DISSERTATION

Dose equivalent measurements in mixed and time varying radiation fields around high-energy accelerators

Sabine Mayer

March, 2003

CERN-THESIS-2003-012
01/03/2003

D I S S E R T A T I O N

Dose equivalent measurements in mixed and time varying radiation fields around high-energy accelerators

ausgeführt zum Zwecke der Erlangung des akademischen Grades
eines Doktors der technischen Wissenschaften
unter der Leitung von

Univ.-Prof. Dipl.-Ing. Dr. techn. Hannes Aiginger
Atominstitut der Österreichischen Universitäten

und

Dr. Thomas Otto
CERN, Schweiz

eingereicht an der Technischen Universität Wien
Fakultät für Technische Naturwissenschaften und Informatik

von

Dipl.-Ing. Sabine Mayer

Matrikelnummer: 9425780
1110 Wien, Krausegasse 4-6/7/4

Wien, im März 2003

To my father.

Kurzfassung

Die Messung der Umgebungs-Äquivalentdosis in Streustrahlungsfeldern rund um Hochenergieteilchenbeschleuniger stellt eine große Herausforderung im Strahlungsschutz dar. Typischerweise tragen unterschiedliche Strahlungskomponenten (Photonen, Neutronen, geladene Teilchen, Myonen,…) mit unterschiedlichen Energien zur Gesamt-Äquivalentdosis bei. Die Strahlungsfelder werden durch Strahlverluste im Beschleuniger hervorgerufen, die während der Beschleunigung oder bei der Auskoppelung des Strahls zu nachfolgenden Experimenten auftreten. Eine zusätzliche Komplikation für die Messung der Äquivalentdosis ergibt sich aus der Tatsache, dass der Teilchenstrahl gepulst ist. Ein ideales Dosimeter für den operationellen Strahlenschutz sollte in der Lage sein, die Äquivalentdosis auch für derart stark gepulste Strahlenfelder mit einer Vielzahl von unterschiedlichen Strahlungskomponenten messen zu können.

Das Ziel der vorliegenden Arbeit war herauszufinden, ob sich eine Ionisationskammer betrieben als „Rekombinationskammer“ und ein gewebe-äquivalenter Proportionalzähler (TEPC), der die Varianz-Kovarianz Methode verwendet (Sievert-Instrument), zur Äquivalentdosismessung in gepulsten Strahlungsfeldern eignen. Die Resultate dieser Methoden werden einerseits mit denen herkömmlicher TEPC-Messgeräte (d.h. HANDI-TEPC) und andererseits mit der Gesamt-Äquivalentdosis, resultierend aus Einzelbeiträgen von verschiedenen Strahlungsmonitoren, verglichen. Diese Monitore (z.B. Argon-Kammer, Wasserstoff-Kammer, REM-Instrument) sind jeweils nur auf eine Strahlungskomponente sensitiv. Obwohl das HANDI-TEPC-Messgerät normalerweise das bevorzugte Referenzinstrument in unbekannten Strahlungsfeldern am CERN ist, eignet es sich nicht zur Messung von stark gepulsten Strahlungsfeldern, die unerwünschte „pile-up“-Effekte hervorrufen.

Die Grundlage für die Messung in einem unbekannten Strahlungsfeld bilden die Kalibrierung und ausführliche Charakterisierung des Messgerätes unter Referenz-bedingungen in den Feldern von Kalibrierquellen. Dies ist für eine präzise und verlässliche Messung in unbekannten Strahlungsfeldern unerlässlich.

Sodann gilt es, das Messgerät in realistischen gemischten Referenzfeldern, die jedoch unter kontrollierten Bedingungen erzeugt werden, zu testen. Solch ein Referenzfeld findet sich am CERF-Strahlplatz (CERN-EU high energy reference field) des CERN. Neben Photonen und Myonen bietet dieses Referenzfeld hauptsächlich Neutronen in einem

weiten Energiebereich, der von thermischen Energien bis hin zu einigen hundert GeV reicht. Bei CERF wird das HANDI-TEPC-Messgerät zur Messung der Gesamt-Äquivalentdosis verwendet. Deshalb wurden die Ergebnisse der Rekombinationskammer und des Sievert-Instruments mit denen des HANDI-TEPC-Messgeräts verglichen. Der Vergleich fand sowohl an verschiedenen Referenzpositionen sowie bei unterschiedlichen Strahlungsfeldintensitäten statt. Einen besonderen Stellenwert hat die Bestimmung der Hintergrundstrahlung am CERF-Strahlplatz. Wie sich herausgestellt hat, liefert die Hintergrundstrahlung einen nicht vernachlässigbaren Beitrag zur Gesamt-Äquivalentdosis, der eine starke Abhängigkeit von der Referenzposition zeigt. Bei CERF zeigten die Resultate der Messungen mit den unterschiedlichen Messgeräten sehr gute Übereinstimmung.

Schließlich wurden die Messgeräte in einem unbekannten, gemischten Streustrahlungsfeld mit kurzen Pulsen auf der so genannten „PS-Bridge“ getestet. Auf der „PS-Bridge“ wird der Teilchenstrahl des PS-Beschleunigers durch eine 260 cm dicke Betonplatte abgeschirmt. Der Teilchenstrahl des PS-Beschleunigers ist stark gepulst, wobei die Strahlungspulse oft nur eine Länge von 10 µs erreichen. In diesem Feld war das HANDI-TEPC-Messgerät aufgrund von „pile-up“-Effekten nicht in der Lage verlässliche Ergebnisse zu liefern. Die Rekombinationskammer und das Sievert-Instrument jedoch ermöglichten auch unter diesen Bedingungen eine Messung der Gesamt-Äquivalentdosis.

Abstract

Measurements of ambient dose equivalent in stray radiation fields behind the shielding of high-energy accelerators are a challenging task. Several radiation components (photons, neutrons, charged particles, muons, etc.), spanning a wide range of energies, contribute to the total dose equivalent. The radiation fields are produced by beam losses interacting with structural material during the acceleration or at the ejection to experimental areas or other accelerators. The particle beam is usually not continuous but separated in “bunches” or pulses, which further complicates dose measurements at high-energy accelerators. An ideal dosimeter for operational radiation protection should measure dose equivalent for any composition of radiation components in the entire energy range even when the field is strongly pulsed.

The objective of this work was to find out if an ionisation chamber operated as a “recombination chamber” and a TEPC instrument using the variance-covariance method (“Sievert Instrument”) are capable of assessing the ambient dose equivalent in radiation fields with short pulses. The results are compared to those of a conventional TEPC instrument (HANDI-TEPC) and to the total dose equivalent values obtained from the suitable combination of readings from instruments currently used at CERN. These instruments are a combination of several detectors with different characteristics measuring individual dose fractions (i.e. an argon-filled chamber, a hydrogen-filled chamber and a rem ionisation chamber). The HANDI-TEPC is usually the preferred reference instrument in mixed radiation fields of unknown composition at CERN, but in strongly pulsed fields it fails because of pile-up effects.

Although the mixed stray radiation fields differ strongly from those applied in standard calibration, the first step in using a radiation protection instrument is the intensive study and characterisation of the detector behaviour in reference fields of calibration sources. This forms the basis for improving the reliability and accuracy of measurements in unknown radiation fields.

The next step is to test the detectors in mixed reference fields, which simulate workplace fields but are produced under laboratory conditions. At CERN, an opportunity for such a reference field is realized by the CERF-field (CERN-EU high-energy reference field). The field provides a mixed field of mainly neutrons ranging from thermal energies up to hundreds of GeV accompanied by photons and muons. At CERF the HANDI-TEPC is

used as a reference instrument for the total dose equivalent. For this reason the results of the recombination chamber and Sievert Instrument were compared to those of the HANDI-TEPC for several reference locations and different beam intensities. In particular, the background radiation at CERF was studied, which has a non-negligible influence on the total dose equivalent and is strongly dependent on the reference location. At CERF, a very good agreement between the results obtained with the various instruments was found.

Finally the instruments were investigated in an unknown mixed stray radiation field with short pulses on the "PS-bridge". This PS-bridge is a location where 260 cm of concrete shield the beam line of the PS accelerator. The operation of the PS at CERN is composed of a supercycle of 16.8 s divided in 14 cycles of 1.2 s each. The duration of the particle pulse can be as short as 10 μs. In such a field the HANDI-TEPC was not able to resolve the single events within one particle pulse because of pile-up effects. The recombination chamber and the Sievert Instrument, however, appear to be capable of assessing the total dose equivalent correctly provided that the response is interpreted carefully by using appropriate corrections and calibration factors.

Contents

Chapter 1

Introduction

Radiation dosimetry in the vicinity of high-energy accelerators is the entire process of acquisition of physical parameters of the radiation field and its interaction with matter and the interpretation of these measurements in terms of quantities needed for the purpose of radiological protection. [IAE88]. McCaslin *et al.* give six reasons for radiation measurements at particle accelerators [McC81]:

- Routine radiation surveys for radiation protection purposes
- Interpretation of the readings of personal dosimeters
- Environmental monitoring
- Accident dosimetry
- Beam intensity measurements
- Radiation measurements in regions of high radiation intensity, to permit an understanding of radiation environment so that reductions in intensity may be made (e.g. by the addition of shielding or changes in operating conditions).

This thesis deals with the complexity of measurements in mixed stray radiation fields at CERN's accelerators. Before interacting, the accelerated beam is essentially monoenergetic, consisting of only one particle type. Passage trough the accelerator structure, experimental equipment or thin shielding will lead to the partial development of electromagnetic and hadronic cascades and the production of many types of particle distributed over a wide range of energies [IAE88]. Behind thick shieldings these cascades are usually well developed and uncharged particles (photons, neutrons) dominate the radiation field. Although in most cases neutrons contribute the highest fraction to the dose equivalent, other components of the mixed field such as gamma radiation and charged

particles have to be correctly assessed as well. All these components, spanning a wide range of energies contribute to the total dose equivalent. In addition the radiation intensity is generally not constant in time, but can be highly structured. Depending on the type of accelerator and the extraction mode of the accelerated particle, the stray radiation fields are slowly varying in time or pulsed (e.g. at the PS accelerator: two pulses of 10 μs separated by 1.2 s in a supercycle of 16.8 s). An ideal dosimeter for operational radiation protection at an (high-energy) accelerator should measure dose equivalent for any composition of radiation in the entire energy range independently of the time structure. Such an instrument could be used as reference instrument for direct field calibration of simpler monitor devices applied for routine protection work.

The PhD thesis focuses on the determination of total dose equivalent in mixed radiation environments around high-energy accelerators. The aim of the thesis project is to investigate and compare the potential of two different single detector methods for the measurement of dose equivalent in mixed stray radiation fields even when they are strongly pulsed. In static stray radiation field conventional TEPC (tissue equivalent proportional counters) are known to measure reliably the total dose equivalent, but in strongly pulsed radiation fields they fail. The two promising methods attempting to measure the dose equivalent directly even in strongly pulsed fields are the *recombination chamber* [Zie62, Zie81] and the *Sievert Instrument* [Kyl97]. The respective measurement principles (ionisation chamber and measurement of recombination characteristics, variance-covariance measurement of a TEPC) are known to measure the radiation protection quantity *H*(10)* well and are likely to be not dependent on temporal distributions of absorbed dose. The approach taken to investigate the potential of the two candidates is divided into the following steps:

The basis for improving the reliability and accuracy of measurements in unknown fields is the investigation of the measuring instrument under reference condition. First intensive study and characterisation of the detector behaviour during calibration processes in fields of reference sources (e.g. ^{137}Cs, ^{60}Co, ^{238}Pu-Be, etc.) have to be carried out. Dosimeters used to measure the ambient dose equivalent, *H*(10)*, require calibration with respect to this quantity. Calibration is the process in which the calibration factor (quotient of conventionally true value by the indicated value) of a dosimeter is determined in a reference radiation field of well-known ambient dose equivalent rate under well-specified calibration conditions [Sch99]. A calibrated instrument will measure *H*(10)* correctly under conditions identical with the calibration conditions. However, under different irradiation conditions or with other particle energy distributions, deviations from the true value will occur since dosimeters used in radiation protection practice usually do not have

ideal response characteristics (e.g. the same energy dependence as the fluence to dose equivalent conversion function) [Sch99]. For that reason the instruments also have to be tested in mixed reference fields. At CERN an opportunity is provided by the CERF-field [Mit02]. The CERF-field simulates closely a workplace field encountered around high-energy accelerators but it is produced under laboratory conditions. Here the dosimeter characteristics can be investigated and different dosimeters can be compared under identical and reproducible conditions.

In order to show the utility of the recombination chamber and the Sievert Instrument in a strongly pulsed stray radiation field measurements were performed in a strongly pulsed, unknown field (e.g. at the PS-bridge of the PS accelerator). The results are compared to the HANDI-TEPC, which is used as reference device for mixed radiation at CERF, and to monitoring systems.

In Chapter 2 the dosimetric quantities used in the present work are defined.

Chapter 3 gives an introduction to the recombination chamber and the applied recombination method. The characterisation and calibration of the chamber carried out in the calibration laboratory are described in detail.

The principles of the Sievert Instrument are presented in Chapter 4. An introduction to the variance-covariance method is given. Moreover the determination of the appropriate measurement parameters during an elaborate calibration process is explained.

Chapter 5 presents an overview of the monitoring devices used in this work. The HANDI-TEPC, high-pressure ionisation chambers and rem counters are described.

Chapter 6 reports results from measurements in the calibration laboratory. Experiments with two neutron "insensitive" ionisation chambers i.e. a CO_2-filled chamber of type G5 and an argon-filled chamber of type IG5 in order to determine the photon contribution to ambient dose equivalent in the given geometry, are carried out in the field of a ^{238}Pu-Be source in the calibration laboratory. These straightforward measurements are confronted with the more elaborated complex method using a recombination chamber REM-2, which allows determining the low-LET component of a mixed radiation field in addition to the measurement of dose equivalent. Moreover the measurements with the Sievert Instrument in the ^{238}Pu-Be are presented. Finally the field of a ^{241}Am-Be source is studied.

Chapter 7 comprises the experiments carried out in the CERF-field. After introducing the CERF-field and the measurement conditions, the investigations with the detectors at different beam intensities are treated separately in detail. Particular attention is paid to the

background radiation encountered at CERF. Then an intercomparison between the already established HANDI-TEPC and the other two candidates for single detector dosimetry is carried out. In addition measurements with an argon-filled and a hydrogen-filled chamber are described.

Chapter 8 is dedicated to the experiments in a strongly pulsed stray radiation field. The recombination chamber and the Sievert Instrument were tested behind a 260 cm concrete shielding on the so-called PS-bridge of the PS accelerator. These investigations were accompanied by measurements with monitor devices routinely used at CERN. Intercomparisons between the used instruments permit an understanding of discrepancies considering the qualitative information on the composition of the radiation field. The experiments and interpretation of the results obtained on the PS-bridge are presented.

Final conclusions are drawn and an outlook is given in Chapter 9.

Appendix A is related to the calibration measurements with the Sievert Instrument. Measurement results and uncertainty considerations are given.

Appendix B includes the uncertainty considerations related to the determination of the photon-contribution of a ^{238}Pu-Be source in Chapter 6.

Appendix C contains the dosimetric results obtained in the CERF-field.

Chapter 2

Quantities in radiation protection dosimetry

Two types of quantities are specifically defined for use in radiation protection: protection quantities, which are defined by the International Commission on Radiological Protection (ICRP), and operational quantities, which are defined by the International Commission on Radiation Units and Measurements (ICRU). The evolution of these protection and operational quantities has led to a system of correlated quantities, which is illustrated by the scheme in Fig. 2-1.

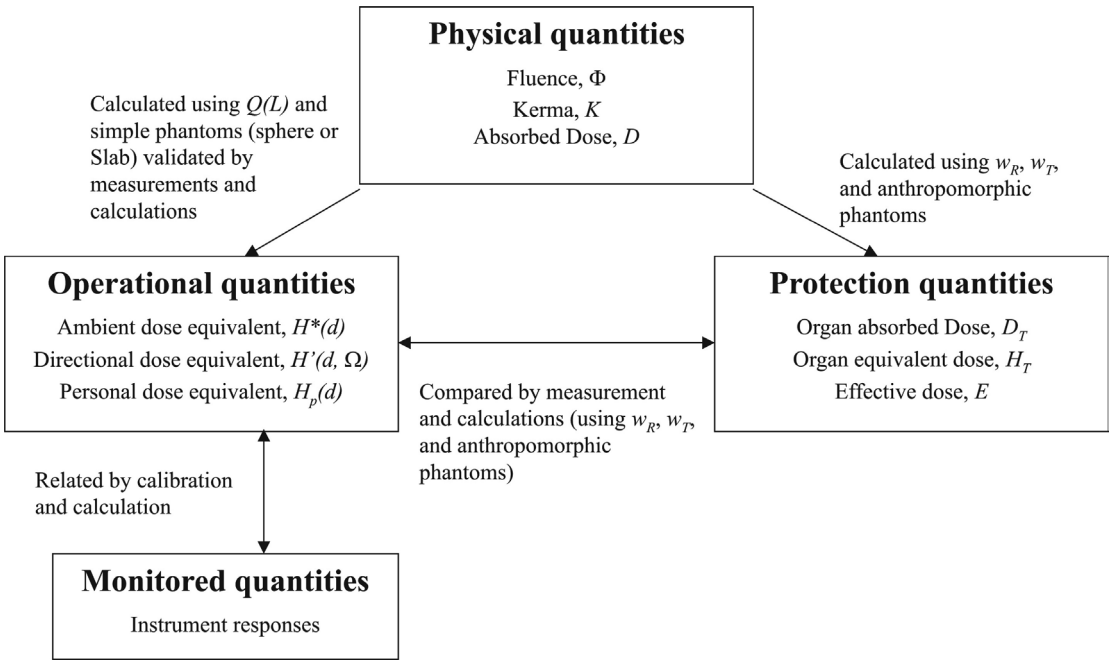

Fig. 2-1 Relationship of quantities for radiological protection monitoring purposes [ICR95]. (Details on quantities and symbols, see below)

The most recent set of protection quantities recommended in ICRP 60 [ICR90] includes the effective dose, E, and the tissue or organ equivalent doses, H_T. These quantities are not directly measurable but are amenable to calculation if the conditions of irradiation are known. The effective dose is assumed to be directly proportional to risk and is used to set exposure limits.

The ICRU has defined a set of operational quantities for area and individual monitoring. They are designed to provide an estimate of protection quantities and to serve as calibration quantities for dosemeters used in monitoring. For area monitoring, the appropriate operational quantities are the ambient dose equivalent, $H^*(d)$, and the directional dose equivalent, $H'(d, \Omega)$. For individual monitoring, the personal dose equivalent, $H_p(d)$, is the appropriate operational quantity.

Both the protection quantities and operational quantities can be related to the basic physical quantities fluence, Φ, air kerma free-in-air, K_a; and the tissue-absorbed dose, D. The physical quantities and the operational quantities are the basis for measuring external radiation. National and international standards laboratories maintain standards and reference fields that are specified and described in terms of these quantities for calibration of instruments and dosemeters.

Conversion coefficients, which relate operational and protection quantities to physical quantities, are calculated using radiation transport codes and the appropriate mathematical models.

2.1 Physical quantities

2.1.1 Fluence, Φ,

is the quotient of dN by da, where dN is the number of particles incident on a sphere of cross-sectional area da.

$$\Phi = \frac{dN}{da} \tag{2.1}$$

Unit: [m^{-2}]

2.1.2 Kerma, *K*,

is a measure of the transfer of energy to secondary charged particles.

$$K = \frac{dE_{tr}}{dm} \tag{2.2}$$

where dE_{tr} is the sum of the initial kinetic energies of all the charged ionising particles liberated by uncharged ionising particles in a material of mass dm.

Unit: Gray [Gy], 1 Gy = 1 Jkg^{-1}

2.1.3 Absorbed dose, *D*,

which is the mean energy imparted $d\varepsilon$ by radiation to a mass element divided by the mass of the element *dm,*

$$D = \frac{d\varepsilon}{dm} \tag{2.3}$$

Unit: Gray [Gy], 1 Gy = 1 Jkg^{-1}

The **energy imparted, ε,** by the ionising radiation to matter in a volume is given by:

$$\varepsilon = R_{in} - R_{out} + \sum Q \tag{2.4}$$

Unit: [J]

where R_{in} is the radiant energy incident on the volume, i.e., the sum of all energies (excluding rest energies) of all those charged and uncharged ionising particles that enter the volume;

R_{out} is the radiant energy emerging from the volume, i.e., the sum of all the energies (excluding rest energies) of all those charged and uncharged ionising particles that leave the volume;

and $\sum Q$ is the sum of all changes of the rest mass energy of nuclei and elementary particles in any interactions that occur in the volume. (In the sum, decreases are denoted by (+) and increases are denoted by (-).) The expectation value of ε, termed the mean energy imparted and denoted $\bar{\varepsilon}$, is closely related to the definition of the absorbed dose, *D*.

In the condition of secondary particle equilibrium, where as many charged secondary particles enter the element *dV* with mass *dm* as leave it, kerma is numerically equivalent to absorbed dose.

2.2 Protection quantities

The protection quantities give a measure of the risk of damage due to ionising radiation and are suitable for defining exposure limits.

2.2.1 Organ absorbed dose

Is the mean absorbed dose, D_T, in a specified tissue or organ of the human body, *T*, given by

$$D_T = \frac{1}{m_T} \int_{m_T} D \cdot dm \qquad (2.5)$$

where m_T is the mass of the tissue or organ, and *D* is the absorbed dose in the mass element *dm*.

Unit: Gray [Gy], 1 Gy = 1 Jkg^{-1}

2.2.2 Equivalent dose, H_T, of an organ or tissue

is the absorbed dose averaged, $D_{T,R}$, over the tissue or organ, *T*, due to radiation *R*, multiplied by the relevant radiation weighting factor, w_R , for radiation, *R*. When the radiation field is composed of radiations with different values w_R , the absorbed dose is subdivided into blocks, each multiplied by its own value of w_R and summed to determine the total equivalent dose, i.e.,

$$H_T = \sum_R w_R D_{T,R} \qquad (2.6)$$

Unit: Sievert [Sv], 1 Sv = 1 Jkg^{-1}

The **radiation weighting factor, w_R,** reflects the different radiobiological effectiveness of the various types and energies of radiation. The Table 2-1 gives the values of radiation weighting factor used for radiological protection purposes as now recommended by ICRP 60 [ICR90].

Table 2-1 Values for radiation weighting factors according to ICRP 60.

Types and energy range of radiation	Radiation weighting factor, w_R
Photons, all energies	1
Electrons and muons, all energies	1
Neutrons, energy	
<10 keV	5
10-100 keV	10
> 100 keV - 2 MeV	20
> 2 – 20 MeV	10
> 20 MeV	5
Protons, other than recoil protons, energy > 2 MeV	5
Alpha particles, fission fragments, heavy nuclei	20

For photons, electrons and muons, the weighting factor is unity, independent of the energy. For neutrons, the radiation weighting factor varies with the neutron energy, E_n. As a supplement to the step function given in Table 2.1, ICRP has defined a smooth w_R function to support the consistency of calculations:

$$w_R = 5 + 17 \cdot e^{\left[\frac{-(\ln(2E_n))^2}{6}\right]} \qquad (2.7)$$

where E_n is the neutron energy in MeV. In practice, only this smooth function is used to calculate neutron-induced body doses.

2.2.3 Effective dose, *E*,

is a summation of the equivalent doses in tissue or organs, each multiplied by the appropriate tissue weighting factor. It is given by the expression

$$E = \sum_T w_T H_T = \sum_T w_T \sum_R w_R D_{T,R} \qquad (2.8)$$

where H_T is the equivalent dose in tissue or organ, T, and w_T is the tissue weighting factor for tissue, T, and accounts for the different susceptibilities of different organs to radiation damage (see Table 2-2). The effective dose can also be expressed as the sum of the doubly weighted absorbed dose in all the tissues and organs of the body.

Unit: Sievert [Sv], 1 Sv = 1 Jkg^{-1}

Table 2-2 Tissue weighting factors

Tissue or organ	Tissue weighting factor, w_T
Gonads	0.20
Bone marrow (red)	0.12
Colon	0.12
Lung	0.12
Stomach	0.12
Bladder	0.05
Breast	0.05
Liver	0.05
Oesophagus	0.05
Thyroid	0.05
Skin	0.01
Bone surface	0.01
Remainder	0.05

2.3 Operational quantities

The operational quantities are used in practice for measurements and individual monitoring.

2.3.1 Dose equivalent, *H*,

One can define a point-quantity dose equivalent:

$$H = D \cdot Q \tag{2.10}$$

Unit: Sievert [Sv], 1 Sv = 1 Jkg^{-1}

where Q is a quality factor which accounts for the biological effectiveness of different radiation types, and are defined in terms of the linear energy transfer, L, of charged particles in water. *Q(L)* values as defined by ICRP 21 [ICR73] and ICRP 60 [ICR90] are given in Table 2–4 and Table 2-5. The dependence of the quality factor Q according to ICRP 21 and ICRP 60 on LET, L, is shown in Fig. 2-2.

The "effective" quality factor Q at a point in tissue is then given by:

$$Q = \frac{1}{D}\int_L Q(L) D_L \, dL \tag{2.11}$$

where D_L is the distribution of D in L.

Dose equivalent quantities are defined on the basis of a phantom known as the ICRU sphere, a 30cm diameter tissue equivalent sphere with a density of 1gcm^{-3} and a mass composition of 76.2% oxygen, 11.1% carbon, 10.1% hydrogen and 2.6% nitrogen.

Conversion factors from physical quantities to operational quantities are calculated by Monte Carlo simulations, using the fundamental relation (2.10).

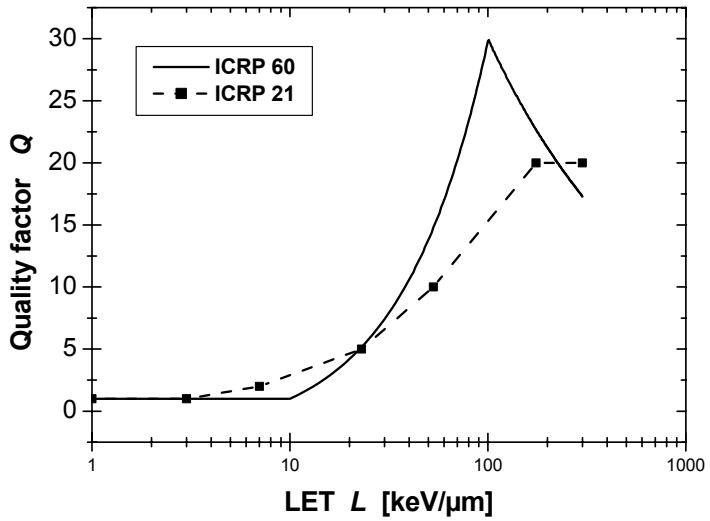

Fig. 2-2 Dependence of the quality factor Q according to ICRP 21 and ICRP 60 on LET, L.

Table 2-3 Relation between quality factor Q and LET, L, recommended in ICRP 21[ICR73]

L in water [keV/ µm]	$Q(L)$
<3.5	1
7	2
23	5
53	10
>175	20

Table 2-4 Relation between quality factor Q and LET, L, recommended in ICRP 60 [ICR90].

L in water [keV/ µm]	$Q(L)$
<10	1
10-100	$0.32L-2.2$
>100	$300 / \sqrt{L}$

2.3.2 Area monitoring

Different dose equivalent quantities are defined for strongly and weakly penetrating, radiation and for area and personal monitoring. Radiation is strongly penetrating if the dose equivalent received by the terminative layer of the skin (0.07 mm) at normal incidence to a broad radiation beam is lower than ten times the effective dose. Radiation is weakly penetrating if for normal incidence the skin dose is higher than ten times the effective dose. The area dose provides an estimate of the effective dose that a person would receive if he stayed at a particular location while the personal dose is a measure of the exposure of an individual to external radiation. The human body influences the radiation field so they are not in general equivalent.

2.3.2.1 Area dose

The area dose is the dose equivalent of soft tissue measured at a specific point (Unit: [Sv]). For strongly penetrating radiation the ambient dose equivalent $H^*(10)$ is used while for weakly penetrating radiation the relevant quantity is the directional dose equivalent $H'(0.07\Omega)$.

The ambient dose equivalent, $H^*(10)$, at a point of interest in a real radiation field is the dose equivalent that would be produced by the corresponding expanded and aligned radiation field at a depth of 10 mm in the ICRU sphere in the opposing direction to the aligned field.

The directional dose equivalent, $H'(0.07\Omega)$, at a point of interest in a real radiation field is the dose equivalent that would be produce d by the corresponding expanded radiation field in the ICRU sphere at a depth of 0.07 mm on a radius in a specified direction Ω. Often the maximum value is used as it is not known a priori what orientation a person will have in the radiation field.

2.3.2.2 Personal dose

The personal dose is the dose equivalent in soft tissue measured at a point on the body surface representative of the radiation conditions prevailing (Unit: [Sv]). Again different quantities are used for strongly and weakly penetrating radiation.

The **personal depth dose equivalent, $H_p(10)$,** is the dose equivalent in ICRU soft tissue at a depth of 10 mm in the body at the location where the personal dosimeter is worn.

The **personal surface dose equivalent, $H_p(0.07)$,** is the dose equivalent in ICRU soft tissue at a depth of 0.07 mm in the body in the location where the personal dosimeter is worn. These values may vary between individuals and depend on the part of the body to which the dosimeter is attached.

2.4 Quantities related to interaction processes

2.4.1 Linear energy transfer (LET), L_D,

is a measure of the energy deposited in a material due to the coulomb interaction.

$$L_D = \left(\frac{dE}{dl} \right)_D \tag{2.12}$$

Unit: [Jm^{-1}], [$keV\mu m^{-1}$]

where dE is the energy lost by a charge particle due to collisions with energy transfers less than a specified value D, while traversing a distance dl. If $D = \infty$, then the energy transfer is said to be unrestricted, and this is often denoted simply by L.

2.4.2 Mean energy expended in gas per ion pair formed, W,

is the quotient of E by N, where N is the mean number of ion pairs formed when initial kinetic energy E of a charged particle is completely dissipated in the gas, thus:

$$W = \frac{E}{N} \tag{2.13}$$

Unit: [J]

Chapter 3

Recombination chamber

The recombination chamber of type REM-2 is designed for measuring absorbed dose, quality factor and dose equivalent of ionising radiation.

Ambient dose equivalent and radiation quality factor are determined by employing the recombination methods, which exploit the effect of the linear energy transfer (LET) of the particle in the process of initial recombination.

In this chapter first theoretical foundations about charge collection in ionisation chambers are given. Then the design of the chamber and the applied recombination method are explained. Moreover this chapter describes the characterisation of CERN's 3 REM-2 recombination chambers before being used for measuring the dose equivalent in mixed radiation fields.

3.1 Theoretical foundations

3.1.1 Charge collection in an ionisation chamber - saturation curve

As the voltage difference between the electrodes of an ionisation chamber exposed to radiation is increased from zero to higher values, the collected current increases almost linearly with voltage. Above a certain voltage the current increases more slowly. It finally approaches asymptotically the saturation current for the given radiation intensity – which corresponds to the current that would be measured if all the ions formed in the chamber by the radiation were able to reach the electrodes [Boa87]. The curve of collected charge or current versus applied voltage is called the saturation curve and is typically of the form shown in Fig.3-1.

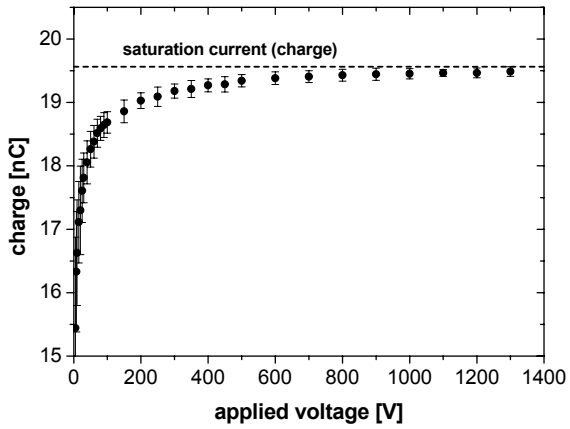

Fig. 3-1 Typical form of a saturation curve measured with an ionisation chamber. The axes are not to scale. At the ordinate, the measured current or charge can be applied.

3.1.2 Mechanisms of recombination

Three pathways for the recombination of ions formed by ionising radiation in gases can be distinguished in theory, although it may often be very difficult to separate them experimentally. These are geminate, initial, and general recombination [Boa87].

Geminate recombination refers to the recapture of an electron by its parent ion or, if the electron has become attached to form a negative ion, the recombination of the latter with the parent positive ion. For practical purposes this pathway can be subsumed under the more general term of initial recombination.

The recombination of positive and negative ions formed within the track of a single ionising particle is called initial recombination. Being an intratrack process, it is independent of the number of tracks formed per second, and thus of the dose rate. It depends only on the initial ion density in each track and the field strength normal to the tracks, since the latter is the electric field component tending to pull the positive and negative ion columns apart.

On the other hand general recombination increases as the average concentration of ions of both signs increases, that is, with increasing dose rate. This sets an upper limit to the dose rate that can be measured accurately by a particular ionisation chamber operating at atmospheric pressure.

An empirical procedure formerly used to distinguish between initial and general recombination in continuously irradiated chambers was to plot the reciprocal of the measured ionisation current I against a suitable function of the applied voltage, U, (field strength) in the chamber. If initial recombination is dominant, one should find a linear relationship between I^{-1} and U^{-1} in the near-saturation region:

$$\frac{1}{I} = \frac{1}{I_S} + \frac{const}{U} \tag{3.1}$$

However, if only general recombination is present the relationship should be

$$\frac{1}{I} = \frac{1}{I_S} + \frac{const}{U^2} \tag{3.2}$$

These relations are approximations, however, based on very simple theoretical models. Since both initial and general recombination are usually present, the graphical extrapolation method at high field strength is not always a reliable method for assessing I_S, the ultimate saturation current.

In Fig. 3-2 we give an example for this empirical procedure in the field of a ^{238}Pu-Be source. The reciprocal charge collected with a recombination chamber is plotted once against the reciprocal applied voltage and a second time against the reciprocal squared, applied voltage. On the basis of these illustrations we see that initial recombination is dominant.

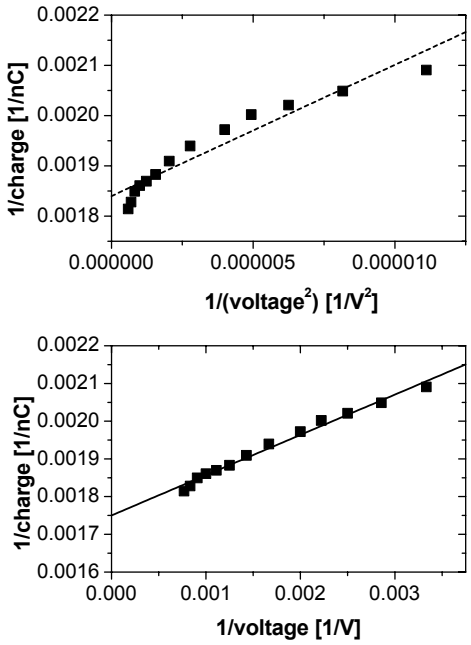

Fig. 3-2 Example for the determination of the saturation current (charge) in a radiation field. Here the procedure is demonstrated for measurements in the field of ^{238}Pu-Be. The approximations demonstrate that initial recombination is dominant.

3.2 Design of the recombination chamber

The recombination chamber REM-2 [Zie62, Zie81] is a high-pressure tissue-equivalent ionisation chamber, manufactured in Poland by POLON-Bydgoszcz [Pol73]. It is filled with a mixture of methane and nitrogen (5% by weight) up to pressure of about 1 MPa. It has a volume of 1800 cm³, a mass of about 6.5 kg and the effective wall thickness is of about 1g/cm², when a point source at the distance of more than 1 m is used.

The chamber contains 25 parallel-plate tissue-equivalent electrodes. The central rod connects 12 collecting electrodes. The polarising electrodes are connected alternately to one of two side rods and thus form two sets of electrodes. These sets can be connected either to the same collecting voltage (summation mode) or to different voltages of opposite polarity (differential mode). For our purposes the basic mode of REM-2 in the experiments was the summation mode.

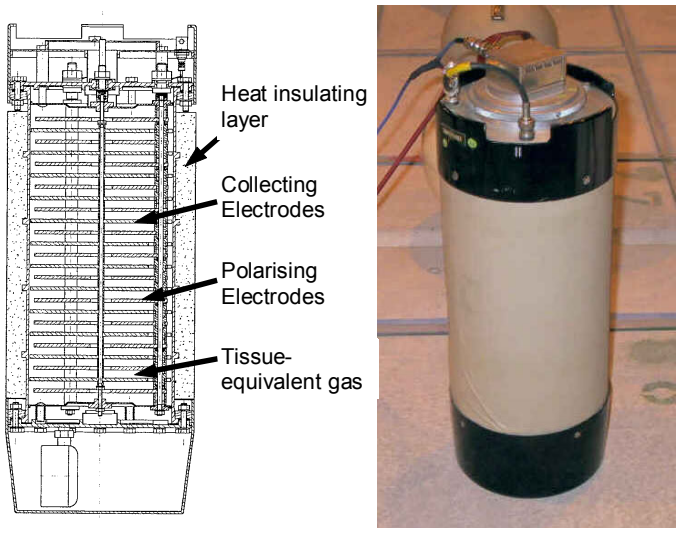

Fig. 3-3 REM-2 recombination chamber with cross section.

The electrodes are 12 cm in diameter and 3 mm thick. The distance between the electrodes is 7 mm. The chamber is accommodated in a cylindrical container made of 1.2 mm thick aluminium alloy. Two steel covers close the container at its ends. A sealed high-resistance element serves as an output for the collecting electrode. Two BNC-2.5 connectors for supply voltages are attached to the lower guard, which is fastened to the lower cover. The same guard is used to connect the chamber with an electrometer. The cylindrical part of the chamber is surrounded by a heat-insulation layer made of foamed polystyrene, which virtually eliminates the effect of fast variations in the ambient temperature on the chamber current. A picture of the REM-2 chamber and its cross section is shown in Fig. 3-3.

The chamber is supplied with a voltage such that the occurrence of initial ion recombination in the whole volume of the chamber is ensured. The charge (current) measured by an electrometer is proportional to the effectiveness of ion collection. From the collected charges (currents) of saturation and recombination it is possible to deduce the quality factor and thus the dose equivalent of the measured radiation. The utility of the recombination chamber for dosimetry of ionising radiation was verified experimentally several times by Golnik *et al.* [Gol85, Gol92, Gol94] and Zielczynski *et al*. [Zie96, Zie99, Zie00].

Table 3-1 Technical data of the REM-2 chamber in summation mode [Pol73].

Sensitivity	0.1pA/(μGy.h)	
Measuring ranges	5 μGy/h – 300 mGy/h	
Background	≤ 0.1 pA	
Angular characteristics	-30% – +10%	
Input capacitance	550 ± 50 pF	
Output resistance	≧ 10^{14} Ω	
Saturation voltage	1000 – 1500 V	
Recombination voltage	< 100 V	
Mass	6.5 ±0.3 kg	
Gas filling	3-10*10^5 N/m^2 (=0.3-1 MPa)	(1 mbar = 100 Pa = 100 N/m²)
Gas leakage	0.2 *10^5 N/m^2 (=0.02 MPa) per year	2 – 6.67 % per year
Temperature range	5° - 35 °C	Measuring error 0.5 %/°C

3.3 Recombination method

Recombination chambers make use of the phenomenon of initial recombination of ions in gases. Initial or columnar recombination is recombination along the track of an ionising particle, and is of utmost interest here as it can be related to the quality factor of the radiation. Initial recombination is less for radiation with small LET, and hence low Q, than for radiation with high LET, as high LET radiation deposits its energy in dense tracks or clusters so that in the presence of a weak electric field the migration time is long enough for the ions to recombine [Cos84].

Using initial recombination of ions for measuring Q and $H^*(10)$ was first proposed by Zielczynski in 1962 [Zie62] and Sullivan in 1963 [Sul63]. Sullivan assumes that the saturation curve of an ionisation chamber can be described as

$$I = KV^n \tag{3.3}$$

where I is the ionisation current, K is a linear function of the dose rate, V is the applied potential and n is the recombination number; n is a monotonic function of the quality factor and independent of the dose rate. This method has been used with a variety of

ionisation chambers by Distenfeld *et al.* [Dis66], Sullivan [Sul69] and Cossairt *et al.* [Cos84] and was found to be suitable for measuring the quality factor, and hence ambient dose equivalent in mixed radiation fields around accelerators. In practice however, the method is rather complex as *n* depends on the chamber design, and the composition and pressure of the filling gas, and special investigations are required for each chamber. The present work follows a simpler procedure developed by Zielczynski and Golnik [Zie80, Gol88, Zie94, Gol96b]:

3.3.1 Recombination index of radiation quality Q_R

The recombination index of radiation quality Q_R proposed by Zielczynski *et al.* [Zie80] is a measurable quantity, which can be determined using the recombination chamber operated under conditions of initial recombination of ions. Q_R is evaluated using the following formula,

$$Q_R = \frac{1 - f_{mix}}{1 - f_\gamma} \tag{3.4}$$

and

$$f_R = \frac{I(U_{R^+}) + \left|I(U_{R^-})\right|}{I(U_{S^+}) + \left|I(U_{S^-})\right|} = \frac{q(U_{R^+}) + \left|q(U_{R^-})\right|}{q(U_{S^+}) + \left|q(U_{S^-})\right|} \tag{3.5}$$

where

f_R is the ion collection efficiency at a special chosen recombination voltage U_R. Averaging over the charges (currents) collected at both polarities *(+ ...positive polarity or -... negative polarity)* of the applied voltage U reduces the effects of electrical charges collected on other aspects of the measuring equipment such as the cables and charge memory effect (where electrical charge is collected on the non conducting parts of the tissue equivalent electrode surface and reduces the effective value of the voltage between the electrodes [Zie01])

$q(U_R)$ charge collected at the recombination voltage U_R

$q(U_S)$ charge collected at the saturation voltage U_S

f_γ ion collection efficiency in a γ–reference field of a ^{137}Cs source

f_{mix} ion collection efficiency at the same voltages (U_R, U_S) in an unknown radiation field

Q_R signifies that U_R should be chosen so that $f_\gamma = \frac{100 - R}{100}$. It was found that Q_4 (R = 4) was the best approximation of the quality factor for radiation protection purposes because its dependence on LET was quite similar to the LET dependence of the radiation quality factor defined in the ICRP 21 recommendations [ICR73]. In practice it is hard to determine U_R so that f_γ is exactly 96% and the results are acceptable if $0.95 < f_\gamma \leq 0.96$ [Zie01].

In the past, the radiation quality index Q_4 was used as a good approximation of the radiation quality factor according to the quality factor definition in ICRU 21. In the more recent recommendations of ICRP, ICRP 60 [ICR90], Q_4 is considered as an independent parameter dependent on restricted LET, L_Δ, with an energy cut-off Δ of about 500 keV (see Fig.3-4).

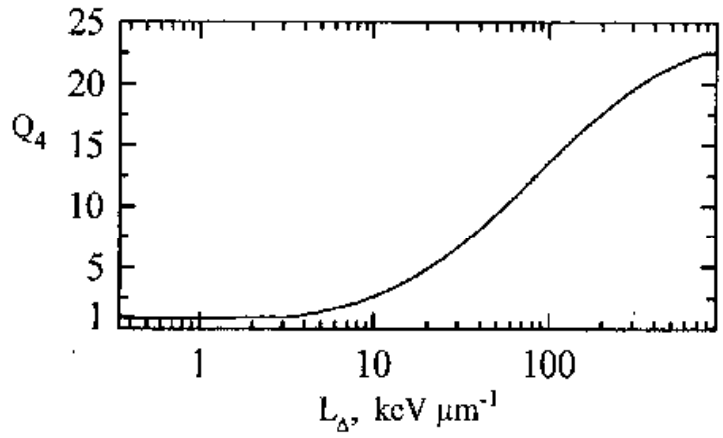

Fig. 3-4 Radiation quality index Q_4 as a function of restricted LET.

To take advantage of the fast determination of the quality factor with the concept of the radiation quality index Q_4, this procedure was adjusted to the quality factors defined in ICRP 60 by Golnik *et al.* [Gol96b] by introducing a new quantity Q_{4new} which is an empirical function of Q_4 such that,

$$\begin{aligned} Q_{4new} &= Q_4 && \text{for } Q_4 \le 5 \\ Q_{4new} &= Q_{ICPR60}(L_R) && \text{for } 5 < Q_4 < 11 \text{ and } Q_4 > 20 \\ Q_{4new} &= 20 && \text{for } 11 \le Q_4 \le 20 \end{aligned} \tag{3.6}$$

where

$$L_R = \frac{L_0 f_\gamma Q_4}{1-(1-f_\gamma)Q_4} \tag{3.7}$$

is a single effective LET value which replaces the LET spectrum for the radiation, and $L_0 = 3.5$ keV/μm.

One has to note that the quantity Q_{4new} can be rigorously defined only for a fictitious radiation field with a single LET value. Golnik [Gol96b] has therefore developed another approach ("fitting method") to determine the radiation quality factor, as given by the *Q(L)* relationship in the ICRP Report 60 [ICR90]. The method is based on the mathematical analysis of the saturation curve. The measurements and calculations are much more tedious than in the case of Q_4, because the whole saturation curve must be determined.

3.3.2 Determination of the low LET dose fraction

On the basis of the analysis of the saturation curves, the "fitting method" described by Golnik [Gol96a], allows in addition to determine the low and high LET components in a mixed radiation field.

For determining the low LET dose fraction Golnik applies a fitting procedure, where first the values of f_{mix} are plotted versus f_γ. Then the following equation is fitted to the experimental data:

$$f_{mix} = \mathcal{D}_{low} \cdot f_\gamma + \sum_{j=2}^{6} \mathcal{D}_j \cdot s_j \tag{3.8}$$

where $\mathcal{D}_{low}$ is the low LET component of the absorbed dose
f_γ is the ion collection efficiency in a γ reference field of a ^{137}Cs source
$\mathcal{D}_j$ are the dose fractions associated with the considered LET intervals
s_j are the analytical functions of f_γ given by equation:

$$s_j = \frac{L_0}{L_{\Delta,j+1} - L_{\Delta,j}} \cdot \frac{f_\gamma}{1 - f_\gamma} \ln \frac{\left| 1 + \left(1 - f_\gamma\right) \cdot \left(\frac{L_{\Delta,j+1}}{L_0 - 1} \right) \right|}{\left| 1 + \left(1 - f_\gamma\right) \cdot \left(\frac{L_{\Delta,j}}{L_0 - 1} \right) \right|} \tag{3.9}$$

where

L_0 is a scaling factor, L_0=3.5 keV/µm

The procedure gives results for the dose fractions $\mathcal{D}_j$ and the low LET dose fraction $\mathcal{D}_{low}$., which is usually the dose from photons to absorbed dose of mixed radiation. Here, "low" is associated with the LET range from zero to 20 keV/µm.

The complete derivation of the fitting function of f_{mix} and of the analytical functions s_j can be found in the work of Golnik [Gol96a].

3.4 Calibration and characterisation of the recombination chamber

CERN has three REM-2 recombination chambers, serial no. 021, 027 and 004. All investigations were carried out in the CERN TIS-RP calibration hall [McL01]. The calibration hall has a constant temperature of 20 °C and allows the distance of the chambers from the source to be set to an accuracy of 1 cm using a laser alignment system. A variable high voltage power supply was used to polarise the chamber. The voltage was read from a digital voltmeter in the range from 5-1000 V and from the dial on the power supply for voltages exceeding the range of the voltmeter. The collected charge, q, was measured using a PTW-UNIDOS electrometer connected to the chamber using electrometrical cables.

3.4.1 Determination of the recombination voltage and sensitivity

Saturation curves for the chambers in a radiation field of a ^{137}Cs source at an ambient dose equivalent rate of $H^*(10)$ = 2.00±0.02 mSv/h were obtained for both polarities by applying a succession of voltages ranging from 5 to 1300 V, to the chamber and measuring the charge collected over 100 s. Initially, 5 measurements were made at each voltage to ensure that the measurements were stable. It was established that the 1st measurement after the voltage had been changed was substantially different, due to dark current while the power supply stabilised, but there was very small variation in the subsequent measurements so only 3 measurements were made at each voltage after ensuring that enough time had elapsed for the power supply to stabilise.

The complete saturation curves were determined twice for chamber 004 and 027 in this manner realigning the chamber each time. Slightly different results were obtained, in agreement with the uncertainty in chamber position, which translates at 2.17 m into a 1 %-uncertainty in dose rate. These variations are also within the standard uncertainty of the calibration source, which has been evaluated to ±5% at the 95% confidence level [Ott99]. Further measurements were made around the values of U_S and U_R so that the results for each voltage give the saturation curves in Fig.3-5. As can be seen from the figures the saturation curves are slightly different for different polarities due to the effects of electrical charges collected on other aspects of the measuring equipment such as the cables and charge memory where electrical charge collects on the non conducting parts of the tissue equivalent electrode surface and reduces the effective value of the voltage between the electrodes [Zie01].

The saturation current, I_S, is reached when all ions formed in the chamber are collected at the electrodes. Such a saturation current is usually not achievable for high-pressure ionisation chambers, as the maximum voltage is limited by electron multiplication and sometimes by increasing dark current. Therefore, the saturation current has to be determined by the extrapolation procedure explained in 2.2.2.
Linear extrapolation to the zero value of U^{-1} gives the reciprocal charge collected at saturation (reciprocal saturation current I_S^{-1}). The graphical determination of the saturation current is demonstrated in Fig. 3-6.

Values for U_R and f_γ determined for the recombination chambers available at CERN are listed in Table 3-2. In addition the sensitivity, $R_D = I_S/D$, to absorbed dose, D, is shown.

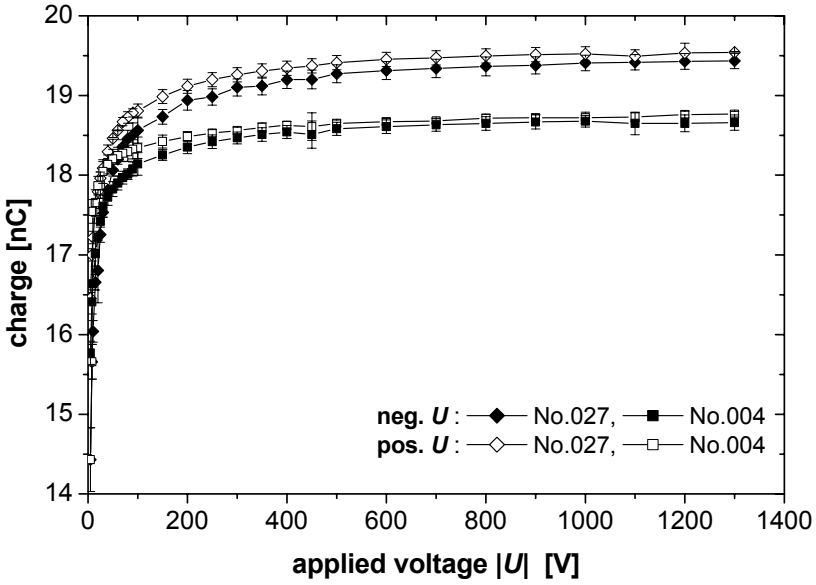

Fig. 3-5 Saturation curves measured at both polarities of applied voltage for chambers 027 and 004 in a γ field of a ^{137}Cs source. The ambient dose equivalent rate is *H*(10)* = 2.00±0.1 mSv/h at a distance of 2.169±0.02 m.

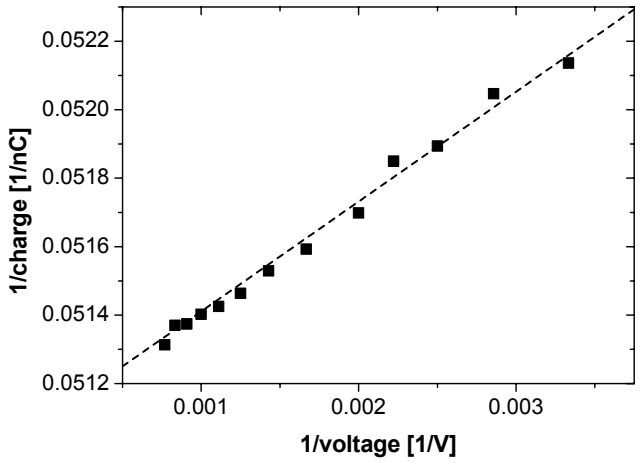

Fig. 3-6 Determination of the saturation current (charge collected at saturation) for the chamber 027 in the field of ^{137}Cs.

Table 3-2 Values of sensitivity, R_D, recombination voltage, U_R, and ion collection efficiency, f, at U_R, determined at an ambient dose equivalent rate of 2.00±0.02 mSv/h at a distance of 2.169±0.01 m, in a radiation field of a ^{137}Cs source in the CERN TIS/RP calibration hall. Comparisons are with values measured in 1992 by Zielczynski and Golnik [Zie92].

Chamber	2001 R_D [μC/Gy]	1992 R_D [μC/Gy]	Change in sensitivity [%]	2001 U_R [V]	2001 f_γ
021	346.01 ± 1.88	369	-6.23	70	0.958 ± 0.002
027	349.23 ± 2.09	369	-5.36	70	0.954 ± 0.006
004	336.24 ± 1.70	356	-5.47	40	0.957 ± 0.004

Chambers 021 and 027 have higher sensitivity and recombination voltages than chamber 004 probably due to lower pressure in chamber 004. The values for sensitivity in 2001 are considerably lower than those in 1992 especially for chamber 021. Zielczynski and Golnik [Zie92] state that the gas leakage from the chambers 027 and 004 is less than <0.2% per year, this corresponds to at most a 1.8% fall in pressure since 1992, while sensitivities have fallen by over 5%. It would be expected that the sensitivity is proportional to pressure so one reason for the lower sensitivities could be due to the use of a different electrometer, because all sensitivities are lower by about –5.5%. Zielczynski and Golnik did all the measurements with a Keithley 642 electrometer [Zie92]. Another possible reason for the underestimation could be the difference in absolute calibration of radiation fields in the calibration laboratory conditions of the new (used in this work) and the old calibration laboratory (used in 1992).

As the ionisation current is small, it is important to eliminate possible sources of dark current, such as drift in the voltage supplying the chamber, and temperature fluctuations. The dark current was measured in the same experimental set up as described above, but in the absence of the source. It fluctuated around zero for all voltages being at most ±3 pC for a measurement made over 100 s. This is consistent with the 10^{-14} A reported by Golnik [Gol96a]. It is also at the same order of magnitude as would be expected assuming a natural background dose rate of 100 nGy/h with a sensitivity of 350 μC/Gy, although this should not fluctuate over the time interval used and is masked by other effects.

At the used dose rates the dark current is negligible, but at lower dose rates it may be significant. The fluctuations complicate the subtraction of the dark current, however if many measurements are made the fluctuations should cancel. The dark current (charge) was much higher, around 0.237 nC for the first measurement when the power supply was turned on and around 25 nC after a change in voltage due to the time taken for the power supply to stabilise. For this reason no measurements were made until the voltmeter reading showed that the voltage had stabilised (usually 60 s to 100 s).

3.4.2 Sensitivity to small changes in position and angular dependence

As stated above the accuracy of the distance of the chamber from the source should correspond to an uncertainty in the charge collected at a distance of 2.169 m of around 1%. This was tested for the chamber 027.

The chamber was aligned using the laser, and the ionisation charge was collected at 4 different voltages. Without realigning the chamber it was moved 1 cm closer and 1cm, further away from the source, and the measurements repeated. As it can be seen from Fig. 3-7 the uncertainties are slightly larger than expected. Although the largest error probably comes from the alignment of the chamber with the laser, there is also an error from setting the distance of the chamber from the source.

The orientation of the chamber was also investigated. Measurements were made at 1200 V rotating the chamber 90° about its cylindrical axis and realigning it each time. Differences in the charge collected were again about 1%, see Table 3-3. Most likely they are dependent on the accuracy, to which the chamber can be positioned, rather than to internal structure of the chamber. More measurements with an improved alignment support would be needed to confirm this.

In order to detect any effects due to the relative position of source and chamber measurements were also made with the chamber shifted to the extreme right and left of the calibration stand. The difference between these measurements was 1.5%, which is again most likely due to differences in distance from the source.

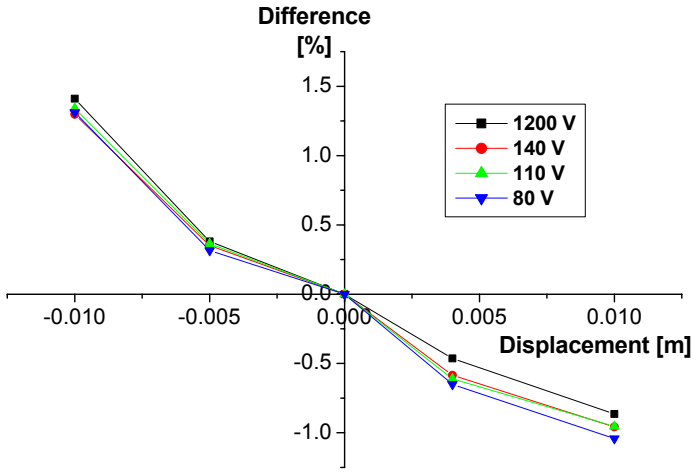

Fig. 3-7 Variation in ionisation charge collected at 4 different voltages due to small displacements from a central position of 2.169 ± 0.01 m of a ^{137}Cs source, giving a dose equivalent rate of 2.00±0.1 mSv/h, in the CERN TIS/RP calibration hall

Table 3-3 Angular dependence of the ionisation charge collected over 100 s at 1200 V in a reference γ field from a ^{137}Cs source in the CERN TIS/RP calibration hall. Ambient dose equivalent rate is 2.00±0.02 mSv/h at a distance of 2.169±0.01 m.

Voltage across chamber	Rotation	Charge collected in nC	% Difference from median value	Comments
1200	0 ± 10°	19.38 ± 0.18	-0.49	
1200	90 ± 10°	19.44 ± 0.18	-0.17	
1200	180 ± 10°	19.47 ± 0.18	0.04	
1200	270 ± 10°	19.61 ± 0.18	0.70	Cables between source and detector
Mean		19.47		

Chapter 4

Sievert Instrument

One of the very few successful attempts to employ a new technique for dose equivalent measurements in mixed radiation fields is the variance-covariance method [Kel84]. This method forms the basis of the measurements with two tissue-equivalent proportional counters known as the Sievert Instrument [Kyl97].

The present work gives an introduction to the variance-covariance method and the Sievert Instrument, which was kindly provided by the Swedish radiation protection institute (SSI) for measurements during the summer of 2002 at CERN. This chapter contains the detector parameters and calibration factors needed for the analysis of measurements at CERN.

4.1 Theoretical foundations

4.1.1 Microdosimetry and the variance-covariance method

During the development of experimental microdosimetry the variance-covariance method emerged as a functional technique for radiation measurements due to a collaboration between the laboratory of Harald Rossi at Columbia University and the Swedish Radiation Protection Institute in Stockholm. The basis of the method has been derived from studying microdosimetric quantities, microdosimetric distributions and their moments by applying statistical relations [Kel84]. The principles of experimental microdosimetry are explained well in the paper of Waker [Wak95]. The successful application of this technique is documented in a series of papers by Kyllönen *et al*. [Kyl97, Kyl01a, Kyl01b, Kyl01c].

All mechanisms for radiation interaction with matter are stochastic by nature and require statistical descriptions. The definitions of microdosimetric quantities (e.g. ICRU 60, [ICR98]) use the term *event*, denoting the interaction of correlated particles. The energy absorbed (imparted) in an event includes also energy absorption from secondary particles such as delta electrons [Kel85, ICR83].

Consider a small object with energy imparted from j events where the energy is transferred in k energy transfer points in each event. The energy imparted in the object is the sum

$$\varepsilon = \sum_j \left(\sum_k \varepsilon_{j,k} \right) = \sum_{j,k} \varepsilon_{j,k} \ . \tag{4.1}$$

The energy imparted in the object is proportional to the number of events and is described by a dose-dependent distribution $f(\varepsilon,D)$. This distribution has a probability for events with no energy deposition and this zero-event probability increases with decreasing dose. The single event distribution, $f_1(\varepsilon)$, describes the energy imparted in an object from exactly one event. This distribution is characteristic for the radiation field and is dose independent. This frequency distribution of energy imparted, $f_1(\varepsilon)$, describes the probability of having an energy deposition in the range ε to $\varepsilon + d\varepsilon$, and the average energy imparted in an event is the expectation value

$$\bar{\varepsilon}_F = \int_0^\infty \varepsilon \cdot f_1(\varepsilon) \cdot d\varepsilon \ . \tag{4.2}$$

Often also the dose distribution from single events, $d_1(\varepsilon)$, is of interest. This distribution describes the fraction of dose given by energy depositions in the range ε to $\varepsilon+d\varepsilon$. The dose (or energy) weighted average is given by

$$\bar{\varepsilon}_D = \int_0^\infty \varepsilon \cdot d_1(\varepsilon) \cdot d\varepsilon = \int_0^\infty \varepsilon \cdot \left(\frac{\varepsilon}{\bar{\varepsilon}_F} f_1(\varepsilon) \right) \cdot d\varepsilon = \frac{\overline{\varepsilon_F^2}}{\bar{\varepsilon}_F} \tag{4.3}$$

which is seen to be the ratio of the second and first moments of the single-event distribution.

Two other important microdosimetric quantities are the specific energy, z, and the lineal energy, y. These and their moments are found from the moment of energy imparted.

$$z = \frac{\varepsilon}{m} \qquad \bar{z}_F = \frac{\bar{\varepsilon}_F}{m} \quad \bar{z}_D = \frac{\bar{\varepsilon}_D}{m} \tag{4.4}$$

$$y = \frac{\varepsilon}{\bar{l}} \qquad \bar{y}_F = \frac{\bar{\varepsilon}_F}{\bar{l}} \quad \bar{y}_D = \frac{\bar{\varepsilon}_D}{\bar{l}} \tag{4.5}$$

Here m and $\bar{l}$ are the mass and mean chord length of the object. The units are *Gy* for z and *keV/μm* for y, and these quantities are the microdosimetric analogues to the macroscopic absorbed dose and LET. If the average number of events, n, is known, the absorbed dose is simply given by

$$D = n \cdot \bar{z}_F \,. \tag{4.6}$$

The relative variance of the single-event spectrum can, as any distribution, be written in terms of the first and second moments.

$$V_1(\varepsilon) = \frac{\bar{\sigma}_\varepsilon^2}{\bar{\varepsilon}_F^2} = \frac{\overline{\varepsilon_F^2} - \bar{\varepsilon}_F^2}{\bar{\varepsilon}_F^2} = \frac{\overline{\varepsilon_F^2}}{\bar{\varepsilon}_F^2} - 1 = \frac{\bar{\varepsilon}_D}{\bar{\varepsilon}_F} - 1 \tag{4.7}$$

When several events contribute to the energy imparted the relative variance is the sum of the term V_1/n, related to fluctuations of event size, and the term $1/n$ (Poisson distribution), due to variations of event number. The total relative variance in a multiple event spectrum is given by

$$V_R = \frac{V_1}{n} + \frac{1}{n} = \frac{\overline{\varepsilon_F^2}}{n\bar{\varepsilon}_F^2} = \frac{\bar{\varepsilon}_D}{n\bar{\varepsilon}_F} = \frac{\bar{z}_D}{n\bar{z}_F} = \frac{\bar{z}_D}{D} = \frac{\bar{l} \cdot \bar{y}_D}{m \cdot D} \,. \tag{4.8}$$

This is the basis for the variance method. A tissue-equivalent proportional counter (TEPC) is used to measure the average and the variance in the absorbed dose in time intervals (typically 0.1 s or 0.3 s) that include multiple events. The dose weighted average of lineal energy, $\bar{y}_D$, (or any of the three microdosimetric quantities) is then given by the relation above.

Since all variance contributions are measured, also a varying beam intensity will be seen as an additional variance. A correction using two detectors can be applied in such cases [Kel84]. If the detectors are exposed to the same beam variations, this can be detected as a covariance between these two signals. The $\bar{y}_D$ can then be determined with the corrected equation

$$\bar{y}_D = \frac{(V_R - C_R) \cdot m \cdot D}{\bar{l}} \tag{4.9}$$

where C_R is the relative covariance. Expressed more explicitly for e.g. detector 1, the $\bar{y}_D$ is determined from

$$\bar{y}_D = \frac{\left(\frac{\overline{q_1^2} - \bar{q}_1^2}{\bar{q}_1^2} - \frac{\overline{q_1 q_2} - \bar{q}_1 \bar{q}_2}{\bar{q}_1 \bar{q}_2} \right) \cdot \bar{q}_1 \cdot \frac{W}{e}}{\bar{l}} \tag{4.10}$$

where q_1 and q_2 are the charges generated in the gas of the two detectors, and W/e is the average energy required to produce an ion pair.

The quality factor, $Q(L)$, is defined by ICRP in terms of linear energy transfer in water, L. After substituting the linear energy transfer L with the lineal energy, the quantity $\bar{y}_D$ is proportional to the dose mean quality factor in a first approximation.

$$\bar{Q}_D = \int_0^\infty Q(y) d(y) dy = c_0 + c_1 \bar{y}_D + c_2 \overline{y_D^2} + \ldots \tag{4.11}$$

Here $d(y)$ denotes the dose distribution of the lineal energy, y, and the c_i are constants.

Finally a first order approximation of the dose equivalent is given by

$$H^* = N D_{gas} \bar{Q}_D = N \cdot \frac{\bar{q} \cdot \frac{W}{e}}{m_{gas}} \cdot (c_0 + c_1 \bar{y}_D) \tag{4.12}$$

where N denotes a calibration factor from a suitable reference source, $\overline{q}$ is the average measured charge and m_{gas} is the mass of the detector gas. The constants c_i are chosen to minimise the difference between H^* and the ambient dose equivalent $H^*(10)$.

4.2 Design of the Sievert Instrument

The Sievert Instrument (Fig.4-1) was developed for radiation protection applications and cosmic ray measurements based on two tissue-equivalent proportional counters (TEPC) applying the variance-covariance method. The instrument can be employed in the variance method by using only one detector to limit the size and weight of the equipment for cosmic radiation applications, where no important intensity variations have been observed [Kyl01b]. If the field variations are longer than the integration time (100 ms) a covariance correction can also be applied using only one detector. However, in the case of short intensity variations such as a pulsed radiation field, a second detector is needed using the variance-covariance method to resolve the field variation from a microdosimetric fluctuation.

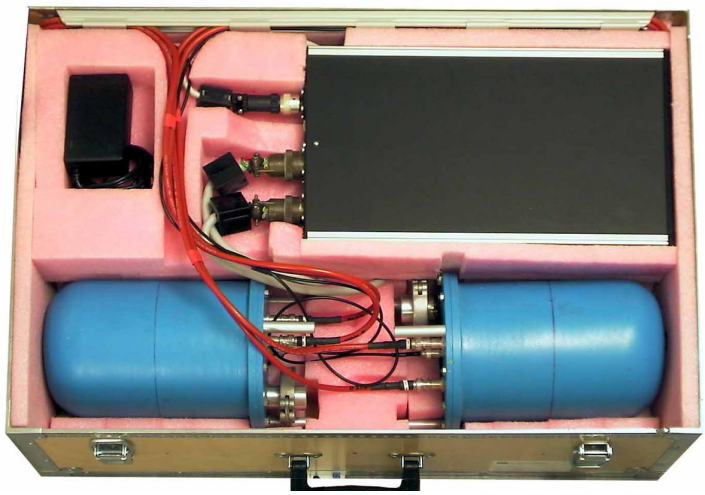

Fig. 4-1 Sievert Instrument arranged in a wooden box to be transportable for flight measurements. The box has dimensions of 67 cm × 47 cm × 21 cm and a total weight of 22 kg [Kyl02b].

Two detectors with electronics and power supply can be carried in a wooden box (67 cm × 47 cm × 21 cm) with total weight of 22 kg. If only one detector is needed a cabin bag (50 cm × 40 cm × 20 cm) can be used to reduce weight to 14 kg. The detectors have a sensitive volume of 1.2 litres achieved by a cylindrical shape with a height and a diameter both of 11.5 cm. In Fig.4-2 one detector and its vertical section is illustrated. The wall of the detector is made of 5 mm thick tissue-equivalent A-150 plastic surrounded by a 3.9 litre vacuum tight container of 2 mm Al. Field shaping tubes at distances corresponding to 80% of the wall high voltage are used to improve the shape of the internal electrical field. The detectors are filled with propane based tissue-equivalent gas at a pressure of 1.48±0.01 kPa and 1.46±0.01 kPa. With a propane based tissue-equivalent gas filling of 1.45 kPa the detectors simulate tissue-volumes of 3 µm diameter or 2 µm mean chord length. The filling parameters are listed in Table 4-1.

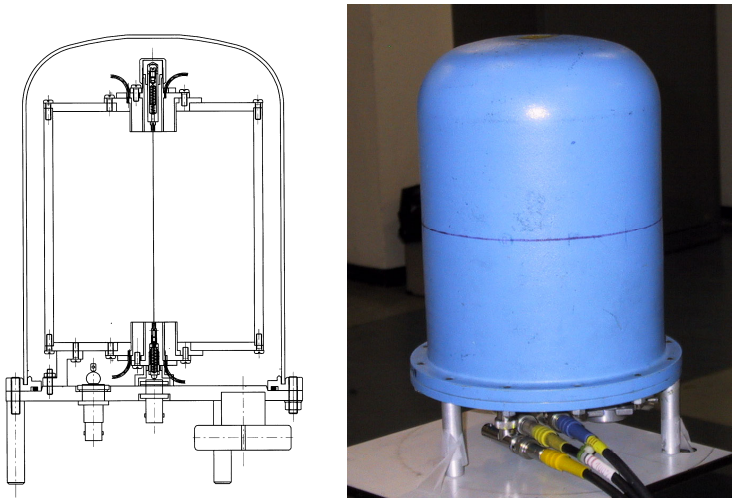

Fig. 4-2 Cross section and picture of one TEPC of the Sievert Instrument. The cross section was kindly provided by the Swedish Radiation Protection Institute [Kyl97].

Table 4-1 Detector filling parameters [Kyl02b]

	TEPC **A** (TE1.2 ser. no. 01)	TEPC **B** (TE1.2 ser. no. 02)
Gas	Propane based TE	Propane based TE
Filling date	2002-01-17	2001-05-09
$p_{filling}$ [kPa]	1.48 ± 0.01	1.46 ± 0.01
$m_{filling}$ [mg]	32.4 ± 0.2	32.4 ± 0.2
D/H(10)-response for p=1.5 kPa*	0.99	0.99

The principal set-up of the Sievert Instrument is shown in Fig. 4-3. The two TEPCs are supplied with high voltage up to 900 V, which is set by the user usually in the range of 600 V to 900 V. Both of the TEPCs can be controlled independently. The electric charge is determined every 100 ms from the voltage increase over a 1 nF capacitor in the electrometer. The data unit serves for saving the measured data in a main unit memory of 7.9 MB. The power is supplied by a lead battery, 12 V (12 Ah), of which up to 9 Ah are used. With two detectors, the operational time is restricted by the battery-charge to 18 h (= 9Ah/0,5A). It can be read out via an externally connected PC. A Geiger-Mueller tube, Philips ZP1201, is also included in the data unit box in order to give an independent estimate of gamma radiation dose.

The instrument determines absorbed dose, D, to detector gas and dose-average lineal energy, $\bar{y}_D$, from multiple-event measurements. The *W/e*-value in low LET fields is 26.8 eV and a value of 28 eV is used for mixed radiation fields. However, in monoenergetic fields a W/e-value of 30 eV is applied [Kyl01b, Kyl02a].

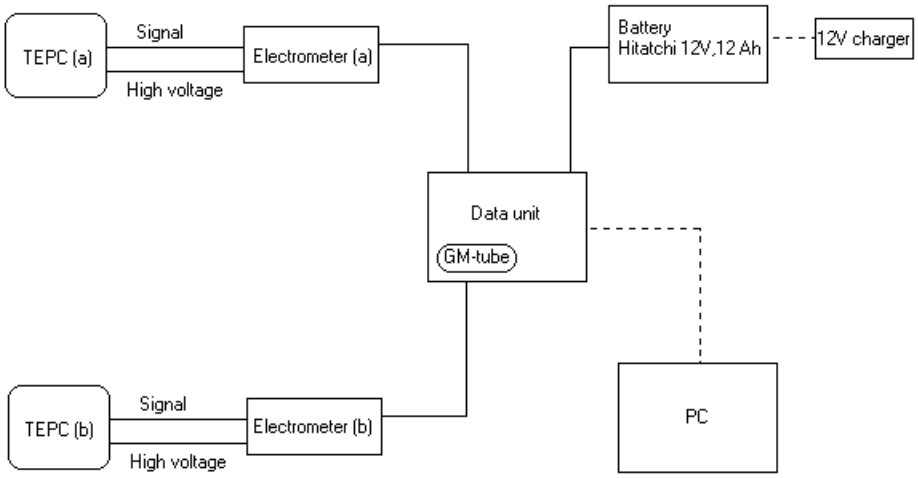

Fig. 4-3 Principle set-up of the Sievert Instrument. PC and the 12V charger are an independent unit, which can be connected with the Sievert Instrument. The figure is provided by Kyllönen [Kyl02b].

4.3 Detector status and calibrating

Calibrating and evaluating the parameters necessary for further measurements with the Sievert Instrument means to first determine the saturation current. For this purpose, one applies a positive detector voltage to avoid gas multiplication. Then, the gas-multiplication factors for different applied negative detector voltages have to be ascertained. Finally the mean lineal energy measured with the instrument in the calibration field has to be measured.

The detectors were calibrated on the 6th of June 2002 in the calibration laboratory of the Swedish Radiation Protection Institute SSI and on the 25th of July 2002 in the calibration laboratory of TIS-RP at CERN. We used a ^{137}Cs gamma field with $H^*(10)$ = 10.8 mSv/h at SSI at a detector-source distance r = 2.5 m. At CERN we varied the distance r from 1.1 to 2.5 m obtaining reference dose equivalent rates from 2.3 to 9.2 mSv/h. Irradiating at different distances served as a reproducibility check.

The saturation current I_{sat} was determined by measuring at two positive voltages (200 V and 400 V) on the detector walls, which is sufficient to calculate a correction factor for incomplete collection charge in an ionisation chamber according to IAEA recommendations [IAE00], and thus to calculate the saturation current of the detectors.

The gas amplification factor M was then determined as the ratio between the measured current at various negative voltages and the saturation current. The measured current was averaged over 100 measurement points at each dose rate. Furthermore the determined amplification factors were averaged over different dose rates. The statistical measurement uncertainty of M was calculated using common error propagation laws. The saturation currents and the gas multiplication factors for detector **A** are listed in Table A-1 and for detector **B** in Table A-2 in Appendix A. The average values for the working pressure, mass and multiplication factors, necessary for further evaluations in the calibration laboratory, the CERF-field and the PS-bridge, are presented in Table 4-2.

Table 4-2 Working parameters determined out of calibration measurements at the Swedish Radiation Protection Institute and at CERN. Detailed results are presented in the Appendix B.

	TEPC **A** (TE1.2 ser. no. 01)	TEPC **B** (TE1.2 ser. no. 02)
$p_{working}$ [kPa]	1.445 ± 0.3	1.378 ± 0.03
$m_{working}$ [kg]	(3.14 ± 0.62) E-05	(2.98 ± 0.59) E-05
M (200V)	2±0.1	2±0.1
M (300V)	3±0.1	4±0.1
M (400V)	7±0.2	9±0.3
M (500V)	17±0.5	22±0.6
M (600V)	41 ± 1	56 ± 2
M (700V)	106 ± 3	149 ± 4
M (800V)	274 ± 8	397 ± 11
M (900V)	752 ± 21	1080 ± 31
$\bar{y}_D$ [keV/µm]	1.647±0.024	1.703 ± 0.025

The measurement of the mean lineal energy $\bar{y}_D$ took place in the field of ^{137}Cs (source no. 3609) at five distances with dose equivalent rates ranging from 1 mSv/h to 7.6 mSv/h, in the field of ^{137}Cs (source no. 3740) at 517 µSv/h and in the field of ^{137}Cs (source no. 3739) at 59 µSv/h. At each distance the detector voltages were varied. For determining the mean lineal energy $\bar{y}_D$ an averaged energy required to produce an ion pair, *W/e,* of 26.8 J/C was used. The time constant of 0.1 s for measurements and evaluation was chosen. In Table 3-2 the $\bar{y}_D$-values averaged over all measurements and evaluated for a ^{137}Cs-field are presented. Again the detailed results for all measurements at different equivalent dose rates and different detector voltages are summarised in Table B-3 and Table B-4 in Appendix B. The measurements at different distances with the same source giving only small dose equivalent differences serve as reproducibility check. As linearity check measurements with different sources (having different activities) were carried out. The results of $\bar{y}_D$ are presented only with the statistical uncertainties. The slightly different $\bar{y}_D$-values between the two detectors are due to different internal gas pressures and hence simulated object sizes.

Kyllönen *et al.* [Kyl01a] established three $\bar{Q}_D(\bar{y}_D)$ relations for three mixed low LET and neutrons field categories shown in Table 4-3 and Fig. 4-4. The first of these is taken for fields with neutrons below a few MeV, the second for fields with neutrons of all energies,

and the third for neutrons above a few MeV. In addition in Table 4-3 one can find the calculated $\overline{Q}_D$-values and resulting calibration factors N for both detectors. The $\overline{Q}_D(\bar{y}_D)$ relations are illustrated in Fig. 4-4 together with the *H*(10)* responses between 32 keV and 1.25 MeV for these three relations in photon fields [Kyl01a, Kyl97].

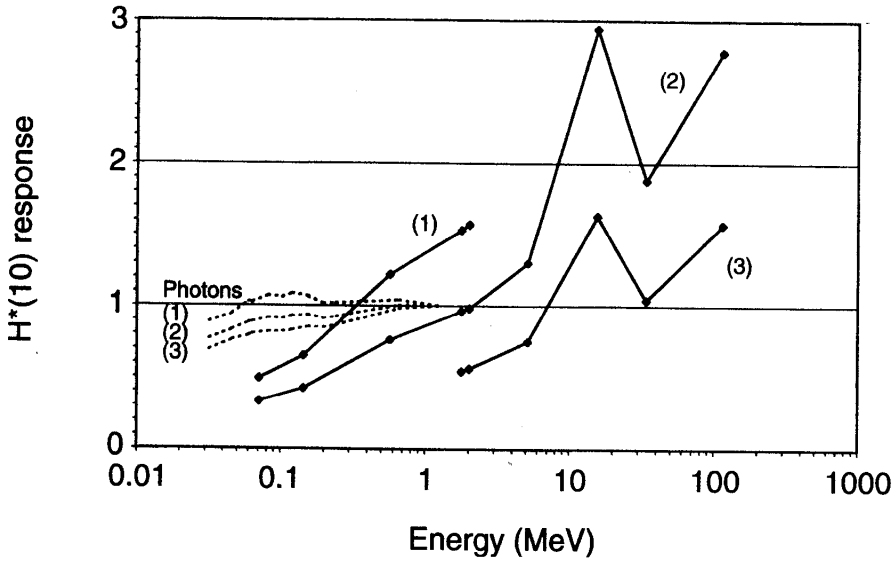

Fig. 4-4 *H*(10)* response in neutron fields between 71 keV and 115 MeV with different *Q(y)* relations. (1) $\overline{Q}_D = 0.52 + 0.28\bar{y}_D$; (2) $\overline{Q}_D = 0.73 + 0.17\bar{y}_D$; (3) $\overline{Q}_D = 0.88 + 0.09\bar{y}_D$. The H*(10) responses for the three relations in photon fields are also shown as dotted lines. The plot is taken from the work of Kyllönen *et al.* [Kyl01a].

Table 4-3 Three $\overline{Q}_D(\bar{y}_D)$ relations for mixed low LET and neutron fields taken from [Kyl01a] and the resulting $\overline{Q}_D(^{137}Cs)$ and calibration factor N from a ^{137}Cs field.

Neutrons	$\overline{Q}_D(\bar{y}_D)$	Detector **A** $\bar{y}_D = 1.647 \pm 0.084$		Detector **B** $\bar{y}_D = 1.703 \pm 0.079$	
		$\overline{Q}_D(^{137}Cs)$	N	$\overline{Q}_D(^{137}Cs)$	N
(1) below a few MeV	$\overline{Q}_D = 0.52 + 0.28\bar{y}_D$	0.98 ± 0.02	1.0295	1.00 ± 0.02	1.013
(2) of all energies	$\overline{Q}_D = 0.73 + 0.17\bar{y}_D$	1.01 ± 0.02	1.0001	1.02 ± 0.02	0.991
(3) above a few MeV	$\overline{Q}_D = 0.88 + 0.09\bar{y}_D$	1.03 ± 0.02	0.9824	1.03 ± 0.02	0.978

4.3.1 Reproducibility check with ^{137}Cs

The detectors were exposed to the radiation of a ^{137}Cs source at different distances. The main aim of the irradiations with ^{137}Cs was to check that measurements were reproducible with high accuracy even with different applied voltages. For that reason the response *H*/H*(10)* has been evaluated and is shown in Fig. 4-5 and 4-6. In this relative comparison no uncertainties are included. The detailed results of the measurements can be found in Appendix A, Table A-7 for detector **A** and Table A-8 for detector **B**. For evaluations of *H** a (*W/e*)-value of 26.8 J/C was taken. A time constant for measurements and evaluations of 0.1 s has been used. The uncertainty of the dose equivalent *H** is calculated from the quadratic sum of statistical uncertainty estimations for the absorbed dose (1%) and for the quality factor (1%), and from uncertainty considerations coming from other influences (source, distance, electrometer, etc.) of 5%.

It can be seen that in static fields with a dose equivalent rate from 60 µSv/h to 8 mSv/h different detector voltages do not affect the measurements.

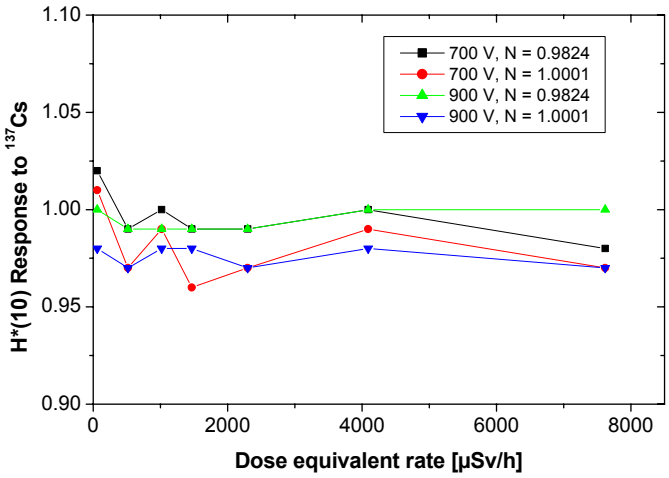

Fig. 4-5 *H*(10)* response to ^{137}Cs for different dose equivalent rates determined by detector **A**.

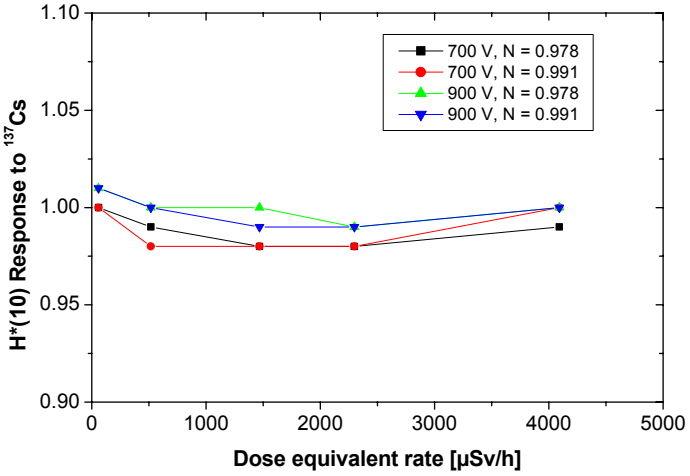

Fig. 4-6 *H*(10)* response to ^{137}Cs for different dose equivalent rates determined by detector **B**.

Chapter 5

Detectors for radiation monitoring

Here a brief description of the detectors used for monitoring and comparing results is given.

5.1 HANDI-TEPC

The Homburg Area Neutron DosImeter (HANDI) [Kun92] is a portable instrument based on a low-pressure tissue-equivalent proportional counter (TEPC) and electronics (Fig. 5-1). The spherical TEPC has a wall thickness of 0.15g/cm² and is filled with propane based tissue-equivalent gas simulating a tissue sphere with a diameter of 2 µm. Because of the low gas density, the homogeneity in the gas and the wall composition, the criteria for application of the Bragg-Gray principles are nearly fulfilled. The determination of the dose quantities and quality factors from the measurement of electrical charge in a TEPC have been summarised by Menzel *et al.* [Men89] in an intercomparison of microdosimetric dose equivalent meters. In order to facilitate the following discussions of this work the principles and relationships are reproduced.

The evaluation of absorbed dose, *D*, in the wall of a TEPC is done using the relation

$$D = \frac{W}{e} \cdot \frac{q_e}{m} \qquad (5.1)$$

where q_e is the charge produced in the cavity, *e* the electron charge. *W* is the (average) *W* value and *m* the mass of gas in the cavity.

Using pulse-height analysis usually calibrated in terms of lineal energy, $y = e/l$ (e the energy of each single event deposited in the cavity gas and l the cavity mean chord length), this instrument measures in real time absorbed dose in the dynamic range from 0.05 up to 1500 keV/µm by which the quality factor is determined [Lim97] according to relation

$$Q = \int_0^\infty q(y)d(y)dy \qquad (5.2)$$

where $d(y)$ is the probability density of absorbed dose in lineal energy y. The functions $q(y)$ are chosen to approximate $Q(L_\infty)$ by setting $y = L_\infty$. The pulse height distributions over lineal energy are often simply called microdosimetric spectra.

Total dose equivalent is then determined according to

$$H = Q \cdot D\,. \qquad (5.3)$$

At CERN the system is calibrated in a ^{60}Co gamma field in terms of absorbed dose. Note that for gamma radiation the quality factor is equal to 1 by definition and thus the absorbed dose is equal to the dose equivalent.

Fig. 5-1 HANDI-TEPC

5.2 High-pressure ionisation chambers IG5

High-pressure ionisation chambers are useful where information on spectral distribution is not required – e.g., for field measurements or as an inexpensive monitoring device.

At CERN two kinds of filling gases are in use: hydrogen (→ "**hydrogen chamber**") or argon (→ "**argon chamber**"). The chamber wall is a steel cylinder, to withstand the high pressure of about 2 MPa, and a gas volume of 5 litres extends between the two electrodes made from aluminium. The ionisation current is the sum of two components: a wall component due to ionisation of the gas by secondary electrons emerging from the wall, and a gas component due to secondaries originating in the gas. The chambers are manufactured by CENTRONIC, UK, and have a diameter of 185 mm and a length of 430 mm.

Argon-filled chambers manufactured for estimating dose equivalent from photons and charged particles in mixed fields, where neutrons have energies of less than approximately 5 MeV, as in the nuclear industry [Ott02]. Photons ionise the gas by secondary electrons and charged particles are detected by direct ionisation. Hydrogen-filled chambers provide the additional capability to detect neutrons. In nuclear industry, hydrogen-filled and argon-filled chambers are used as a "matched pair" with equal photon sensitivity to estimate the photon- and the neutron – component of a mixed field [Ott03]. Neutrons generate recoil protons in hydrogen, which in turn ionise the gas. The ionisation processes have different cross sections in gas than in tissue-equivalent material and therefore it cannot be expected that the high-pressure ionisation chambers indicate a quantity like ambient dose equivalent $H^*(10)$. The energy response of these chambers is in fact only poorly known: the documentation from the manufacturer states sensitivities as current per dose equivalent rate without defining the radiation energy or the measured quantity in case of photons. In hydrogen-filled chambers, a response curve is given for neutrons without stating if its origin is from experiment or from theoretical considerations. The first attempt to characterise these chambers was done by Otto [Ott02]. He calculated the response functions to neutrons and photons with the Monte Carlo simulation program FLUKA [Fas93, Fas97a, Fas97b] (see Fig.5-2 and 5-3).

High-pressure chambers are generally used to measure very low dose rates and then general recombination is negligible. However, in the case of repetitive pulsed radiation the amount of general recombination may be considerable. Here we face the problem, that no data about the general recombination in these chambers is available.

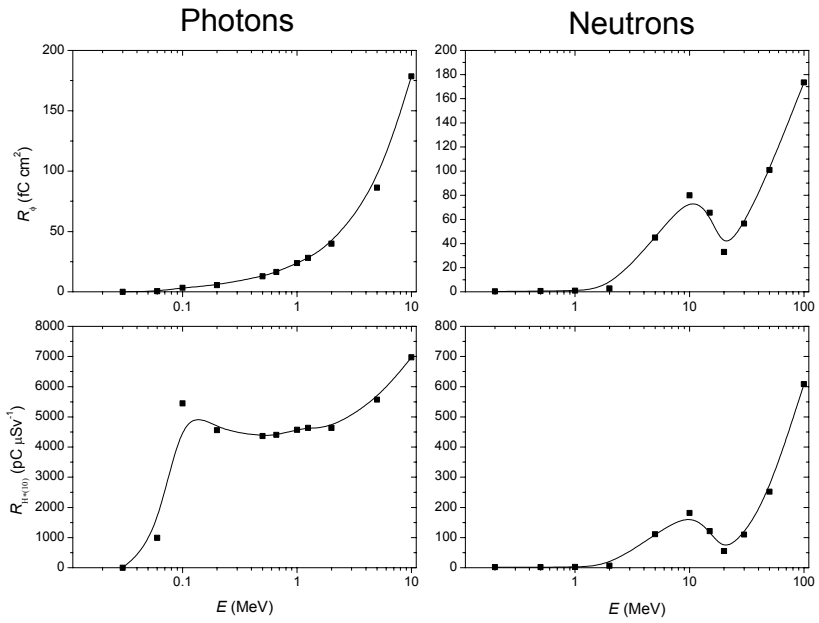

Fig. 5-2 Calculated response of the argon-filled IG5-chambers to photons and to neutrons by Otto [Ott02]. The top row shows the fluence response, the bottom row shows the response to ambient dose equivalent *H*(10).* The lines indicate the trend only.

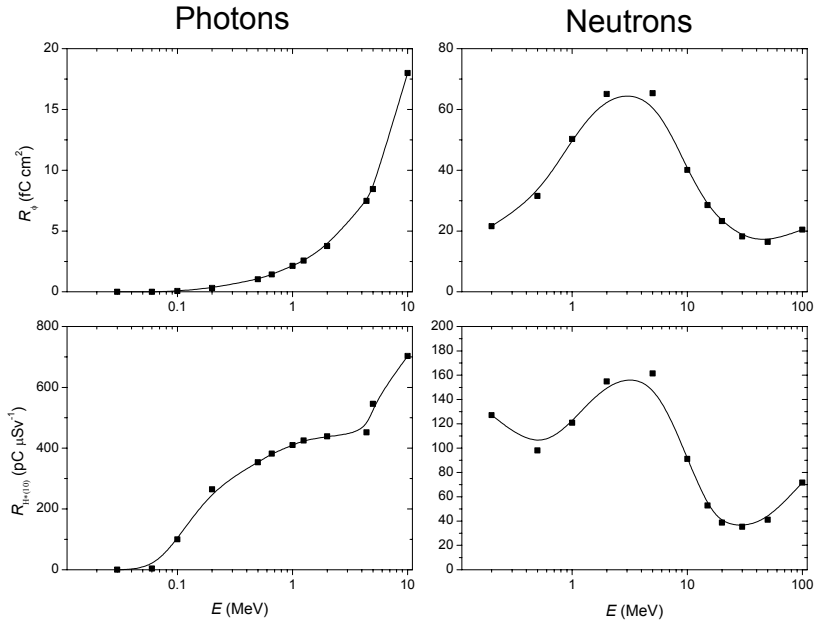

Fig. 5-3 Calculated response of the hydrogen-filled IG5-chambers to photons and to neutrons by Otto [Ott02]. The top row shows the fluence response, the bottom row shows the response to ambient dose equivalent *H*(10).* The lines indicate the trend only.

5.3 High –pressure graphite ionisation chamber of type G5 chamber

The high-pressure G5 type graphite ionisation chamber used in this work was designed and constructed in the Institute of Atomic Energy (IAE) in Swierk, Poland [Gol96a]. The chamber is 115 mm long and 18 mm in diameter (see Fig. 5-4). The distance between the electrodes is 2 mm. It is enclosed in a 0.3 mm thick aluminium envelope and is filled with carbon dioxide up to a pressure of 2.8 MPa. The chamber was used as a "neutron insensitive" detector for neutrons with an energy up to approximately 10 MeV. In such chambers, especially when they are operated at relatively low collecting voltages, the recombination of ions in tracks of high-LET particles is considerably higher than in tracks of low-LET particles. As the result, the relative neutron sensitivity of the chambers is below 3% for neutrons of energies up to 15 MeV provided that the electrical field strength in the chamber cavity does not exceed 200 V/cm [Gol96a]. The chamber can be used for measurements of photon dose rates from 0.5 mGy/h up to 500 Gy/h.

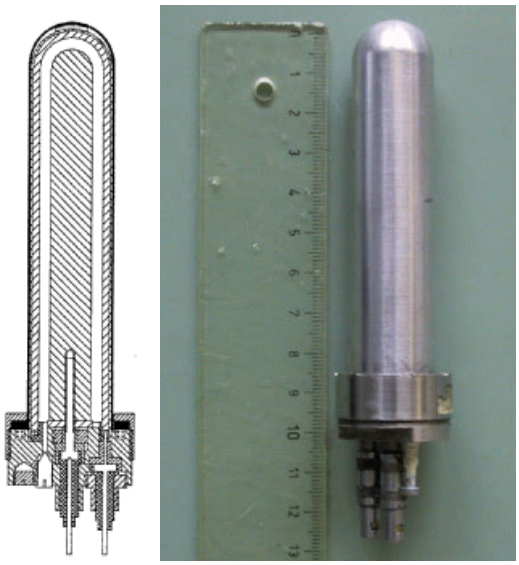

Fig. 5-4 High –pressure graphite ionisation chamber of type G5 chamber, constructed in the Institute of Atomic Energy (IAE) in Swierk, Poland.

5.4 Rem counter EG&G Berthold LB6411

The rem counter of type EG&G Berthold LB6411 contains a ^{3}He proportional counter as thermal neutron detector in the centre of a moderator with a diameter of 25 cm. The proportional counter is sensitive for thermal neutrons and provides an excellent discrimination against gamma radiation. The neutron dose equivalent rate is measured with approximately correct *H*(10)*-response in the energy range from 0.015 eV to 20 MeV [Ott03].

5.5 RIC chamber

The ionisation chamber type RIC (REM Ionisation Chamber) manufactured by CENTRONIC is a portable survey instrument designed for radiation protection service. As detector a BF_3-filled ionisation chamber in a polyethylene moderator of 215 mm thickness is exploited. The advantage of an ionisation chamber compared to a counter is that it shows no dead time effects in pulsed radiation fields. The main disadvantage lies in the lack of discrimination between neutron and gamma radiation. The neutron dose equivalent rate is measured with approximately correct *H*(10)*-response in the energy range from 0.015 eV to 15 MeV [Ott03].

Chapter 6

Measurements in the fields of reference sources

Radioactive sources are frequently used for the calibration of dosimeters, e.g. ^{60}Co or ^{137}Cs sources for photon dosimeters and ^{252}Cf , ^{238}Pu-Be or ^{241}Am-Be sources for neutron dosimeters, since they can provide stable and reproducible calibration conditions. Calibration is the process in which the calibration factor (quotient of conventionally true value by the indicated value) of a dosimeter is determined in a reference radiation field of well-known ambient dose equivalent under well-specified calibration conditions [NCR91].

The calibration laboratory at CERN is equipped with a number of radioactive sources installed in motorized calibration benches and small, transportable, point-like sources. The permanently installed sources used in this work are listed in Table 6-1. For the small ^{241}Am-Be and ^{241}Am sources only a limited database of the calibration laboratory is available, shown in Table 6-2.

Table 6-1 Radioisotope sources at CERN's calibration laboratory [Ott99]. The sources listed are fix-installed in the laboratory.

Radio nuclide	Source no.	Mean energy	Activity (1.1.1999)	$\dot{H}^*(10)$ (d = 2 m; 1.1.1999)
^{137}Cs	3609	662 keV	102.11 GBq	2.45 mSv/h
^{137}Cs	3740	662 keV	14.18 GBq	345 µSv/h
^{137}Cs	3739	662 keV	1.75 GBq	41.5 µSv/h
^{60}Co	1665	1250 keV	21.60 GBq	1.98 mSv/h
^{238}Pu-Be	1120	4.5 MeV	1.85 TBq	364 mSv/h

Table 6-2 Transportable radioisotope sources used in this work, which are available in the calibration laboratory.

Source no.	Mean energy	Activity (1.1.2001)	$\dot{H}^*(10)$ (d = 0.5 m; 1.1.2001)
^{241}AmBe (474)	4.3 MeV	not provided	not provided
^{241}Am (3724)	60 keV	3.8 GBq	45.97 µSv/h

6.1 The ^{238}Pu-Be source

The ^{238}Pu-Be radionuclide source in the TIS-RP-calibration laboratory is used as secondary standard for calibrating neutron detectors and dosimeters. The source is mounted on an automatic calibration bench. It is located behind a 40 cm thick concrete shielding wall with a window of 40 x 40 cm². It has a neutron emission of approximately 10^8 1/s [Ott99] whose mean energy is 4.5 MeV. The activity is 1.81 TBq and the half-life of the source is 87.7 years. In Table 6-3 the characteristics of the actinide ^{238}Pu are presented.

The neutron spectrum of ^{238}Pu-Be is similar to the one of ^{241}Am-Be, the source recommended in ISO standard 8529-1 [ISO01]. The advantage of the ^{238}Pu-Be source is its higher neutron fluence for the same source mass, allowing a more compact design of the source and the significantly smaller contribution of photons to the radiation field. The emission of the source can be traced back to international standards by the use of a transfer instrument, a moderated neutron detector (rem counter) of type EG&G Berthold LB6411 [Ott98].

The total emission of the source contains a component of photons due to decay processes and is accompanied by neutron scattering. Neutrons are scattered from the walls, ceiling, and floor of the room and from the air in the room. They are also scattered from extraneous objects in the room. Until now the photon component of the source and the scattering component are not quantified and so the quality factor of the ^{238}Pu-Be field is only estimated. For this reason more detailed information about the ^{238}Pu-Be source in the laboratory by means of investigations with several detectors is desirable.

In case of determining the photon contribution of the ^{238}Pu-Be source one possible method is the measurement of count rates as a function of distance between source and detector [Nac72]. This was done with two different chambers, an argon chamber (type IG5) and a graphite chamber (type G5) [May02e, May02f].

Table 6-3 αβγ-Table [Wah01] of Plutonium Isotope ^{238}Pu .
* γ-emission (absolute intensity per 100 decays and in equilibrium); ** α-, β-decay (intensity per 100 decays) ∑ 100%; *** spontaneous fission

Isotope $t_{1/2}$	Decay E in MeV	Branch intensity** in %	Production Daughter-nuclide & Eγ	E-list in I-order in keV	γ-& X-intens.* in %
	Q_α=5.59320				
^{238}Pu	→ α: 5.49903	70.91	→^{234}U (2.445*105y)		
	→ α: 5.4563	28.98	→ γ: 43.498^{int,E2}	43.50	0.00395
	→ α: 5.3577	0.105	→ γ: 99.853^{int,E2}, 43.50	99.85	0.00735
	→ α: 5.2056	0.0030	→ γ: 152.720^{E2}, 99.85,43.50	152.72	0.000937
			→ X: L_β	17.069	5.2
			→ X: L_α	13.600	4.2
			→ X: L_γ	20.366	1.15
			→ X: L_l	11.620	0.25
			→ X: L_η	15.400	0.102
87.7(3)y	→ sf:***	1.85E-10			
int=^{241}Am (43.42, 0.073%), ^{241}Pu (44.20, 0.17%)					
int=^{228}Ac(99.51, 1.26%)					

A more complicated method, which allows determining the low and high LET components in a mixed radiation field, is based on the analysis of saturation curves measured with a recombination chamber REM-2. Furthermore this method delivers information about the average quality factor of this field.

6.1.1 Information obtained from the count rate at different distances from the source

The count rate (dimension: s^{-1}) for a point source in a scattering environment can be expressed as

$$\dot{A}(r) = a + \frac{b}{r^2} \qquad (6.1)$$

where the heuristic parameter a (s^{-1}) describes the count rate caused by indirect (i.e. scattered neutrons and photons produced in (n,γ)-reactions in hydrogenous materials) component, while b (m^2s^{-1}) is a characteristic detector constant which, according to the inverse square distance law, is given by the relation

$$b = \frac{QS}{4\pi} \tag{6.2}$$

where Q (s^{-1}) is the source strength (the source should be isotropic), and S (m^2) the detector sensitivity.

Assuming that the two parameters a and b in equation (6.1) are constants, they are obtained from measurements at more than three points applying a least-squares fit. The absolute value of the quantity a strongly depends on the scattering geometry, but is assumed to be constant over the distance (source-detector) from 50 to 200 cm in which the detector is moved. This is a reasonable assumption when the radiation comes from a point source and the nearest significant scattering object is at least a few meters away from the detector. The quotient a/b can be used as a measure of the importance of scattered radiation. The smaller this ratio the smaller the scatter level in the location of the measurement.

6.1.2 Determination of the photon-contribution using a graphite chamber of G5 type

Measurements were performed with a high-pressure graphite ionisation chamber of G5 type (serial number 8), where the chamber was moved on a support (see Fig. 6-1) to several distances in order to obtain the results for the distance law in the field of ^{238}Pu-Be source. For collecting the charge a PTW-UNIDOS electrometer [PTW98] in charge mode was used. As a working voltage –20 V was chosen. A Keithley 197 multimeter monitored the applied voltage. Prior to the measurements the calibration of the chamber has taken place in the field of a ^{137}Cs source (see Appendix B). A calibration factor of –(1,31±0.05) pC/μSv was found.

Measurements were performed in steps of 0.1 m at distances r from 0.8 m to 1.4 m. At every distance, five charge measurements were made. Before every measurement, any parasitic currents in the measurement system were compensated with the appropriate command of the electrometer.

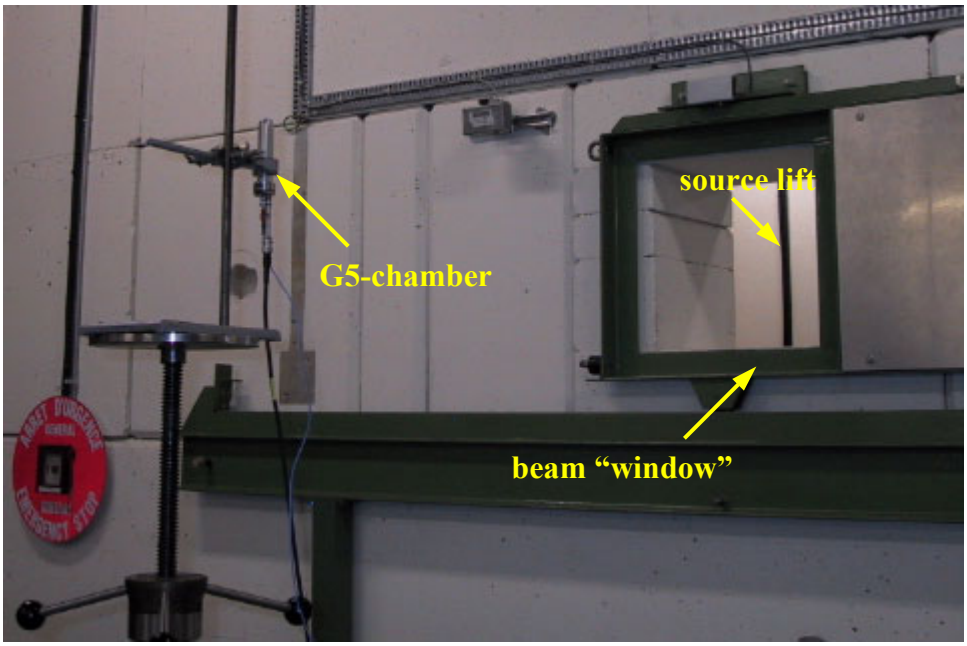

Fig. 6-1 G5 chamber mounted on a support in front of the beam "window".

In Fig. 6-2 the product of the charge with the square of the source-detector distance, r, is plotted over r^2. The trend line $y=ax+b$ of this presentation easily delivers the parameters a and b, because

$$\dot{A}(r) = a + \frac{b}{r^2} \tag{6.3}$$

$$\dot{A}(x) \cdot r^2 = a \cdot r^2 + b \tag{6.4}$$

From the figure, we obtained the contribution of direct radiation (originating predominantly from the ^{238}Pu-Be source) b= –(48.2±2.5) pC/h. Applying the calibration factor of –(1.31±0.05) pC/µSv and considering the measurement uncertainties (see Appendix C), the photon-contribution of the source is (36.8±2.8) µSv/h.

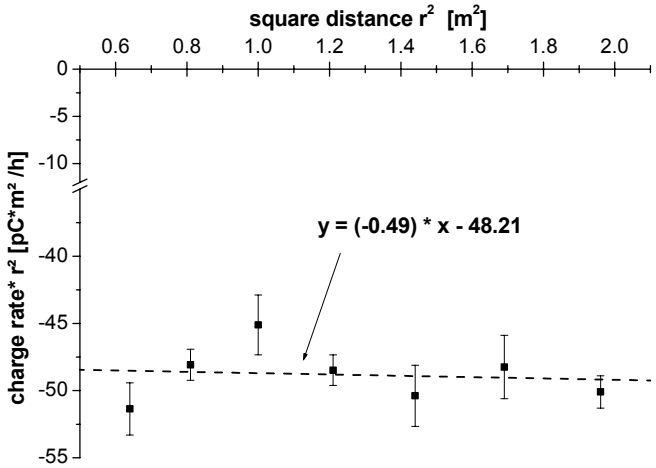

Fig. 6-2 Product of charge rate and distance (detector-source) as a function of the square distance measured with the G5-chamber. The interception value in combination with the calibration factor delivers the photon-contribution of the ^{238}Pu-Be source.

6.1.3 Determination of the photon-contribution using an argon-filled chamber IG5

In multiples of 25 cm, at each distance from the ^{238}Pu-Be source 10 measurements over 200 s were made with the argon chamber, using the automatic data acquisition program in the calibration laboratory. Uncertainties were obtained from the standard deviation in these 10 measurements and additionally an overall uncertainty of 5% related to several other uncertainty influences (i.e. distance, source, data acquisition system, etc) was added. The calibration factor of (300±15) μSv^{-1} was obtained before in a reference ^{137}Cs field.

After setting a trend line over the plotted data in Fig. 6-3 we obtained a value of the axis intercept of (11650±50) cts/h. Applying the calibration factor leads to a dose equivalent H*(10)= 38.7±1.9 µSv/h.

The calculation of the quotient *a/b* gives 0.010 for the G5-chamber and 0.014 for the IG5-chamber. The slightly higher scatter level for the argon-filled chamber could be explained by the fact that these measurements were done at higher distances from the source. At higher distances the scatter becomes progressively more important.

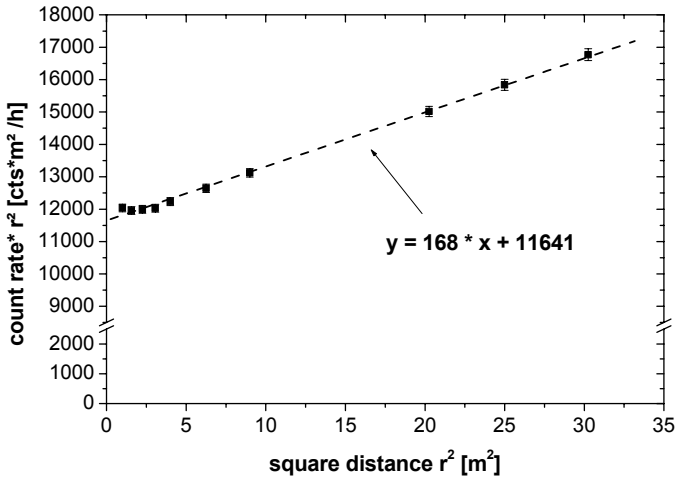

Fig. 6-3 Product of charge rate and distance (detector-source) as a function of the square distance measured with the argon chamber IG5. The interception value in combination with the calibration factor delivers the photon-contribution of the ^{238}Pu-Be source. At distances $r^2 < 2.5$ the measurements have a similar trend to measurements with the chamber G5.

6.1.4 Determination of the photon-contribution with the REM-2 chamber

Complete saturation curves were obtained for the recombination chamber REM-2 (No. 027), in a reference γ field from a ^{137}Cs source, by applying a succession of voltages in the range from 8 to 1300 V and measuring the charge collected over 100 s. The chamber was positioned in a distance of 2.17 m with a dose rate of 2 mGy/h. A variable high voltage power supply was used to polarise the chambers and the voltage was read from a digital voltmeter KEITHLEY 167 in the range from 5-1000 V and from the dial on the power supply between 1000 and 1300 V, which was out of the range of the voltmeter. The collected charge q was measured using a PTW-UNIDOS electrometer connected to the chamber using electrometrical cables. In this procedure a calibration factor of K=348.9 μC/Gy was found. Since former response of REM-2 chambers to ambient dose equivalent investigations showed that the used gas filling - a mixture of methane and nitrogen - causes a slightly higher sensitivity to neutrons up to 5 MeV, the calibration factor was

corrected to the response from ^{238}Pu-Be using a correction factor of 1.18 [Gol96a]. This delivered a corrected calibration factor of K_{corr} = 411.4 µC/Gy.

This operating sequence was repeated for the field of the ^{238}Pu-Be source at a distance of 2.18 ± 0.01 m, and a reference neutron dose rate of 300 µSv/h. The saturation curve measured in the ^{238}Pu-Be field is shown together with the saturation curve measured in the reference ^{137}Cs field in Fig. 6-4. One can clearly see a faster decrease of the ^{238}Pu-Be saturation curve in ion collection efficiency with decreasing voltage due to higher recombination. After plotting f_{mix} against f_γ (Fig. 6-5), equation (3-7) was fitted to the graph using a MATLAB procedure [Gol02]. The recombination method delivered a photon contribution of $\mathcal{D}_{low}$ = 17.46±0.87% to absorbed dose for the ^{238}Pu-Be source. For the photon contribution a standard uncertainty of 5% was assumed derived from the experience with the behaviour of the instrument. Here, the scattered photon contribution is neglected, since it is very small as demonstrated in the measurements mentioned before. This gives an equivalent dose rate of H^*_{photon}= (39.90±2.79) µSv/ h in 1 m distance from the source within the given geometry including scattering photons. In addition the quality factor for the ^{238}Pu-Be source was determined to Q = 8.6±0.4 by means of analysis with the fitting procedure.

The Table 6-4 presents the very good agreement between the different detectors used to determine the photon contribution of the ^{238}Pu-Be source in 1 m distance.

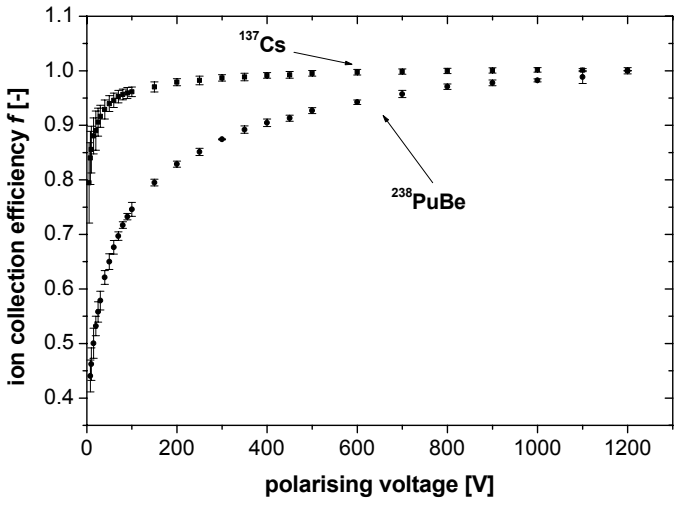

Fig. 6-4 Saturation curves determined with a recombination chamber REM-2 in the field of a ^{137}Cs source and a ^{238}Pu-Be source.

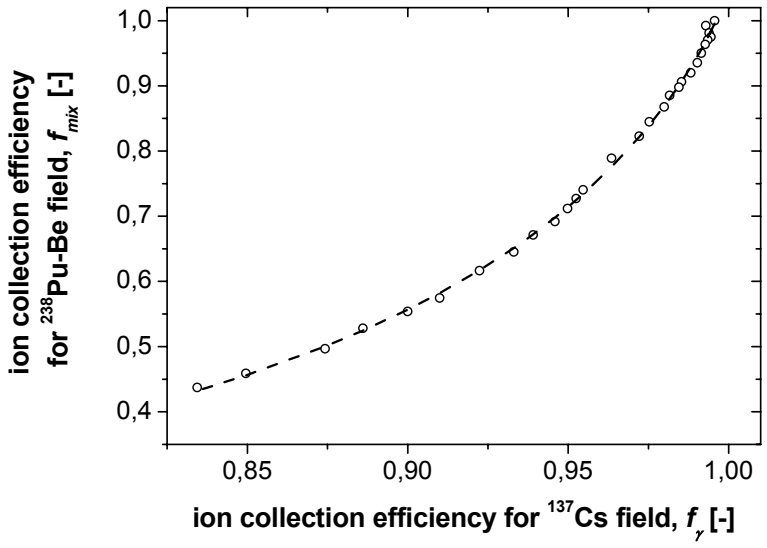

Fig. 6-5 The same experimental points as in Fig. 6-4, but f_{mix} is plotted as a function of f_γ.

Table 6-4 Photon-contribution in 1m distance from the ^{238}Pu-Be source given for different detectors.

Detector	Graphite Chamber G5	Argon Chamber IG5	Recombi. Chamber REM-2
Photon Contribution $H^*(10)_{photon}$ [µSv/h]	36.8±2.76	38.73±1.94	39.90±2.79

6.1.5 Measurements with the Sievert Instrument in the ^{238}Pu-Be field

Measurements were performed in several distances in the field of the ^{238}Pu-Be radionuclide source with the Sievert Instrument. The evaluations were carried out first with a (*W/e*)-value of 30 J/C recommended for fields dominated by neutrons and then with a (*W/e*)-value of 28 J/C recommended for mixed radiation fields [Kyl01b, Kyl02]. The Sievert Instrument measures the total dose equivalent. However, in the calibration laboratory there are given only reference ambient dose equivalents for the neutron component determined by a moderated neutron detector (transfer instrument) [Ott99]. For comparing the dose equivalents, we subtracted the photon contribution, which was determined above with three independent detectors, from the total dose equivalents measured by the Sievert Instrument in this geometry. We evaluated the difference between the neutron dose equivalents, D_{iff}, taking the relation $\overline{Q}_D = 0.73 + 0.17\overline{y}_D$ (usually for fields with neutrons of all energies ;Table 6-5, Table 6-7, Table 6-9, Table 6-11) and the relation $\overline{Q}_D = 0.88 + 0.09\overline{y}_D$, (usually for fields dominated of neutrons above a few MeV; Table 6-6, Table 6-8, Table 6-10, Table 6-12). In addition the dose equivalents were measured at different detector voltages.

Table 6-5 Detector A: Measurements in the field of ^{238}Pu-Be. A (*W/e*)-value of **30 J/C** is chosen. For determining the total dose equivalent *H** with the Sievert Instrument the relation $\overline{Q}_D = 0.73 + 0.17\overline{y}_D$ was taken.

Distance [m]	Voltage [V]	$\overline{y}_D$ [keV/µm]	Q	D [µGy/h]	H^* [µSv/h]	$H^*(10)_{photon}$ [µSv/h]	$H^*(10)_{neutron}$ [µSv/h]	D_{iff} [%]
1.1	700	51.7±2.6	9.5±0.4	165.5±3.3	1574.4±211.8	30.6±2.2	1230.6±36.9	25.4
	900	52.3±2.6	9.6±0.4	166.3±3.3	1600.8±215.4			27.6
1.5	700	51.2±2.6	9.4±0.4	88.4±1.8	833.7±112.2	17.8±0.9	635.9±19.1	34.9
	900	52.7±2.6	9.7±0.4	87.3±1.7	845.7±113.8			36.8
2	700	54.4±2.7	10.0±0.4	48.1±1.0	479.8±64.5	10.2±0.5	353.6±10.6	32.8
	900	56.4±2.8	10.3±0.4	48.8±1.0	503.0±67.7			39.4
2.5	600	57.5±2.9	10.5±0.4	30.3±0.6	318.1±42.8	6.7±0.3	227.9±6.8	36.7
	700	49.8±2.5	9.2±0.4	30.4±0.6	279.4±37.6			19.7
	800	48.0±2.4	8.9±0.4	29.7±0.6	264.0±35.5			12.9
	900	51.4±2.6	9.5±0.4	30.9±0.6	292.8±39.4			25.5

Table 6-6 Detector A: Measurements in the field of ^{238}Pu-Be. A (*W/e*)-value of **30 J/C** is chosen. For determining the total dose equivalent *H** with the Sievert Instrument, the relation $\overline{Q}_D = 0.88 + 0.09\bar{y}_D$ was taken.

Distance [m]	Voltage [V]	$\bar{y}_D$ [keV/µm]	Q	D [µGy/h]	H^* [µSv/h]	$H^*(10)_{photon}$ [µSv/h]	$H^*(10)_{neutron}$ [µSv/h]	D_{iff} [%]
1.1	700	51.7±2.6	5.4±0.2	165.5±3.3	898.6±120.9	30.6±2.2	1230.6±36.9	-29.5
	900	52.3±2.6	5.5±0.2	166.3±3.3	912.7±122.8			-28.3
1.5	700	51.2±2.6	5.4±0.2	88.4±1.8	476.2±64.1	17.8±0.9	635.9±19.1	-27.9
	900	52.7±2.6	5.5±0.2	87.3±1.7	481.9±64.8			-22.0
2	700	54.4±2.7	5.7±0.2	48.1±1.0	272.7±36.7	10.2±0.5	353.6±10.6	-25.8
	900	56.4±2.8	5.8±0.2	48.8±1.0	285.1±38.4			-22.2
2.5	600	57.5±2.9	5.9±0.2	30.3±0.6	180.1±24.2	6.7±0.3	227.9±6.8	-23.9
	700	49.8±2.5	5.3±0.2	30.4±0.6	159.9±21.5			-32.7
	800	48.0±2.4	5.1±0.2	29.7±0.6	151.7±20.4			-36.4
	900	51.4±2.6	5.4±0.2	30.9±0.6	167.2±22.5			-29.6

Table 6-7 Detector A: Measurements in the field of ^{238}Pu-Be. A (*W/e*)-value of **28 J/C** is chosen. For determining the total dose equivalent *H** with the Sievert Instrument, the relation $\overline{Q}_D = 0.73 + 0.17\bar{y}_D$ was taken.

Distance [m]	Voltage [V]	$\bar{y}_D$ [keV/µm]	Q	D [µGy/h]	H^* [µSv/h]	$H^*(10)_{photon}$ [µSv/h]	$H^*(10)_{neutron}$ [µSv/h]	D_{iff} [%]
1.1	700	48.2±2.4	8.9±0.4	154.5±3.1	1379.0±185.5	30.6±2.2	1230.6±36.9	9.6
	900	48.8±2.4	9.0±0.4	155.2±3.1	1402.0±188.6			11.4
1.5	700	47.8±2.4	8.9±0.4	82.5±1.7	730.3±98.2	17.8±0.9	635.9±19.1	18.1
	900	49.2±2.5	9.1±0.4	81.5±1.6	740.6±99.6			19.8
2	700	50.8±2.5	9.4±0.4	44.9±0.9	420.1±56.5	10.2±0.5	353.6±10.6	15.9
	900	52.6±2.6	9.7±0.4	45.5±0.9	440.4±59.3			21.7
2.5	600	53.6±2.7	9.8±0.4	28.3±0.6	278.5±37.5	6.7±0.3	227.9±6.8	19.3
	700	46.4±2.3	8.6±0.3	28.4±0.6	244.7±32.9			4.5
	800	44.8±2.2	8.3±0.3	27.7±0.6	231.4±31.1			-1.4
	900	48.0±2.4	8.9±0.4	28.9±0.6	256.4±34.5			-9.6

Table 6-8 Detector A: Measurements in the field of ^{238}Pu-Be. A (*W/e*)-value of **28 J/C** is chosen. For determining the total dose equivalent *H** with the Sievert Instrument, the relation $\overline{Q}_D = 0.88 + 0.09\overline{y}_D$ was taken.

Distance [m]	Voltage [V]	$\overline{y}_D$ [keV/µm]	Q	D [µGy/h]	H^* [µSv/h]	$H^*(10)_{photon}$ [µSv/h]	$H^*(10)_{neutron}$ [µSv/h]	D_{iff} [%]
1.1	700	48.2±2.4	5.1±0.2	154.5±3.1	792.0±106.6	30.6±2.2	1230.6±36.9	-38.1
	900	48.8±2.4	5.2±0.2	155.2±3.1	804.3±108.2			-37.1
1.5	700	47.8±2.4	5.1±0.2	82.5±1.7	419.8±56.5	17.8±0.9	635.9±19.1	-36.8
	900	49.2±2.5	5.2±0.2	81.5±1.6	424.7±57.1			-31.3
2	700	50.8±2.5	5.4±0.2	44.9±0.9	240.2±32.3	10.2±0.5	353.6±10.6	-34.9
	900	52.6±2.6	5.5±0.2	45.5±0.9	251.1±33.8			-31.9
2.5	600	53.6±2.7	5.6±0.2	28.3±0.6	158.5±21.3	6.7±0.3	227.9±6.8	-33.4
	700	46.4±2.3	5.0±0.2	28.4±0.6	141.0±19.0			-41.0
	800	44.8±2.2	4.8±0.2	27.7±0.6	133.8±18.0			-44.2
	900	48.0±2.4	5.1±0.2	28.9±0.6	147.3±19.8			-38.2

Table 6-9 Detector B: Measurements in the field of ^{238}Pu-Be. A (*W/e*)-value of **30 J/C** is chosen. For determining the total dose equivalent *H** with the Sievert Instrument, the relation $\overline{Q}_D = 0.73 + 0.17\overline{y}_D$ was taken.

Distance [m]	Voltage [V]	$\overline{y}_D$ [keV/µm]	Q	D [µGy/h]	H^* [µSv/h]	$H^*(10)_{photon}$ [µSv/h]	$H^*(10)_{neutron}$ [µSv/h]	D_{iff} [%]
1.5	700	50.0±2.5	9.2±0.4	86.2±1.7	789.5±106.2	17.8±0.9	635.9±19.1	21.4
	900	55.5±2.8	10.1±0.4	87.1±1.7	877.0±118.0			35.1
2	700	54.6±2.7	9.9±0.4	47.8±1.0	474.1±63.8	10.2±0.5	353.6±10.6	31.2
	900	53.5±2.7	9.7±0.4	48.7±1.0	474.4±63.8			31.3
2.5	700	53.7±2.7	9.8±0.4	30.6±0.6	298.7±40.2	6.7±0.3	227.9±6.8	28.2
	900	52.8±2.6	9.6±0.4	31.4±0.6	301.8±40.6			29.5

Table 6-10 Detector B: Measurements in the field of ^{238}Pu-Be. A (*W/e*)-value of **30 J/C** is chosen. For determining the total dose equivalent *H** with the Sievert Instrument, the relation $\overline{Q}_D = 0.88 + 0.09\overline{y}_D$ was taken.

Distance [m]	Voltage [V]	$\overline{y}_D$ [keV/µm]	Q	D [µGy/h]	H^* [µSv/h]	$H^*(10)_{photon}$ [µSv/h]	$H^*(10)_{neutron}$ [µSv/h]	D_{iff} [%]
1.5	700	50.0±2.5	5.3±0.2	86.2±1.7	454.1±61.1	17.8±0.9	635.9±19.1	-31.4
	900	55.5±2.8	5.7±0.2	87.1±1.7	500.2±67.3			-24.1
2	700	54.6±2.7	5.7±0.2	47.8±1.0	270.8±36.4	10.2±0.5	353.6±10.6	-26.3
	900	53.5±2.7	5.6±0.2	48.7±1.0	271.4±36.5			-26.1
2.5	700	53.7±2.7	5.6±0.2	30.6±0.6	170.8±23.0	6.7±0.3	227.9±6.8	-28.0
	900	52.8±2.6	5.5±0.2	31.4±0.6	172.8±23.3			-27.1

Table 6-11 Detector B: Measurements in the field of ^{238}Pu-Be. A (*W/e*)-value of **28 J/C** is chosen. For determining the total dose equivalent *H** with the Sievert Instrument, the relation $\overline{Q}_D = 0.73 + 0.17\overline{y}_D$ was taken.

Distance [m]	Voltage [V]	$\overline{y}_D$ [keV/µm]	Q	D [µGy/h]	H^* [µSv/h]	$H^*(10)_{photon}$ [µSv/h]	$H^*(10)_{neutron}$ [µSv/h]	D_{iff} [%]
1.5	700	46.7±2.3	8.6±0.4	80.5±1.6	691.7±93.1	17.8±0.9	635.9±19.1	6.0
	900	51.8±2.6	9.4±0.4	81.3±1.6	767.9±103.3			18.0
2	700	51.0±2.5	9.3±0.4	44.6±0.9	415.1±55.9	10.2±0.5	353.6±10.6	14.5
	900	49.9±2.5	9.1±0.4	45.5±0.9	415.5±55.9			14.6
2.5	700	50.1±2.5	9.2±0.4	28.5±0.6	261.6±35.2	6.7±0.3	227.9±6.8	11.9
	900	49.3±2.5	9.0±0.4	29.3±0.6	264.3±35.6			13.1

Table 6-12 Detector B: Measurements in the field of ^{238}Pu-Be. A (*W/e*)-value of **28 J/C** is chosen. For determining the total dose equivalent *H** with the Sievert Instrument, the relation $\overline{Q}_D = 0.88 + 0.09\overline{y}_D$ was taken.

Distance [m]	Voltage [V]	$\overline{y}_D$ [keV/µm]	Q	D [µGy/h]	H^* [µSv/h]	$H^*(10)_{photon}$ [µSv/h]	$H^*(10)_{neutron}$ [µSv/h]	D_{iff} [%]
1.5	700	46.7±2.3	5.0±0.2	80.5±1.6	400.2±53.8	17.8±0.9	635.9±19.1	-39.9
	900	51.8±2.6	5.4±0.2	81.3±1.6	440.4±59.3			-33.5
2	0.978	700	51.0±2.5	5.3±0.2	44.6±0.9	10.2±0.5	353.6±10.6	-35.5
		900	49.9±2.5	5.3±0.2	45.5±0.9			-35.3
2.5	0.978	700	50.1±2.5	5.3±0.2	28.5±0.6	6.7±0.3	227.9±6.8	-36.9
		900	49.3±2.5	5.2±0.2	29.3±0.6			-36.1

Investigations with a recombination chamber in the field of the ^{238}Pu-Be source delivered an estimation for its quality factor of 8.62 ± 0.43 [May02d, May02e]. As it can be seen from the tables, if the relation for "neutrons of all energies ($\overline{Q}_D = 0.73 + 0.17\overline{y}_D$)" is taken, the resulting quality factor is slightly higher than expected. The relation for "neutrons above a few MeV ($\overline{Q}_D = 0.88 + 0.09\overline{y}_D$)" underestimates the quality factor. Using the simple retrograde calculation by dividing the reference ambient dose equivalent for neutrons plus the photon dose equivalent by the measured absorbed dose, results in a quality factor of about 8.2 by taking a (*W/e*)-value of 28 J/C, which is in good agreement within measurement uncertainties with the value determined by the recombination chamber. Evaluations with a (*W/e*)=30 J/C, which was taken by Kyllönen [Kyl01b] for investigations with monoenergetic neutrons, turned out to be too high. The tables demonstrate that a value of (*W/e*)=28 J/C recommended for mixed radiation fields gives better agreement within measurement uncertainties. An explanation for that could be that the field of the ^{238}Pu-Be source has a non-negligible contribution of photon radiation.

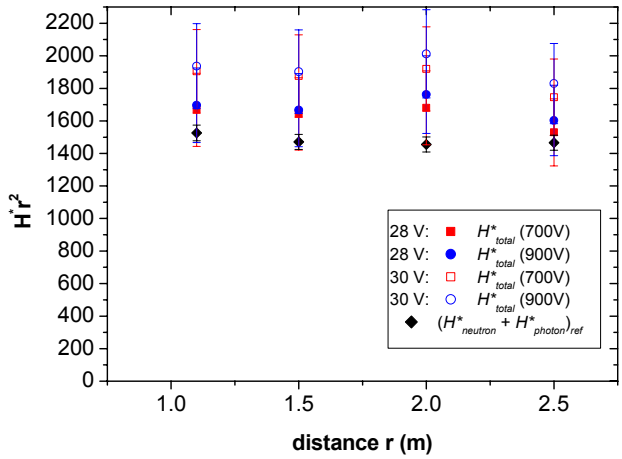

Fig. 6-6 Dose equivalent multiplied by square distance over distance measured for the ^{238}Pu-Be source (source no.1120).

6.1.6 Measurements in a ^{241}Am and an ^{241}Am-Be field

Measurements were performed in the field of a ^{241}Am source and a ^{241}Am-Be source on the optical bench (see Fig. 6-7) in the calibration laboratory. Detector **A** was placed in different distances from the source supplied with a high voltage of 900 V. In case of the ^{241}Am source the dose equivalent was determined as $H^* = N \cdot D \cdot (0.52 + 0.28\bar{y}_D)$, where N = 1.0295 is the *H*(10)*-calibration factor for ^{137}Cs. A mean energy spent per unit charge produced, (*W/e*), of 26.8 J/C for the gamma field was used. The measurements were performed in distances from 0.3 to 1.5 m between the source and the detector centre. In Fig. 6-8 we plot the dose equivalent times square-distance against the detector-source distance. An ideal gamma emitter would deliver in this presentation a constant value for the dose equivalent. Here we also have contribution from scattering events to the total

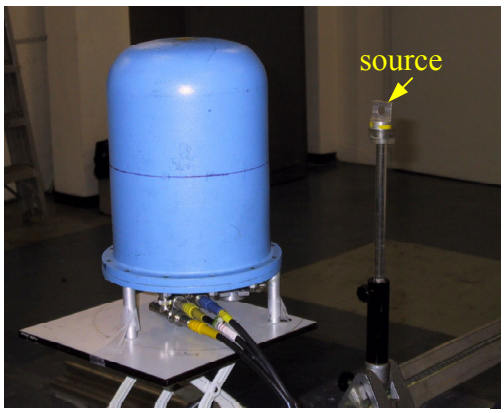

Fig. 6-7 Sievert detector in front of ^{241}Am-Be source.

dose equivalent. In Table 6-13 the results of the measurements with the Sievert detector in the ^{241}Am field are presented. In addition the deviation of the measured dose equivalent to the reference values, *H*(10),* given by the database of the Radiation Protection Group for this source are noted. However, reference values for the ^{241}Am source were only given for three distances.

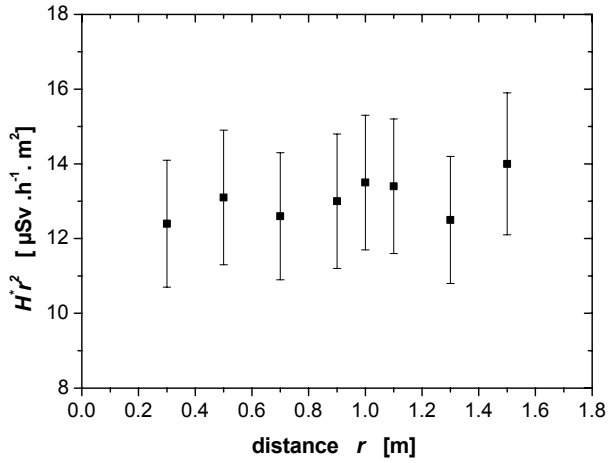

Fig. 6-8 Dose equivalent times square-distance as a function of distance for the ^{241}Am source.

Table 6-13 Detector A: Measurements on the optical bench with the ^{241}Am source (No. 3724) applying a detector voltage of 900 V and a calibration factor N = 1.0295. The relationship $\overline{Q}_D = 0.52 + 0.28\overline{y}_D$ for evaluating the quality factor is taken. A time constant of 0.1 s is chosen. (*W/e*)=26.8 J/C.

Distance [m]	$\overline{y}_D$ [keV/µm]	*Q*	*D* [µGy/h]	*H** [µSv/h]	*H*(10)* [µSv/h]	D_{iff} [%]
0.3	2.8±0.1	1.3±0.05	106.3±2.1	137.9±18.6		
0.5	3.0±0.2	1.4±0.1	38.6±0.8	52.6±7.1	45.9±2.3	14.54
0.7	2.8±0.1	1.3±0.05	19.7±0.4	25.8±3.5		
0.9	2.9±0.1	1.3±0.05	12.0±0.2	16.1±2.2		
1	3.1±0.2	1.4±0.1	9.8±0.2	13.5±1.8	11.9±0.6	13.48
1.1	3.1±0.2	1.4±0.1	8.0±0.2	11.1±1.5		
1.3	2.8±0.4	1.3±0.05	5.8±0.1	7.4±1.0		
1.5	3.1±0.2	1.4±0.1	4.4±0.1	5.6±0.8	5.7±0.3	9.18

The same set up was used for measurements with the ^{241}Am-Be source. The measurement results for the Sievert Instrument in the field of the ^{214}Am-Be source are presented in Table 6-14. In Fig. 6-9 the dose equivalent multiplied by the quadrate of the distance is plotted versus distance. The dose equivalent was determined according to $H^* = N \cdot D \cdot (0.73 + 0.17\bar{y}_D)$ with N = 1.0001 as the *H*(10)*-calibration factor for ^{137}Cs. Here, a mean energy spent per unit charge produced, (*W/e*), of 28 J/C was used. The reason for choosing the (*W/e*)-value of 28 J/C for the field of Am-Be was because of the well known similarities between the spectra of ^{238}Pu-Be and ^{241}Am-Be and the fact, that we obtained in the ^{238}Pu-Be field the best approximation to *H*(10)* with this value.

Table 6-14 Detector A: Measurements with the ^{241}Am-Be source on the optical bench applying a detector voltage of 900 V and a calibration factor N = 1.0001. The quality factor is evaluated according to $\bar{Q}_D = 0.73 + 0.17\bar{y}_D$.

Distance [m]	$\bar{y}_D$ [keV/µm]	Q	D [µGy/h]	H^* [µSv/h]
0.3	8.8±0.4	2.2±0.1	100.7±2.0	223.8±30.1
0.5	9.2±0.5	2.3±0.1	36.9±0.7	84.6±11.4
0.7	9.3±0.5	2.3±0.1	19.1±0.4	44.1±5.9
0.9	9.2±0.5	2.3±0.1	11.5±0.2	26.3±3.5
1	8.7±0.4	2.2±0.1	9.4±0.2	20.8±2.8
1.1	8.7±0.4	2.2±0.1	7.9±0.2	17.5±2.2
1.3	8.8±0.4	2.2±0.1	5.7±0.1	12.7±1.7
1.5	7.8±0.4	2.1±0.1	4.3±0.1	8.8±1.2

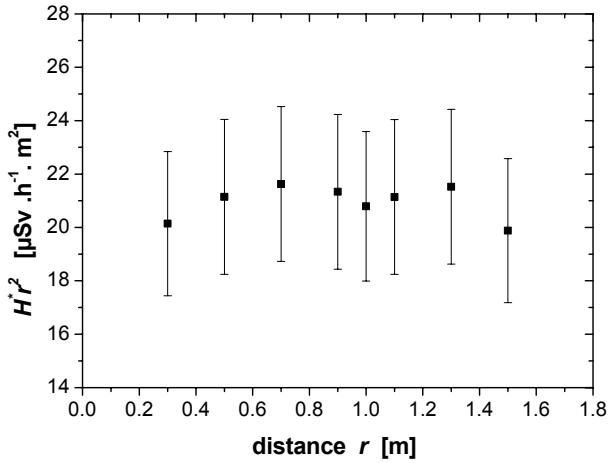

Fig. 6-9 Dose equivalent times square-distance as a function of distance for the ^{241}Am-Be source.

The reason for the irradiations of the Sievert Instrument in the field of ^{241}Am and ^{241}Am-Be in the same geometry was the fact, that the ^{214}Am source permits an acceptable estimate of the dose component coming from 60 keV photons. Therefore appropriate correction can be applied to the measurement results of the Sievert Instrument in the ^{241}Am-Be field in order to obtain a sufficiently accurate estimate of the dose equivalent $H_{n,cal}$ coming from neutrons of this source.

Before subtracting the total dose equivalent measured in the ^{241}Am field the correction factor between fluence rates of the ^{241}Am and the ^{241}Am-Be source was determined to be $F = 0.9$ with an argon-filled IG5-A20 chamber, which is insensitive to neutrons. Then it was possible to subtract the total dose equivalent measured in the ^{241}Am field corrected with F from the total dose equivalent, H^*, measured by the Sievert Instrument in the ^{241}Am-Be field.

$$H^*(^{241}AmBe) - H^*(^{241}Am) \cdot F = H_{n,cal} \tag{6.5}$$

The same correction can be applied also for the dose rates D:

$$D(^{241}AmBe) - D(^{241}Am) \cdot F = D_{n,cal} \tag{6.6}$$

$D_{n,cal}$ denotes the contribution of dose rate corrected by the dose rate obtained from 60 keV photons. If we divide $H_{n,cal}$ by $D_{n,cal}$, we get an averaged quality factor for the neutrons of the ^{241}Am-Be field:

$$\frac{H_{n,cal}}{D_{n,cal}} = Q_{n,cal} \tag{6.7}$$

The results, $H_{n,cal}$, shall serve for comparisons with the measurements done with a rem counter delivering the neutron dose equivalent $H^*(10)_n$. The neutron dose equivalent $H^*(10)_n$ measured with the rem counter in comparison with the neutron dose equivalent $H^*_{n,cal}$ determined for the Sievert Instrument is plotted against the distance between source and detector in Fig. 6-10. The calculated results in comparison with the measured results by the rem counter are listed in Table 6-15, where D_{iff} denotes:

$$D_{iff} = \frac{H_{n,cal} - H^*(10)_n}{H^*(10)_n} \tag{6.8}$$

In Fig. 6-11 the neutron response of the Sievert Instrument to the dose equivalent measured by the rem counter is shown.

Table 6-15 Neutron dose equivalent in the field of the ^{241}Am-Be source. $H^*(10)_n$ denotes the reference values obtained with the rem counter. $D_{n,cal}$ and $H_{n,cal}$ give the contribution of dose rate and dose equivalent rate corrected by the dose rate and dose equivalent rate measured in the field of ^{241}Am by the Sievert Instrument, respectively. $Q_{n,cal}$ results from the quotient $H_{n,cal}/D_{n,cal}$. The last column shows the Difference, D_{iff}, between the calculated value $H_{n,cal}$ and the value measured with the rem counter.

Distance [m]	$H^*(10)_n$ [µSv/h]	$D_{n,cal}$ [µGy/h]	$Q_{n,cal}$	$H_{n,cal}$ [µSv/h]]	D_{iff} [%]
0.3	91.6±4.6	5.0±2.8	19.9±13.0	99.7±34.4	8.8
0.5	35.3±18.7	2.2±1.0	16.6±9.5	37.2±13.0	5.5
0.7	18.7±0.9	1.4±0.5	15.3±7.6	20.9±6.7	11.9
0.9	11.4±0.6	0.7±0.3	16.5±9.2	11.9±4.0	4.0
1	9.9±0.5	0.6±0.3	13.5±7.5	8.6±3.2	-12.9
1.1	6.5±0.3	0.7±0.2	11.1±5.3	7.5±2.7	15.1
1.3	6.1±1.5	0.6±0.2	10.5±4.4	6.1±1.9	-0.7
1.5	4.9±0.2	0.3±0.1	11.3±6.7	3.2±1.4	-34.0

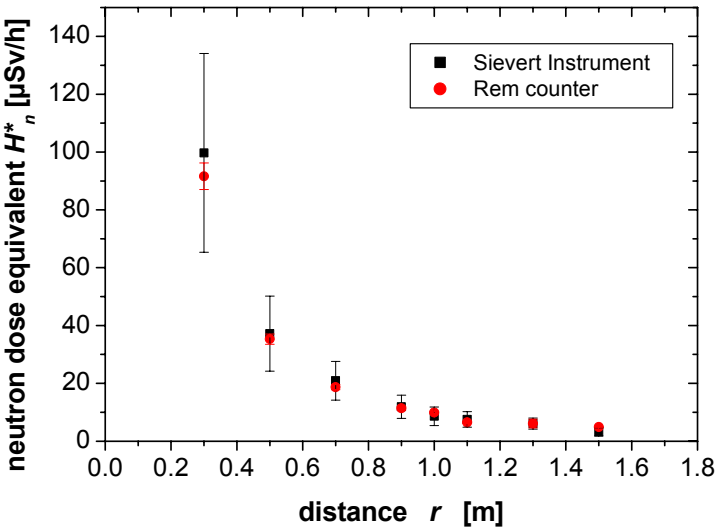

Fig. 6-10 Neutron dose equivalent $H^*(10)_n$ measured with the rem counter in comparison with the neutron dose equivalent $H_{n,cal}$ determined for the Sievert Instrument plotted against the distance between source and detector.

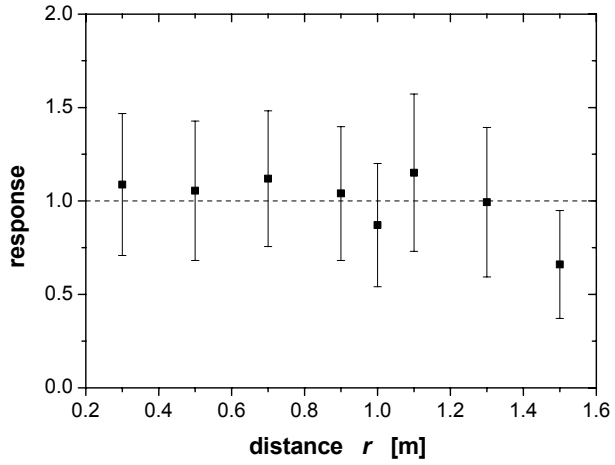

Fig. 6-11 Neutron response $H_{n,cal}/H^*(10)_n$ of the Sievert Instrument to the neutron dose equivalent determined by rem counter.

Chapter 7

Measurements at CERF

The CERN-EC High Energy Reference Field Facility (CERF-field) [Höf94, Bir98] provides a mixed field of mainly neutrons ranging from thermal energies up to hundreds of GeV [Mit01] accompanied by photons and muons. In addition it is sufficiently similar to the cosmic ray field encountered at commercial flight altitudes. The field serves as a reference base for calibration and intercomparison of dosimetric devices in high-energy radiation fields at CERN since 1993.

The neutron component of the field is well characterised as a result of measurements made by groups from across Europe using a wide range of active and passive detectors, and by Monte Carlo simulations carried out at CERN [Fas97b, Fer97]. Unfortunately, the Monte Carlo simulations only model radiation produced in the target, so they are not relevant for the γ and muon components of the field coming principally from elsewhere in the experimental hall. Hence it is very difficult to interpret the results with the help of the simulations. At this time at CERN only the HANDI-TEPC is used to actually measure the total dose equivalent. Therefore, it is presently considered as the best-suited instrument for field calibration in the cosmic radiation field at high commercial flight altitudes [Alb99]. However, also the comparison with other measurement devices is of obvious importance.

The studies at CERF were made to investigate if the results of the Sievert Instrument and the recombination chamber are comparable to the HANDI-TEPC results. For the first time all three chambers are investigated at the same reference positions at several beam intensities. In addition first measurements were carried out with a hydrogen chamber at CERF, which are of fundamental interest because of its widespread use as radiation protection monitor at CERN. Moreover this work contributes to the determination of the muon background at CERF for the measurement period in the year 2002. This background is not exactly reproducible from year to year and has to be measured by instruments sensitive to low-LET radiation.

7.1 CERF-field

The CERF-field is situated on one of the secondary beams from the Super Proton Synchrotron (SPS), in the North Experimental Area on the Prevessin site of CERN. A pulsed hadron beam with a momentum of 120 GeV/c, with a period of 16.8 s and a pulse length of 5.2 s (in 2001) or 4.8 s (in 2002), is fired onto a copper target in a radiation cave. The duration of the radiation pulse within the 16.8 s is denoted as spill. The copper target, 7 cm in diameter and 50 cm in length, can be installed in two different positions in the radiation cave as shown in Fig. 7-1 and Fig. 7-4. The measurements are performed in 90° directions with respect to the incident hadron beam direction behind shieldings of 80 cm of concrete or 40 cm of iron. The radiation intensity in these measurement positions is spatially nearly uniform over a area of 2 x 2 m² and the measurement can be performed in sixteen labelled sub-areas, each 0.5 x 0.5 m² in size. Additional measurement positions are available behind the lateral shielding of the irradiation cave, at the same angles with respect to the targets as for the two roof positions. Shielding is either 80 cm or 160 cm concrete, and at both positions 8 additional exposure locations (arranged in 2 x 4 grids made up of the same 50 x 50 cm^2 elements) are provided. In this work the measurements on the side are only related to the positions with 80 cm shielding (Fig. 7-3). The reference positions are denoted as CTx (concrete top, position number x), ITx (iron top, position number x) or CSx (concrete side, position number x). The nominal measurement locations are at the centre of each square at 25 cm above floor, i.e. at the centre of a 50 x 50 x50 cm^3 air volume, for which the radiation field has been calculated.

By adjusting the beam intensity on the target one can vary the dose equivalent rate at the reference positions, typically in the range from 25μSv/h to 1 mSv/h on the iron roof-shield and from 5 to 600 μSv/h on the 80 cm concrete roof or lateral shield.

The neutron component of the field is well characterised as a result of measurements with a wide range of active and passive detectors, and by Monte Carlo simulations carried out at CERN [Bir97]. The spectrum behind the iron shield is dominated by neutrons in the 0.1 – 1 MeV energy range. The energy distribution behind the concrete shield shows an additional large relative contribution of 10 – 100 MeV neutrons extending to about 1 GeV. In particular, the latter reproduces fairly closely the neutron field produced by cosmic rays at commercial flight altitudes. In relation to the neutron component, the contribution of other hadrons is much lower. The photon fluence from (n,γ)-reactions is almost one order of magnitude less than that of neutrons and the muon fluence is about one further order of magnitude lower.

Unfortunately the Monte Carlo simulations only model radiation produced in the target, and are therefore not relevant for the presence of "concurrent" radiation [Gol99]. The described low-LET background is dominated by muons originating mainly from pion decay in the beam line, with some contribution from pion or photon beam losses upstream or in neighbouring beam lines. This has to be taken into account for ionisation chambers, TEPC and other active devices that have a considerable sensitivity to low-LET radiation. For these instruments it is very difficult to compare the collected results with the simulations. At this time at CERN only the HANDI-TEPC is used to determine the total dose equivalent. For this reason the results of the recombination chamber, the Sievert Instrument and the hydrogen-filled chamber, which are sensitive to all kinds of radiation, can only be compared to the HANDI-TEPC.

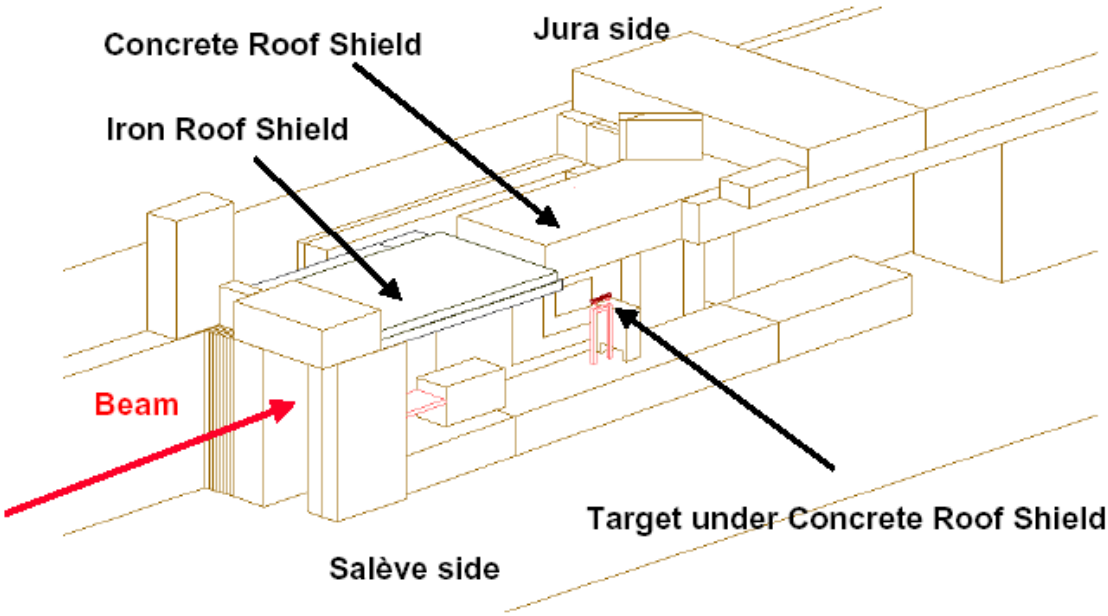

Fig. 7-1 Axonometric view of the CERF facility as modelled in the FLUKA simulation [Mit01]. The side shielding on the Salève side is removed to show the inside of the irradiation cave with the copper target set-up.

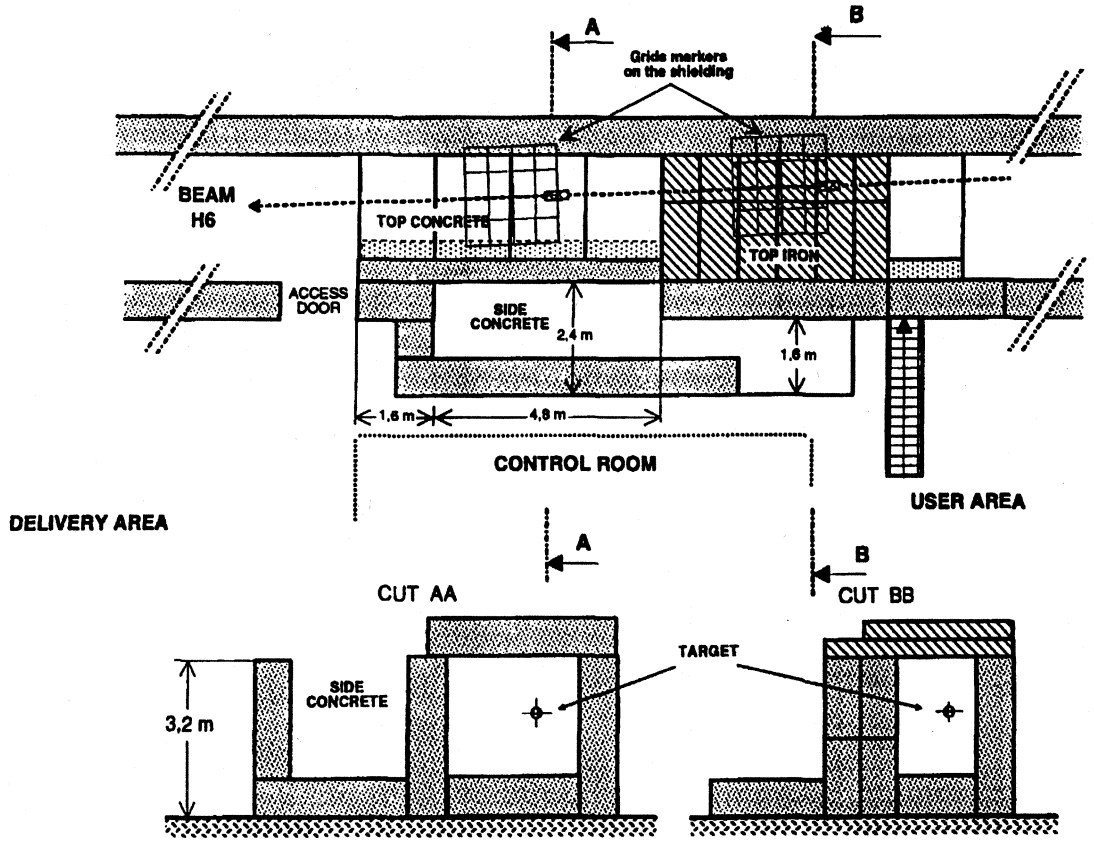

Fig. 7-2 Plan and sectional views of the CERF facility [Nav97].

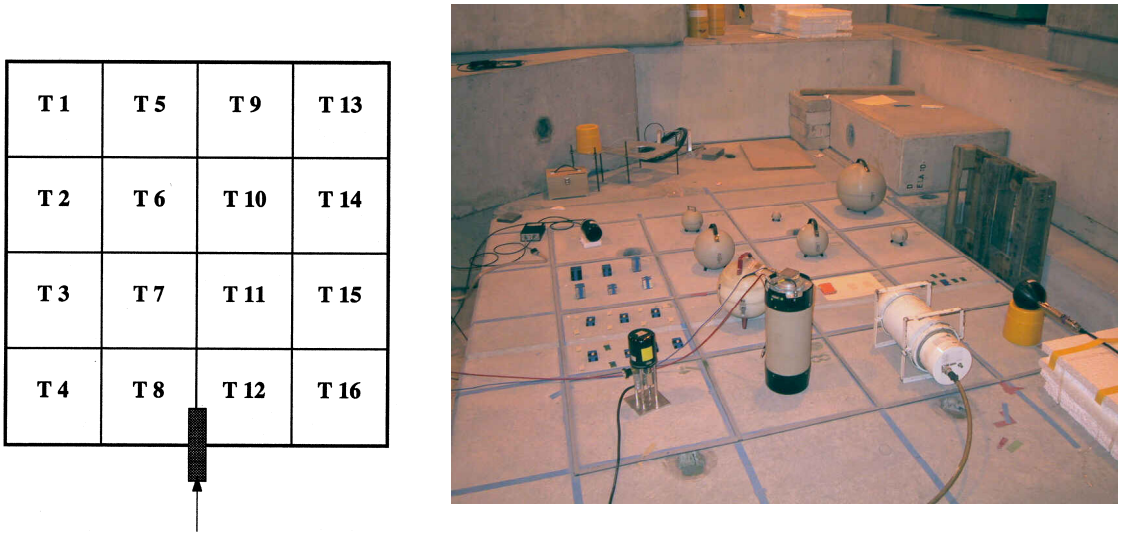

Fig. 7-3 Reference grid with 16 exposure locations used on the concrete and iron roof shields. The picture (right) shows, how the exposure locations are used during a CERF-run.

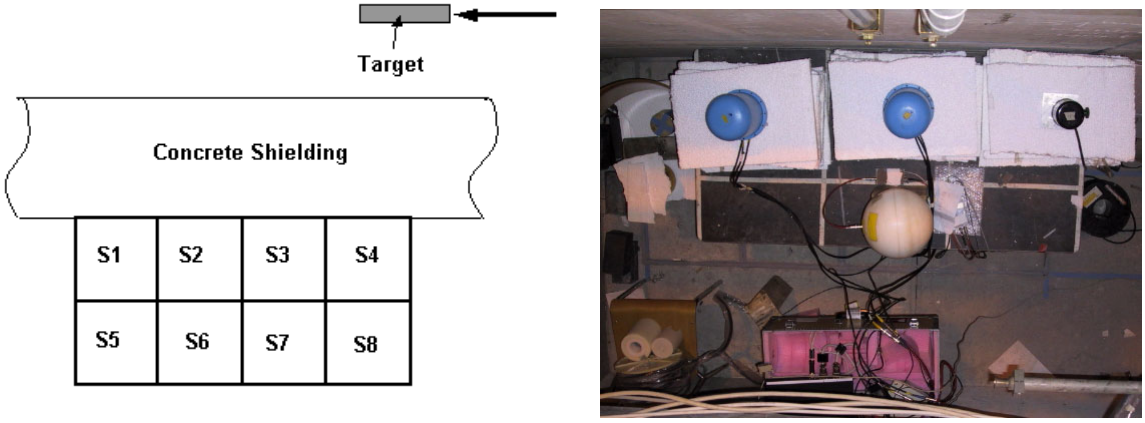

Fig. 7-4 Reference grid with 8 exposure locations used behind the 80 cm concrete side shielding. The detector centres are placed in the height of the incident beam axis by dint of polystyrene slabs.

7.1.1 CERF beam monitor

The intensity of the beam is monitored by an air-filled precision ionisation chamber (PIC) at atmospheric pressure. The chamber is placed in the beam just upstream of the target and is connected to a current-digitising circuit. Usually all measurement results are normalised to its count rate. One PIC count corresponds (within ± 10%) to 2.2 10^4 particles impinging on the target [Mit02]. Typical values of the dose equivalents are 1-2 nSv per PIC count on top of the 40 cm iron roof-shield and 0.3 nSv per PIC count outside the 80 cm concrete shields (roof and side).

7.2 Measurements

Measurements were performed with a set of instruments sensitive for different kinds of radiation at the CERF-runs in August and October 2001 and in June and July 2002. For measurements of the complete mixed radiation field the recombination chamber and the Sievert Instrument was investigated in comparison to the HANDI-TEPC, which is usually taken for this purpose at CERF. An argon-filled chamber was used to measure the part of the radiation field due to photons and charged particles.

Investigations were carried out at different beam intensities in order to characterise the CERF-field and to estimate the "concurrent" background radiation (gamma and muon components of the field originating from other beam lines and long-lived activation products). The determination of the absorbed dose due to the concurrent γ and muon radiation was done in case of the recombination chamber by Golnik *et al*. [Gol98] in 1998. In this work the same method is applied to all instruments sensitive to low-LET radiation.

In the following sections the measurement results are presented separately for each instrument. Normally the measurements have been performed simultaneously on several positions. However, it was not possible to establish a complete mapping of all 16 positions with all instruments used in this work. However, even only one measurement at a certain position is interesting for characterisation of the CERF field.

7.2.1 Measurements with the HANDI-TEPC

Measurements were carried out with the CERN HANDI-TEPC, which was calibrated before the experiments in the field of a ^{60}Co source in the calibration laboratory at CERN. The microdosimetric distributions by the HANDI-TEPC were established using a modified version [Ott99b] of the evaluation program supplied by the manufacturer (Universität des Saarlandes). The main dosimetric parameters determined with the HANDI-TEPC with *Q(L)*-function according to ICRP 60 are shown for different beam intensities in Appendix C (Table C-1). The uncertainties for the measurements were calculated after the suggestion of Sannikov [San94] assuming an overall uncertainty of 5% for TEPC measurements to which the statistical uncertainty is added in quadrature.

The Fig. 7-5 to 7-7 present the microdosimetric distributions in one position on the top of concrete and iron and at the concrete side, respectively. The spectra were recorded at a beam intensity of about 4000 PIC counts per spill for the concrete shielding and at about 1200 PIC counts per spill for iron shileding. When comparing the microdosimetric distributions in absorbed dose, *y.d(y),* remarkable difference in the shape of the peak in the low-LET range at the concrete side positions in comparison to the peaks at both locations on the top positions is noticed. This can be explained by the muon background mentioned above.

The microdosimetric spectrum in dose equivalent, *y.h(y)*, behind the concrete shieldings is characterised by a sharp peak around 100 keV/µm while the spectrum on iron shows a broad peak that extends to higher *y* values. These differences are well explained by the neutron fluence spectra outside the concrete and iron shielding [Aro93a]. A spectrum highly enriched in neutrons with energies less than 1 MeV escapes from the iron shielding, whereas the concrete spectrum is much harder with a considerable contribution of neutrons with energies above 10 MeV. These high energy neutrons produce a relatively large number of events with *y*>200 keV/µm in the microdosimetric spectra, *y.h(y)* [Aro93b].

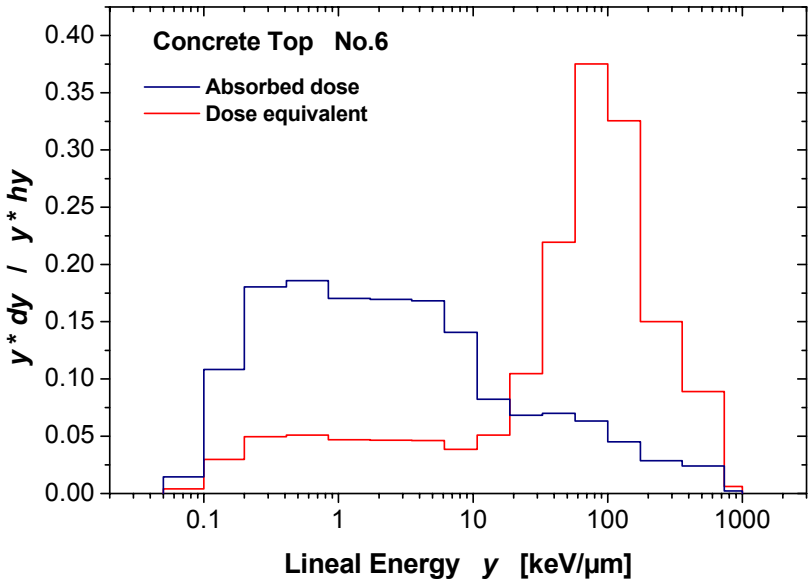

Fig. 7-5 Microdosimetric spectra measured at CT6 at a beam intensity of about 4000 PIC counts per spill on the concrete roof shielding with the HANDI-TEPC.

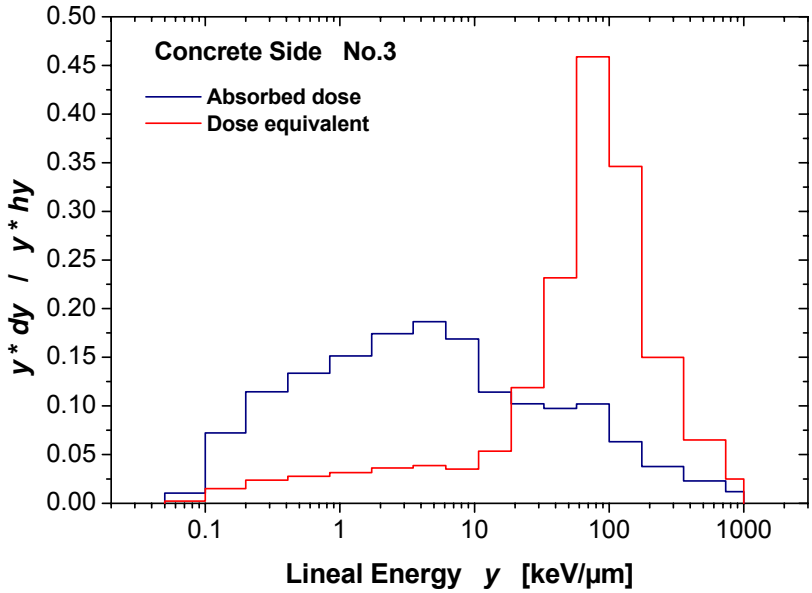

Fig. 7-6 Microdosimetric spectra measured at CS3 at a beam intensity of about 4000 PIC counts per spill on the concrete side with the HANDI-TEPC.

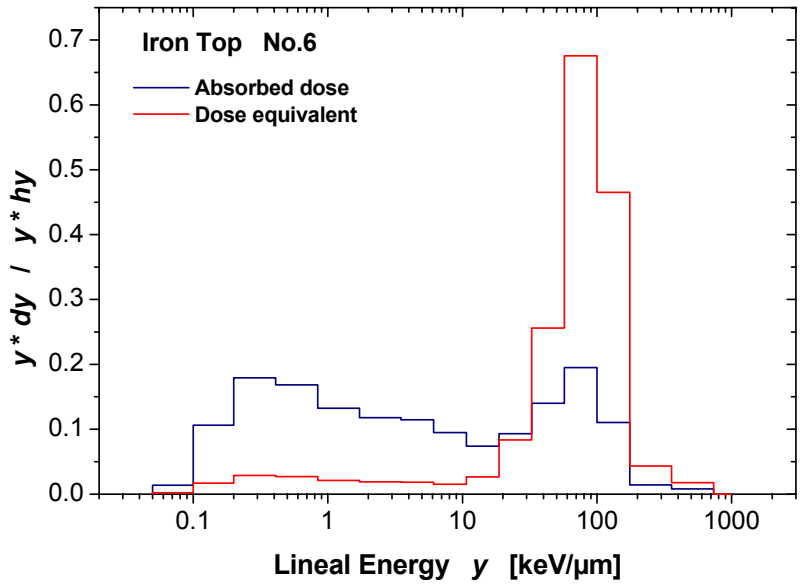

Fig. 7-7 Microdosimetric spectra measured at IT6 at a beam intensity of about 1200 PIC counts per spill on the iron roof shielding with the HANDI-TEPC.

In Fig. 7-8 to 7-10 the concurrent radiation is determined by plotting the absorbed dose per spill versus beam intensity [Gol93,Gol98]. The linear extrapolation of the data set to the zero-axis leads to a concurrent radiation of 161±10 nGy per spill on the concrete top. At the concrete side we don't observe concurrent radiation. Here, the extrapolation line passes through the origin of the coordinate system. On the iron top a linear fit through the data points is not possible. Here we set a trend line, which gives an estimation of the concurrent radiation of 188±25 nGy per spill.

In Fig. 7-11 and 7-12, the main dosimetric parameters are plotted against the beam intensity for several locations at the three different exposure possibilities of concrete top, concrete side and iron top.

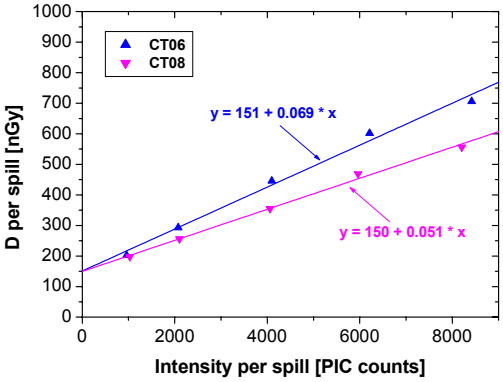

Fig. 7-8 Determination of the "concurrent radiation at on the concrete top.

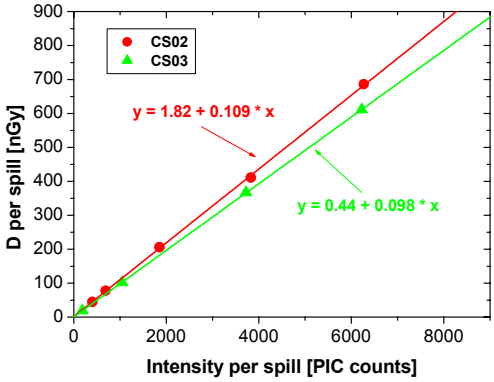

Fig. 7-9 Determination of the "concurrent radiation at on the concrete side.

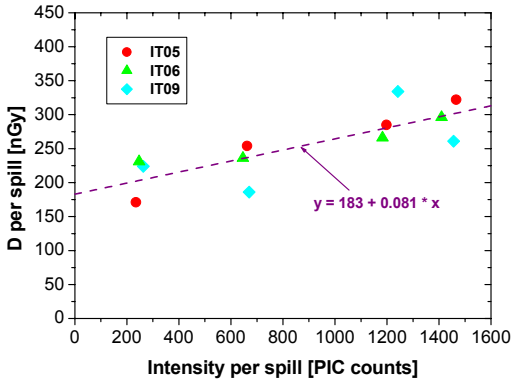

Fig. 7-10 Determination of the "concurrent" radiation on the iron roof shielding. Here the data points are not located on a straight line. For this reason a trend line was drawn.

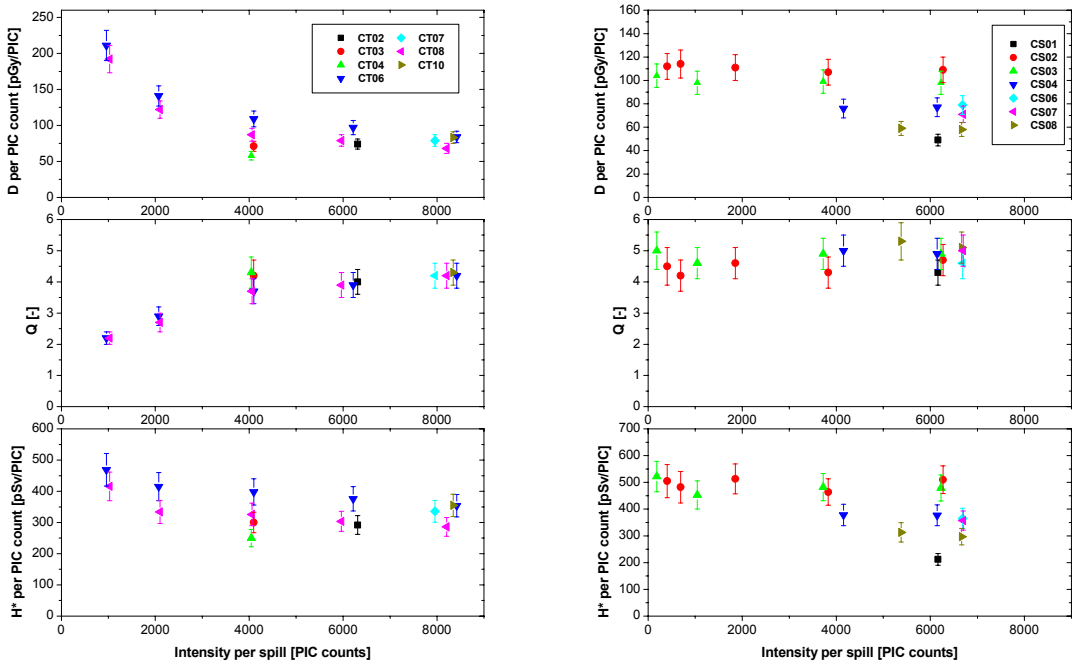

Fig. 7-11 Absorbed dose, quality factor and dose equivalent plotted against beam intensity for the concrete top (right) and the concrete side (left) determined by the HANDI-TEPC. On the concrete side, there is no muon background radiation. The measured dose is nearly constant over beam intensity.

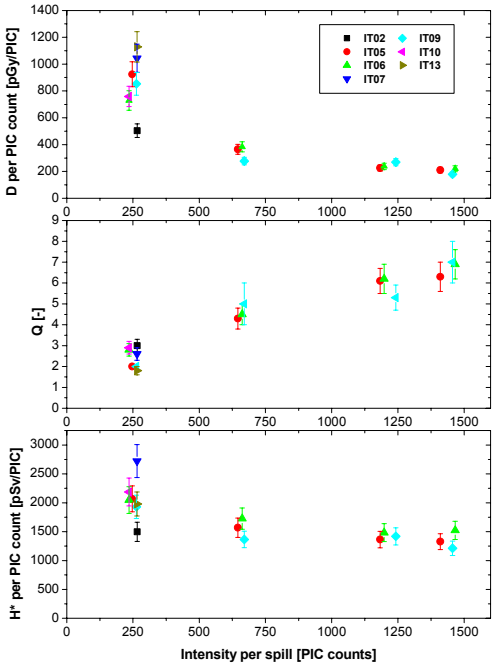

Fig. 7-12 Absorbed dose, quality factor and dose equivalent determined on the iron roof shielding with the HANDI-TEPC. Note the maximum beam intensity of 1500 PIC counts per spill.

7.2.2 Measurements with the recombination chamber

All the measurements at CERF were made with REM-2 chamber 027, as it has the highest sensitivity of the CERN chambers. Before the experiments, the chamber was calibrated in the field of a ^{137}Cs source. The sensitivity was determined to K= 353.6±4.0 μC/Gy. The target was either under concrete, where the measurements were carried out on the top and side, or under iron, where the exposure of the chamber was done on the top. Here the program of the investigations in 2002 is presented:

1. Measurements in location CT06, CS02 and IT02 at various beam intensities for determination of the absorbed dose, the radiation quality index Q_4 and subsequently dose equivalent for studies of the concurrent radiation and the behaviour of the REM-2 chamber in comparison to the other used chambers at beam variation.
2. Measurements at several positions on the top of concrete and iron to obtain a comparison between the positions on the top, respectively.
3. Measurements of full saturation curves of the chamber in locations IT06, CT06 and CS04 for determination of the quality factor according to ICRP 60 by the fitting method of Golnik [Gol93] and the low-LET component.

The influence of the concurrent γ and muon radiation is studied by employing the method of Golnik [Gol93, Gol98]. The total dose per spill is plotted as a function of beam intensity for the positions CT02, CS04 and IT02 in Fig. 7-13 to 7-15. The results obtain for these positions were determined in July 2002. The concurrent radiation is in position CT02 96±20 nGy per spill and in position IT02 124±20 nGy per spill. The measurements without target also contain the assessment of the concurrent dose. As it can be seen from the figures the concurrent dose measured without target agrees very well with the value determined with the method of Golnik. At the side location we don't observe concurrent radiation. Here, the linear fit passes trough the origin of the coordinate system within measurement uncertainties. Note that the results are strongly dependent on reference location and year. The same method applied to the results of October 2001 led to a concurrent dose of 170 ± 20 nGy per spill in CT06 [May02b, May02c].

In Table 7-1 we list the absorbed dose per spill due to concurrent radiation (background radiation) determined earlier with the recombination chamber. In the measurement of October 2001 a slightly higher background radiation was observed.

Table 7-1 Absorbed dose per spill due to the concurrent (background) radiation at position CT06. Values for the years 1993-1998 are taken from Golnik *et al.* [Gol98]. The value of 2001 was determined during experiments at the October run with the recombination chamber [May02c].

CERF – run	1993 (Sept.)	1997 (Sept.)	1998 (April)	2001 (Oct.)
Absorbed dose per spill	140 ± 20 nGy	137 ± 7 nGy	125 ± 10 nGy	170 ± 20 nGy

The main dosimetric parameters determined with the two voltage method (averaged over both polarities), normalised to one PIC count are given for several exposure locations on the top of the concrete and iron shielding, and at the side behind the concrete shielding in the Appendix C (Table C-2). The results are present graphically in Fig. 7-16 and 7-17. As it can be seen from the figures, the beam intensity has an important influence on the results. An average over different intensities leads to wrong interpretations. For this reason the dose equivalent is always presented together with the beam intensity.

It is necessary to underline at this point, that the two voltage method determines the radiation quality index Q_4, which approximates the quality factor defined in ICRP 21 recommendations. Golnik *et al*. [Gol96b] have developed a conversion for the measured radiation quality index into the recent defined quality factor of ICRP 60. In this conversion Golnik *et al.* equate Q_4 with the quality factor according to ICRP 60 below a value of $Q_4 = 5$. This would mean that at CERF no corrections for the radiation quality index have to be introduced. However, in studies at CERF in 1998 Golnik mentions correction coefficients of 1.14 for top locations and 1.25 for the side location at a beam intensity of 4000 – 5000 PIC counts per spill, to make the conversion from ICRP 21 to ICRP 60. In Fig. 7-16 to 7-17 are the uncorrected values of radiation quality index are presented, justified by the fact that the radiation quality factor is the pure physical determined parameter, which does not change by convention. The two voltage method has the big advantage of being very fast which is important for the measurement at different beam intensities in a limited time.

Nevertheless, additionally the time consuming method by fitting the radiation curves was done for one reference position at the top of iron, concrete and at the concrete side. The procedure of measuring the complete saturation curve allows in addition to the determination of the quality factor according to ICRP 60 recommendations the estimation of the low-LET dose component. The saturation curves determined in different reference positions are shown in Fig. 7-18 in comparison to the saturation curve measured in the reference gamma field ^{137}Cs. The results obtained by applying the fitting method (Chapter 3) are presented in Table 7-2.

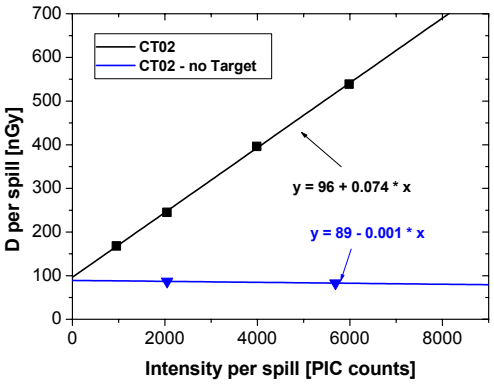

Fig. 7-13 Determination of the "concurrent" radiation with the REM-2 chamber on concrete top.

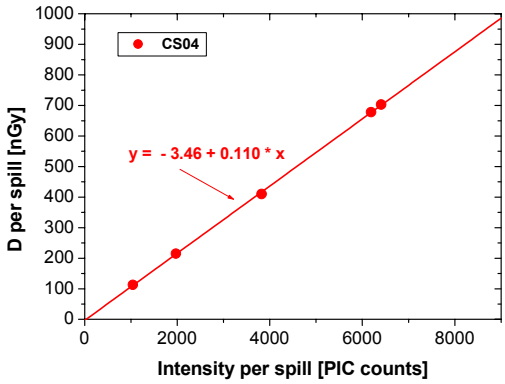

Fig. 7-14 Determination of the "concurrent" radiation with the REM-2 chamber on concrete side.

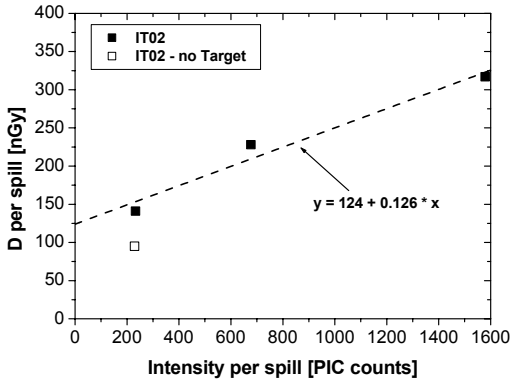

Fig. 7-15 Determination of the "concurrent" radiation with the REM-2 chamber on iron top.

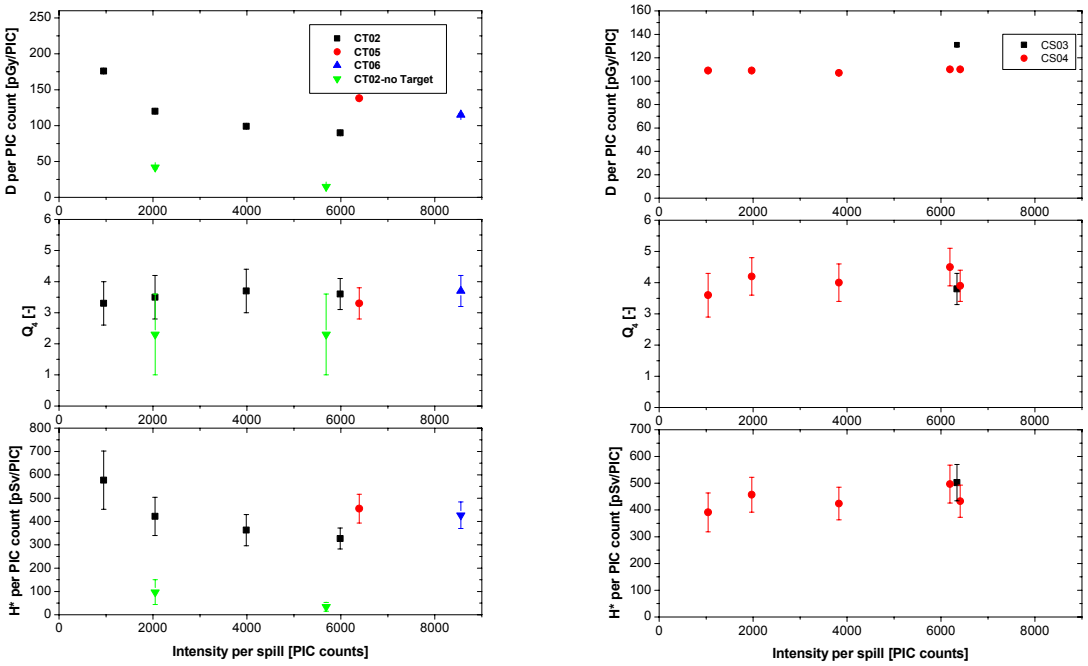

Fig. 7-16 Absorbed dose, radiation quality index and dose equivalent plotted against beam intensity for the concrete top (right) and the concrete side (left) determined by the REM-2 chamber. On the concrete top, two measurements without target have been performed is no muon background radiation. These measurements provide information about the "concurrent" radiation.

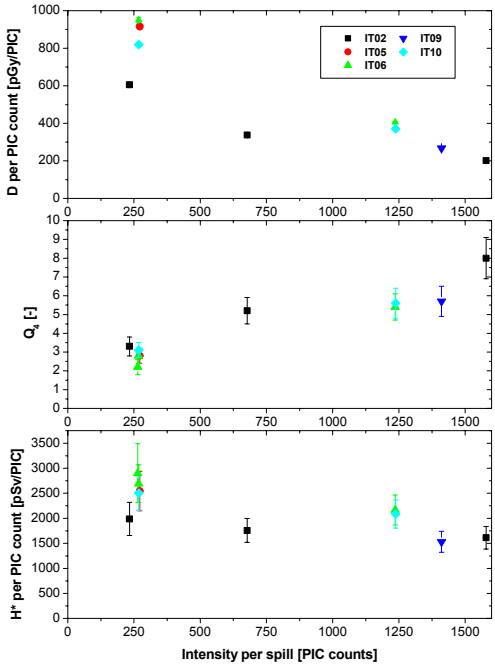

Fig. 7-17 Main dosimetric parameters versus beam intensity for the iron top shielding measured by the REM-2 chamber.

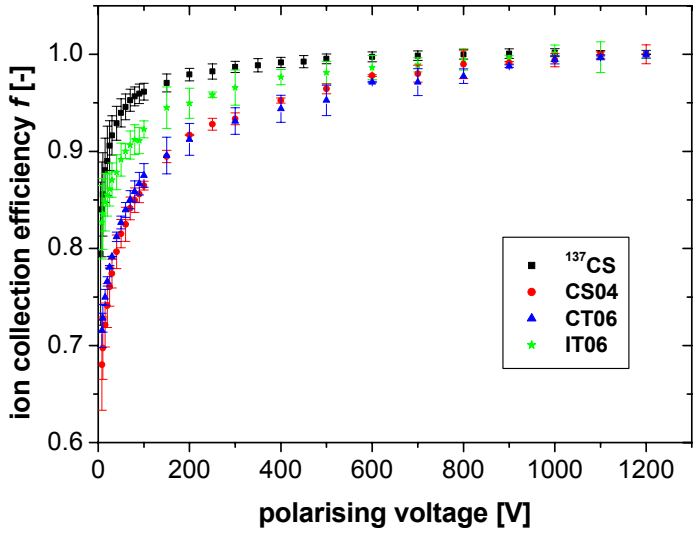

Fig. 7-18 Saturation curves measured in reference positions CT06, CS04 and IT06 at CERF. In addition the saturation curve determined in the field of ^{137}Cs is plotted. Note that the beam intensities were about 8600 PIC counts per spill at CT06, about 6400 PIC counts per spill at CS04 and about 260 PIC counts per spill at IT06.

Table 7-2 Dosimetric parameters evaluated after analysing the complete saturation curves with the fitting method by Golnik [Gol96a].

	CT06	CS04	IT06
Beam Intensity per spill [PIC counts]	8600±153	6399±121	264±15
$\mathcal{D}_{low}$ [%]	75.4±2.8	69.6±2.1	91.9±3.5
$\dot{D}^*(10)_{total}$ [pGy/PIC]	115±1.4	110±1.4	1327±24
Q_{ICRP60}	4.6±0.3	5.6±0.5	2.05±0.2
$\dot{H}^*(10)_{total}$ [pSv/PIC]	530± 35	615±55	2722±136

7.2.2.1 Orientation of the chamber in the field

Because of the cylindrical shape of the chamber, influence of the orientation of the chamber relative to the direction of the beam due to its, investigations were carried out at the CERF-run in August 2001. Measurements were made with the chamber in position 8, with the long axis of the chamber at 3 different orientations: vertical, horizontal and in an angle of 35° to the concrete roof.

Table 7-3 presents the results evaluated according ICRP 21 [May02a]. The quality factors and dose equivalents measured at different orientation are the same within the error bounds. This is consistent with measurements made in position 6 over the iron roof shielding by Golnik 1993 [Gol93], where the absorbed dose measured by the chamber in horizontal and vertical orientations was found to be the same to within 0.5%, and the quality factor was the same within 2%.

Table 7-3 Measurements of dose equivalent, *H**, and quality factor, Q_4, over the concrete roof shielding at CERF. Measurements were done with the REM-2 recombination chamber at different angles to the horizontal and evaluated according to ICRP 21. Beam intensity is 7500 PIC counts per spill.

Orientation	Q_4	H* [pSv/PIC]
Vertical	2.77± 0.55	371 ± 74
Horizontal	2.62 ± 0.31	383 ± 47
35°	2.84 ± 0.53	356 ± 9

7.2.3 Measurements with the Sievert Instrument

Measurements were performed with both detectors **A** and **B** outside the transport box in the reference height of 25 cm above the top concrete and iron shielding and in the distance of 25 cm from the concrete side shielding.

The Sievert detectors were calibrated in a ^{137}Cs field before the CERF-runs in the calibration laboratory at the Swedish radiation protection institute (SSI) and after the CERN runs in the calibration laboratory at CERN (see Chapter 4.3). The working pressures were determined to 1.444 kPa and 1.378 kPa, respectively. The high voltage on both detectors was either 700 V resulting in a gas multiplication factor of 106 for **A** and of 149 for **B** or 900 V with gas multiplication factors of 752 and 1080. The dose equivalent is determined as $H^* = N \cdot D \cdot (0.88 + 0.09\bar{y}_D)$, where the *H*(10)*-calibration factors for ^{137}Cs are *N*=0.9824 for **A** and *N*=0.978 for **B**. A (*W/e*)-value of 28 J/C was used.

In Fig. 7-19 the readings of both detectors are plotted versus time. Here, the pulse structure of the field is resolved. The duration of the particle pulse is 4.8 s within a supercycle of 16.8 s.

The concurrent radiation was graphically determined with the Sievert Instrument to be 178±10 nGy per spill on concrete top and 200±25 nGy per spill on iron top (Fig. 7-20 and 7-22). At the concrete side locations no concurrent radiation was observed (Fig. 7-21).

In the Appendix C (Table C-7) the main dosimetric parameter determined with the Sievert Instrument are listed. The results are presented graphically in Fig. 7-23 and 7-24.

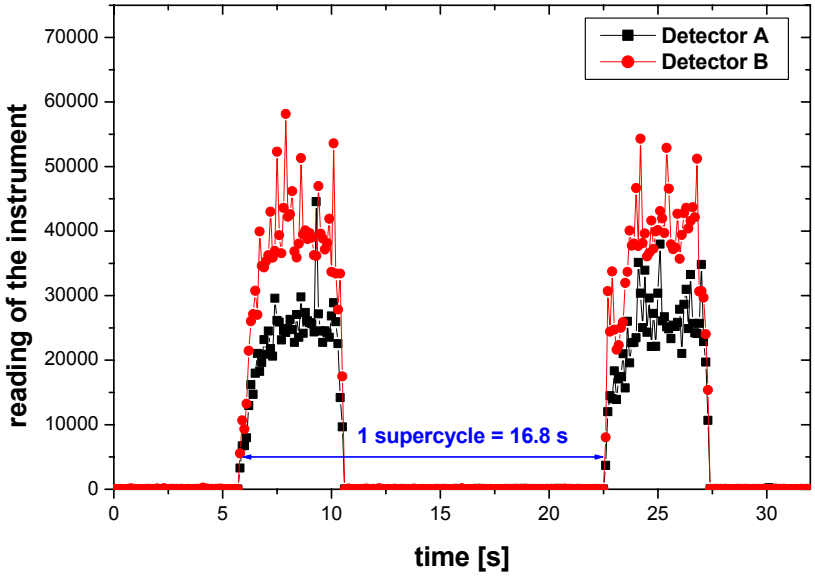

Fig. 7-19 Readings of the Sievert detectors plotted versus time. The duration of the particle pulse is 4.8 s within a supercycle of 16.8 s.

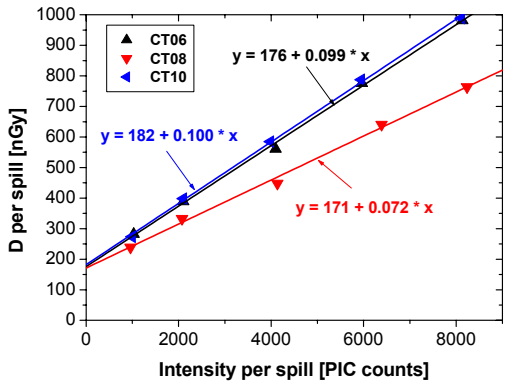

Fig. 7-20 Determination of the "concurrent" radiation with the Sievert Instrument on concrete top.

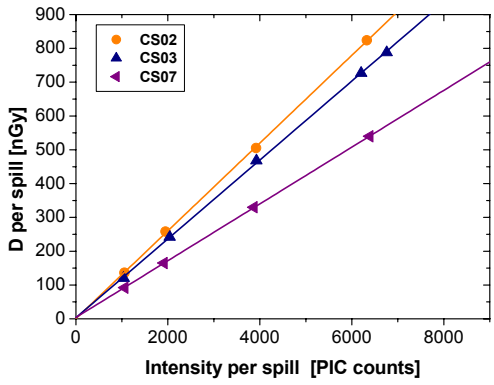

Fig. 7-21 Determination of the "concurrent" radiation with the Sievert Instrument on concrete side.

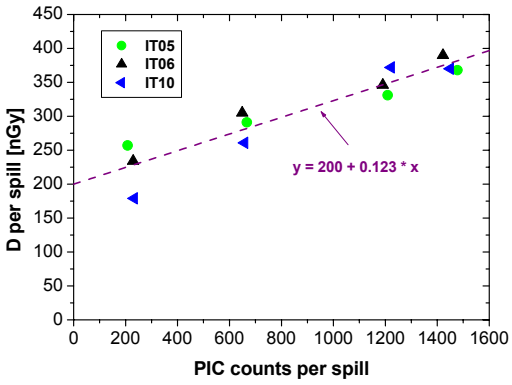

Fig. 7-22 Determination of the "concurrent" radiation with the Sievert Instrument on iron top.

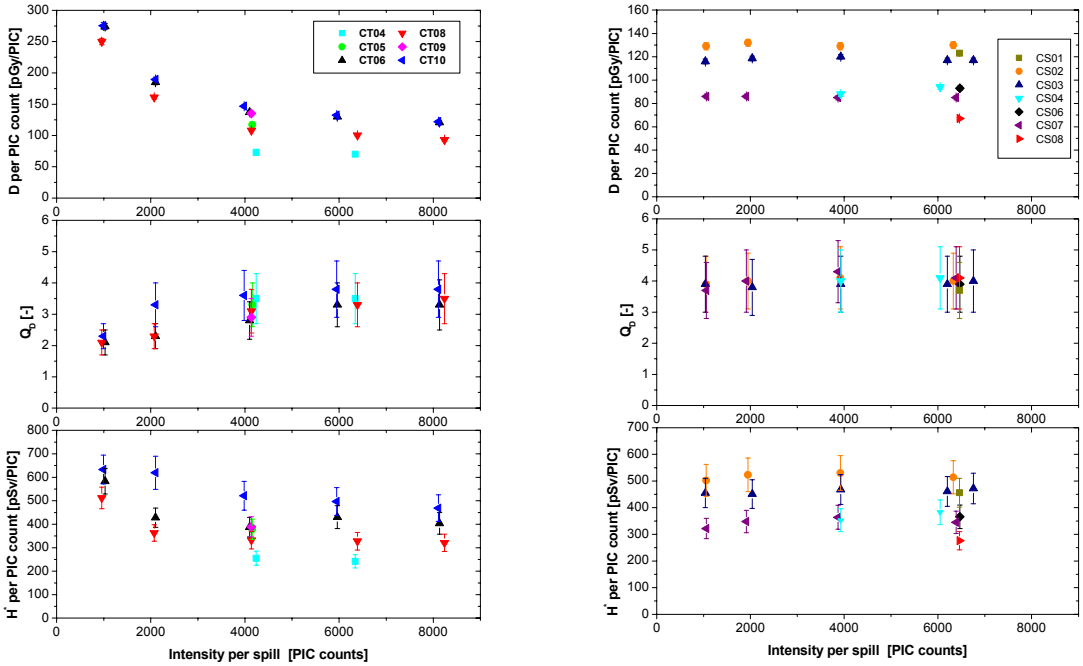

Fig. 7-23 Main dosimetric parameters measured with the Sievert Instrument on the concrete top (right) and concrete side (left) locations.

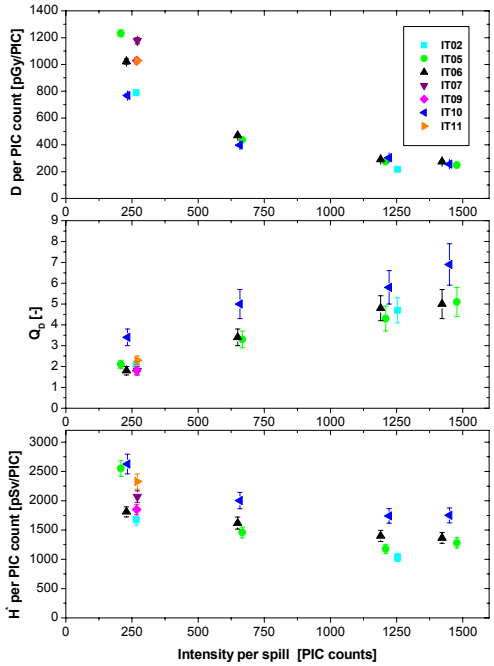

Fig. 7-24 Main dosimetric parameters measured with the Sievert Instrument on the iron roof shielding.

7.3 Intercomparison for the HANDI-TEPC, the REM-2 chamber and the Sievert Instrument

In Fig. 7-25 the intercomparison between the results obtained with the HANDI-TEPC, the REM-2 chamber and the Sievert Instrument behind the concrete shielding is presented. At concrete top we compare the measurements at the reference position CT06 and CT02. At position CT06 we have a series of measurements over beam intensity only for the Sievert Instrument and the HANDI-TEPC. For that reason we compare also the measurement results of position CT02, where the REM-2 chamber shows its dependency on beam intensity. From the figure, we see clearly that all three instruments exhibit the same trend versus beam intensity. The measurement result is heavily dependent on beam intensity and reference position. At the concrete side positions we observe approximately constant measurement results versus beam intensity.

In Fig. 7-26 we present the measurement results determined at the iron top shielding in position IT05 and IT06. Note that the beam intensity varied in a smaller range than at the concrete locations. Nevertheless the measurements exhibit a strong dependency on beam intensity. All three instruments give values of the main dosimetric quantities in very good agreement. At the beam intensity of about 1200 PIC counts per spill the REM-2 chamber shows a slightly higher dose rate and thus a higher dose equivalent rate. This value is interpreted as outlying point.

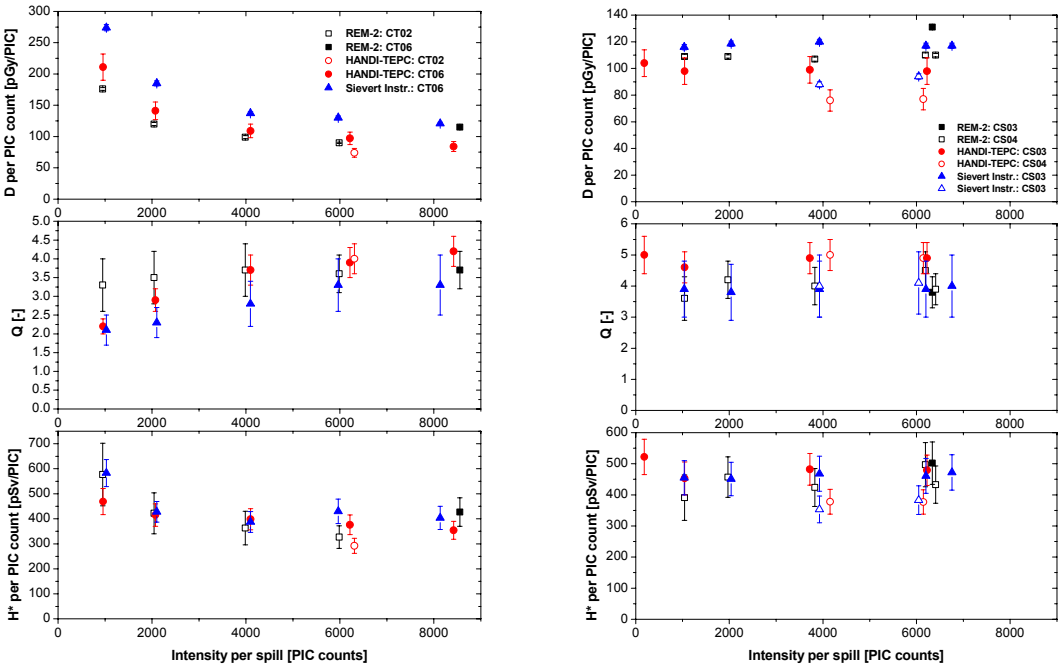

Fig. 7-25 Intercomparison of main dosimetric parameters determined with the REM-2 chamber, the HANDI-TEPC and the Sievert Instrument. On the left side measurements on top of the concrete shielding and on the right side measurements at the side concrete are presented.

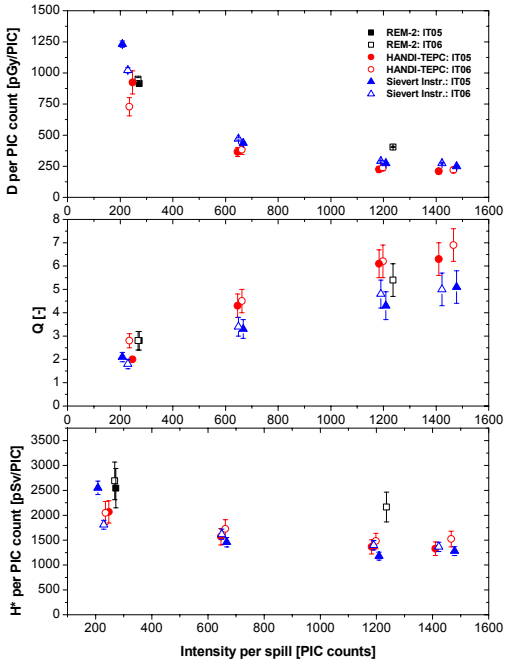

Fig. 7-26 Intercomparison of measurements carried out on iron top. The detectors are the REM-2 chamber, the HANDI-TEPC and the Sievert Instrument.

7.4 Measurements with the argon-filled chamber

The argon-filled chamber of type IG5A20 (serial no.2619), which is largely insensitive to neutrons, was used for measurements of the dose equivalent from photons and charged particles. The calibration factor of the chamber is K_A = 1.01±05 nSv/count determined in a ^{137}Cs reference field.

The results of the dose equivalents normalised to one PIC count are shown versus beam intensity in Fig. 7-27. In addition the graphical determination of the background radiation is demonstrated. On the concrete top shielding the background radiation of 178±10 nGy per spill was found. The measurements without target confirmed this result. At the concrete side positions approximately no concurrent radiation was detected. Here, the linear fit passes through the origin of the coordinate system. On the iron top a concurrent radiation of 189±20 nGy per spill was evaluated. The results for the background radiation agree very well within measurement uncertainties with the results determined by the recombination chamber, the Sievert Instrument and the HANDI-TEPC.

The measurement results are listed in Appendix C (Table C-4).

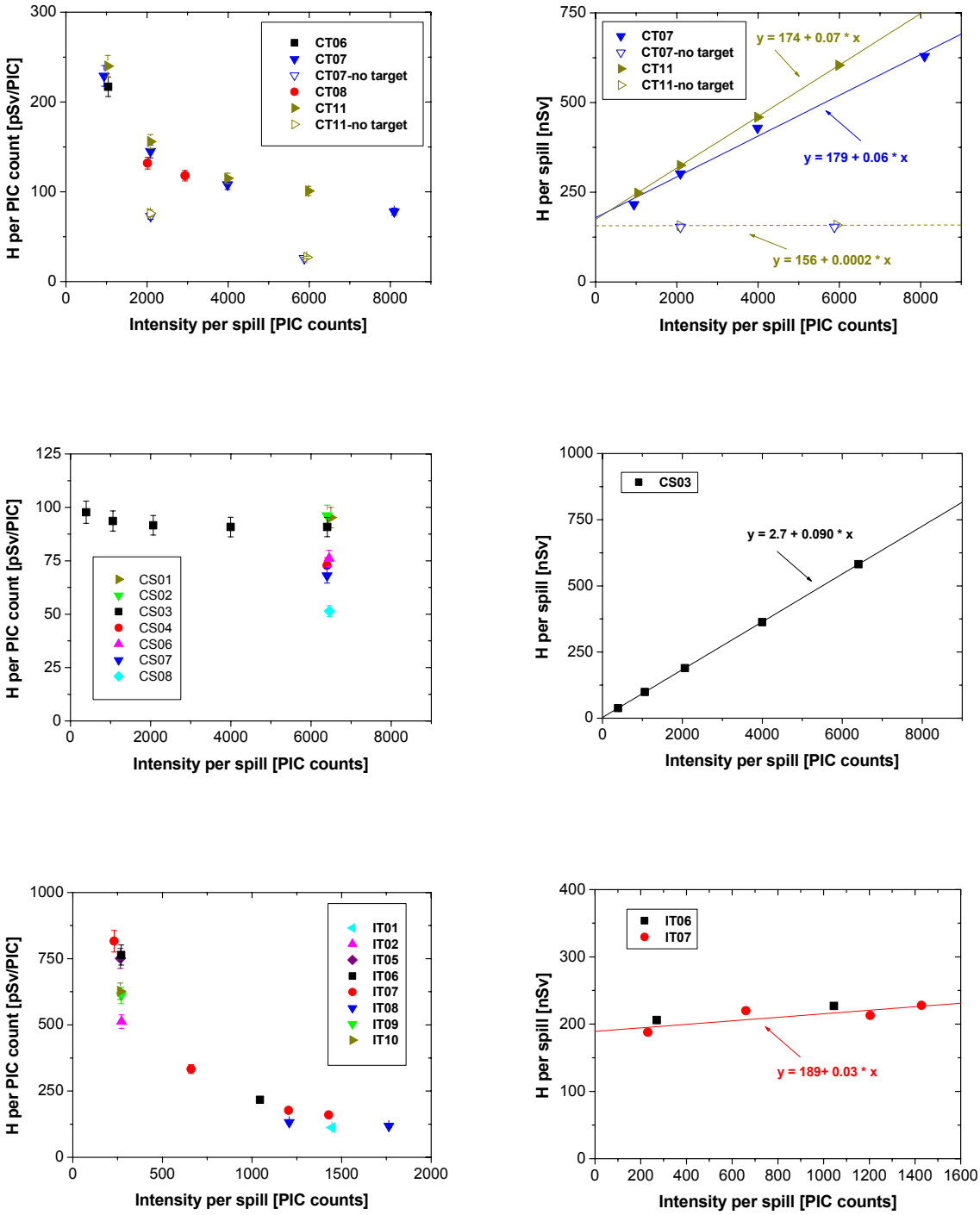

Fig. 7-27 Dose equivalent per PIC count collected with the argon-filled chamber at CERF. The first row presents the results from the concrete top, the second row shows the results from the concrete side and the last row gives the values found on the iron top shielding. On the right side of each row, the dose equivalent measured in one spill is plotted versus beam intensity. Extrapolating the data to the zero-axis gives the background radiation.

7.5 Measurements with the hydrogen-filled chamber

For the measurements at CERF the hydrogen-filled chamber of type IG5H20 (serial no. 07379) was used with a calibration factor of K_H = 7.07±0.5 nSv/count determined in the field of a ^{238}Pu-Be source. The measurement results are averaged over ten measurements each lasting one spill.

In Fig. 7-28 the dose equivalent determined by the hydrogen-chamber is displayed versus beam intensity for the three available field possibilities. In each row, on the left side the dose equivalent rates per PIC count are presented. On the right side the dose equivalents per spill versus beam intensity are plotted for estimation of the background radiation. The measured results are summarised in the Appendix C (Table C-5). The background determination for the concrete side locations gives the expected result that we don't observe background radiation. On the top locations, the chamber indicate a value of 424±50 nSv per spill on concrete top and 800±80 nSv per spill on iron top by extrapolation. Here, the extrapolation method is inapplicable for the hydrogen-filled chamber because of their calibration factor determined in a ^{238}Pu-Be. As seen before, the background radiation is mainly composed of low-LET radiation. Therefore, if we apply a calibration factor of K_{HCs} = 2.53 nSv/count measured in the field of a ^{137}Cs source to the number of counts that we would have at zero intensity, we get as background radiation 152±20 nSv per spill on the concrete top locations and 286±29 nSv per spill on the iron top locations. The result determined for the concrete top agrees with the results determined by the other used instruments. The result determined for the iron top locations is too high. However, not only the results for the background radiation are wrongly determined by the hydrogen-filled chamber. In all top locations the dose equivalent is overestimated by a factor of 2. Only at the side positions the dose equivalent is comparable to the dose equivalent measured by the other chambers. With these measurements we demonstrate, that the hydrogen chamber calibrated in a field of a ^{238}Pu-Be neutron source does not determine correctly the dose equivalent in a mixed radiation field with a non-negligible component of low-LET radiation.

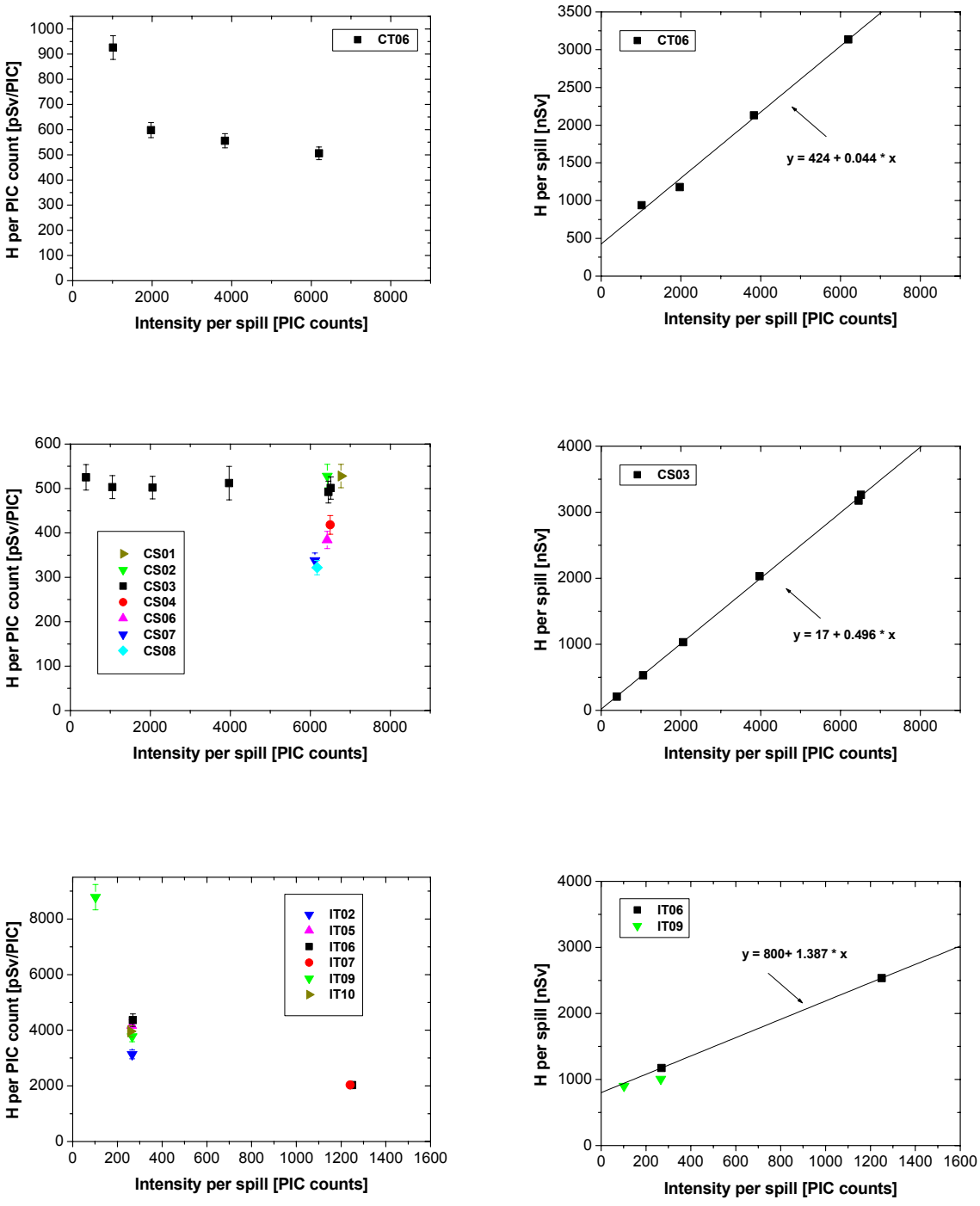

Fig. 7-28 Dose equivalent per PIC count collected with the hydrogen-filled chamber at CERF. The first row presents the results from the concrete top, the second row shows the results from the concrete side and the last row gives the values found on the iron top shielding. On the right side of each row, the dose equivalent measured in one spill is plotted versus beam intensity. Extrapolating the data to the zero-axis gives the background radiation.

7.6 Conclusions for the CERF field

In this work measurements at the CERF field were done with instruments sensitive for all radiation components (i.e. the HANDI-TEPC, the recombination chamber, the Sievert Instrument and the hydrogen-filled chamber). The argon chamber measures dose due to photons and charged particles. All of these chambers have their sensitivity to low-LET radiation in common. This is crucial at the top locations, where the chambers measure an absorbed dose per PIC count that exhibits a non-linear dependence on beam intensity, whereas the same quantity is constant versus beam intensity at the side locations. The reason for this observed behaviour is the "concurrent" radiation due to gamma and muon components of the field originating from other beam lines and long-lived activation products, which is present on the top locations.

As a consequence the concurrent radiation has an influence on the quality factor Q at different beam intensities. At the top location an increase of the quality factor with beam intensity can be seen, which is due to the decrease of the relative contribution of low-LET component to total dose. At the side location the value of Q is constant versus beam intensity.

The agreement in the measurement of total dose equivalent for the HANDI-TEPC, the recombination chamber and the Sievert Instrument is very good at CERF. Up to now the HANDI-TEPC was used as reference instrument for assessing the total dose equivalent at CERF. The HANDI has the main advantage that it provides microdosimetric spectra of the absorbed dose and the dose equivalent according to the ICRP 60 recommendations. However, the HANDI-TEPC suffers from the fact that after each measurement only the final spectrum can be saved. During long measurements several times the beam was lost for a sequence of spills. By averaging over time, this changes the dose rate and the quality factor of the field. This has to be carefully considered for presenting final results as reference values for measurements. On the other hand the Sievert Instrument has the advantage, that it records every 0.1 s the accumulated charge depending on time, so that measurements in certain time intervals can be corrected for evaluating the dose equivalent at a certain beam intensity. The disadvantage of the Sievert Instrument is that it does not provide any information about the spectral distribution. The measurement procedure with the recombination chamber is not automated. This makes the measurements with this chamber very time consuming.

The results of the hydrogen-filled chamber show large discrepancies in dose equivalent to the latter instruments. The calibration of this chamber should be carefully re-examined. The results for the contribution due to low-LET radiation to the CERF-field determined

with the argon-filled chamber are concordant with the results obtained with the other chamber except the hydrogen-chamber. The argon-filled chamber is able to measure correctly the dose equivalent due to low-LET radiation.

Chapter 8

Measurements in a strongly pulsed stray radiation field

Radiation dosimetry at particle accelerators is a difficult task due to the complex nature of the mixed radiation field consisting of electromagnetic radiation, charged and uncharged particles having a wide energy range covering more than 10 orders of magnitude. Apart from the experimental areas supplied with a slow extraction, radiation appears in the form of very short and irregular intense pulses during injection, fast ejection or beam losses in an accelerator.

Measurements were carried out on the PS-bridge, where we face a stray radiation field with short pulses produced by beam losses at the ejection of the PS. The objective of this experiment was to find out if the recombination chamber and the Sievert Instrument are capable of measuring dose equivalent in radiation fields with short pulses by comparing the results with those obtained by the instruments currently used at CERN.

8.1 PS-Complex

Protons with an energy of 50 MeV from the linear accelerator "Linac II" are accelerated to 1.4 GeV in the PS Booster, up to 25 GeV in the PS (proton synchrotron) and finally up to 450 GeV in the SPS (super proton synchrotron). The PS Booster supplies the PS with a maximum intensity of $3.5 \cdot 10^{13}$ protons every 1.2 s having pulse durations of 0.5 to 2 μs. In Fig. 8-1 the PS-complex is shown, where the so-called PS-bridge is indicated by a star. The PS-bridge is a location, which is very easily accessible. Here the PS beam leaves the ground and enters the experimental area, where it is shielded by concrete. The roof of the PS-bridge, where the measurement campaign took place, is of 260 cm concrete.

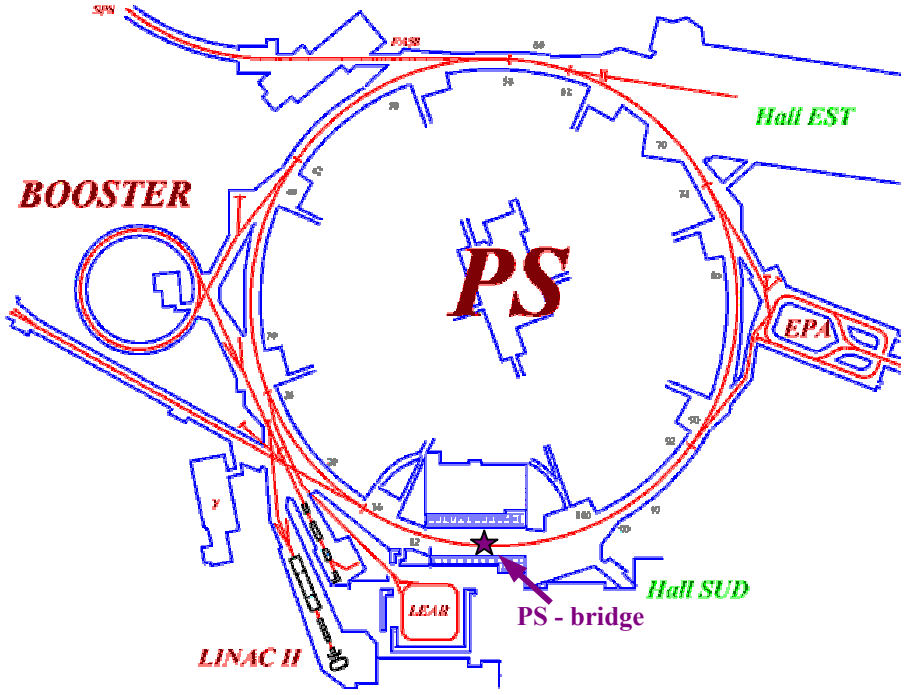

Fig. 8-1 Top view of the PS complex.

The PS machine works with a supercycle of 16.8 s duration, which currently corresponds to 14 Linac cycles (subcycles). The accelerated particles are extracted at the end of the acceleration process. They are sent directly to certain experiments, directed to one or more targets to produce secondary beams downstream or transferred to the SPS accelerator. At the extraction, beam losses take place. Beam losses are the particles, which are not directed anymore along the beam line under controlled conditions. The number of lost particles amounts to typically a few percent of the circulating beam.

The PS feeds successively the SPS, the n_TOF target (time of flight experiment), the AD target and finally the East Experimental Area with the following beams:

SFTPRO (SPS fixed target protons) beam: This beam is used to provide the SPS with protons for fixed target physics. The SPS is fed with two pulses of 1.5 to $3 \cdot 10^{13}$ protons of 14 GeV/c separated by 1.2 s and a pulse duration of 10 µs. The pulse duration of 10 µs results from circulating five times in the PS with each circle lasting for about 2 µs.

TOF (Time of Flight) beam: The n_TOF target is fed with pulses of $7 \cdot 10^{12}$ protons having 20 GeV/c, a cycle of 1.2 s and a pulse duration of 24 ns.

AD (Antiproton Decelerator) beam: The AD beam is used by AD for anti proton production. It is one pulse of $1.5 \cdot 10^{13}$ protons with a momentum of 26 GeV/c, a cycle of 2.4 s and a pulse duration of 1 μs.

EASTB, EASTC (East Area) beams: This beam has two different target destinations: TOF or different experiments of the East Experimental Area. This means that first one high intensity bunch with a momentum of 20 GeV/c is ejected and then the low intensity bunch is re-accelerated up to 24 GeV/c where finally the slow extraction takes place. The high intensity pulse consists of $4 \cdot 10^{12}$ protons and the low intensity pulse of $5 \cdot 10^{11}$ protons. The cycle duration is 2.4 s and the pulse duration is 400 ms in slow extraction mode.

The SPS currently provides $2.5 \cdot 10^{13}$ protons with an energy of 400 GeV, a cycle of 16.8 s and a slow extraction time of 4.8 s, to the North and West Experimental Areas. In Table 8-1 an overview of the different beam properties at CERN' s accelerators is presented [Ben03, Mul02]. One can see the different conditions, which may be encountered while measuring radiation produced by these beams. More detailed information can be taken from the website of the operations group in the AB Division (former PS Division) [www02].

Table 8-1 Proton beams of different properties produced by CERN accelerators in 2002. [Mul02]

Machine	Destination	Kinetic Energy / Momentum	Protons per pulse [10^{13}]	Pulse duration [μs]	Cycle time [s]
Linac 2	PS Booster	0.05 GeV	16	20 – 150	1.2
PS Booster	ISOLDE	1.4 GeV	2 - 3.5	0.5 – 2	1.2
	PS	1.4 GeV	2 - 3.5	0.5 – 2	1.2
PS	AD	26 GeV/c	1.5	1	2.4
	n_TOF	20 GeV/c	0.7	0.024	1.2
	SFTPRO	14 GeV/c	1.5 - 3	10	2 x 1.2
	East Area	24 GeV/c	0.2	$4 \cdot 10^5$	2.4
SPS	West / North Area	400 GeV	2.5	$4.8 \cdot 10^6$	16.8

8.1.1 Illustrating the time structure by measurement with the Sievert Instrument

The time-dependent record of the absorbed dose in the Sievert Instrument allows to illustrate the time structure of beam-losses on the PS-Bridge. The measurements with the Sievert Instrument are presented in section [8.2.3].

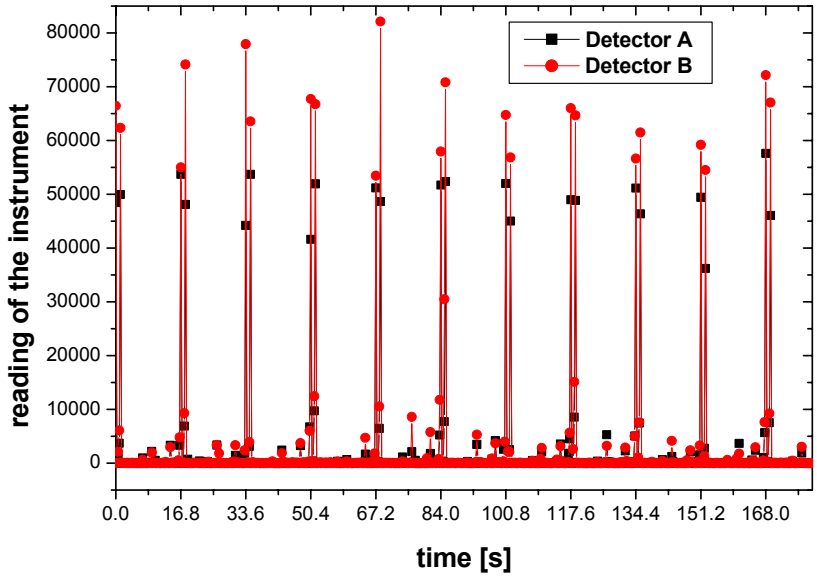

Fig. 8-2 Reading of the Sievert Instrument plotted versus time during ten supercycles of the PS machine. Note that one supercycle is 16.8 s. The short intense pulses are due to beam losses in the machine.

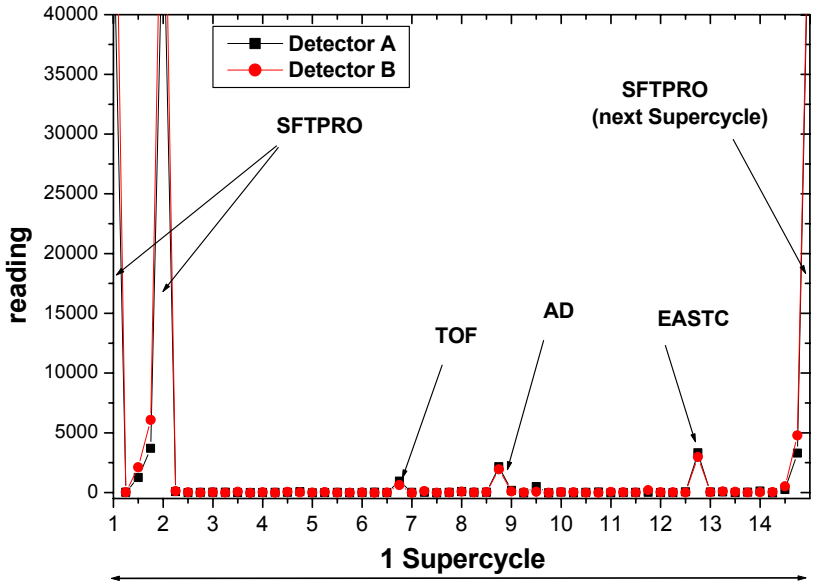

Fig. 8-3 Illustration of one supercycle composed out of 14 subcycles of 1.2 s. On the basis of the ejection order to the experiments one can identify beam losses of beams designed for other experiments by counting the subcycles. A sampling time of 0.3 s is used.

The radiation appears in form of very short pulses and is due to beam losses in the accelerator, Fig. 8-2. As an example, at the ejection from the PS the pulses for the SPS cause two high peaks of radiation, SFTPRO, at the PS-bridge due to a mechanical cutting process at the extraction via a "Septum". These two pulses, each of 10μs and being separated by 1.2 s, are followed by 15.6 s, in which the radiation levels are significant lower. However, in between these SFTPRO pulses some little pulses can be distinguished from the background. On the basis of the knowledge of the ejection order to the experiments one can identify beam losses of beams designed for other experiments, such as TOF, AD or EASTA (see Fig.8-3), by counting the subcycles. The PS control room records the ejection order to the different experiments in minutes.

8.1.2 The structure of the radiation fields encountered around CERN accelerators

At the ejection of the accelerated beams a small part of the beam is lost. As a consequence, high-energy particles interact with matter, mainly shielding material and magnets, creating copious numbers of secondary particles of lower energy like pions, protons, neutrons, electrons and others. Each one of those produces further particles again with lower energy. Particle energies may extend up to the primary particle energy and down to thermal energies, but typically a large fraction of the absorbed dose is deposited by low energy particles [IAE88]. Moreover, primary and secondary particles create radioactive nuclei in the crossed materials, the so-called induced radioactivity.

8.1.3 Expected radiation field

In the 1950s, for the qualitative nature of radiation environments outside thick shielding a general rule was established, showing that neutrons between 0.1 and 10 MeV contribute more than 50% to the dose equivalent of the radiation field; gamma rays and low energy neutrons contribute about 10-20%, and the balance is made up by neutrons greater than 10 MeV in energy. This fact was explained and confirmed by the similarity of the cosmic ray field to the fields outside accelerator shields [IAE88]. The neutron spectrum in a concrete shielding has essentially a 1/E form from thermal energies up to 1MeV. There is a peak, due to evaporation neutrons, in the 1-10 MeV range and a second peak, probably due to intranuclear cascade processes, in the 100 MeV region [Höf84]. While in the forward direction the composition of the radiation field contains the higher energy cascade-generating particles, in the backward direction the lower energy particles produced due to evaporation neutrons dominate, which are emitted isotropically. Since the measurements are located 50 m in backward direction to the point, where the ejection to the SPS accelerator takes place, we expect a neutron dose equivalent produced by evaporation neutrons and its secondaries.

8.2 Measurements and discussion

The measurement equipment was positioned near to the permanently installed monitor chamber PAXS43, which is a hydrogen-filled chamber of type IG5-H20 connected to the radiation protection survey net of CERN. The measurement arrangement is shown in Fig. 8.4. The measurement location is on the top of the PS-bridge, where the beam line is shielded by concrete of 260 cm. The position of the instruments was not changed during the whole experiment, because of the assumption, that the field is nearly constant within this arrangement.

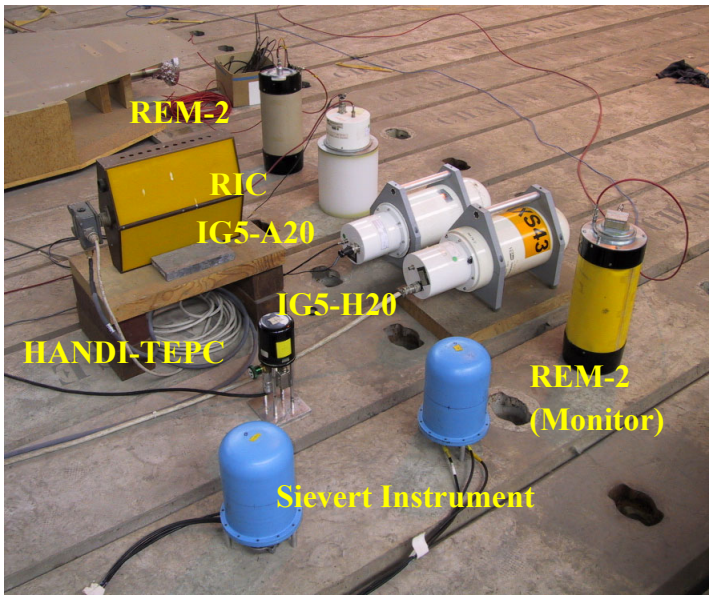

Fig. 8-4 Arrangement of the detectors during the measurement at the PS-bridge.

8.2.1 Hydrogen-filled chamber PAXS43

Hydrogen chambers are useful whenever information on spectral distribution is not required – e.g., for field measurements or as an inexpensive monitoring device.

At the PS-bridge the hydrogen-filled chamber (serial no.2645), PAXS43, is permanently installed and connected to the centralized survey system of the Radiation Protection Group. The calibration factor is K_H = 6.92±0.5 nSv/count determined in the field of ^{238}Pu-Be on the 15th of January 2001. Every 84 s (manually chosen, 84 s is equal to 5 subcycles of 16.8 s) the measurement value was recorded in a file. In Fig.8.5 the record of the 27th of June versus time is displayed. This figure shows that there are periods with

lower measured intensity. For further evaluations we made sure, that they were done during beam time periods of full intensity (exception: background studies). Full intensity means dose equivalent rates of about 80 µSv/h as indicated by the hydrogen-filled chamber. However, this "reference" value of 80 µSv/h is actual debatable at the PS-bridge, since high-pressure chambers are generally used to measure very low dose rates and thus general recombination is not a major problem, but in the case of repetitive pulsed radiation the amount of general recombination may be not negligible. Here we face the problem, that no data about general recombination in these chambers at the PS-bridge is available. We have only measurements for one applied voltage, thus no corrections for pulsed fields applying the simple two voltage method according to Boag [Boa87] could be introduced. Moreover the chambers are calibrated for *H*(10)* in the field of ^{238}Pu-Be, but there does not exist any literature about the suitability of this calibration method for complex radiation fields containing high energy particles. In addition detailed analysis with the recombination chamber gave a higher dose equivalent rate, discussed in Chapter 8.2.5.

Nevertheless the chamber is useful for monitoring (i.e. relative measurements). If appropriate field calibration of this chamber was available, it would deliver fast and reliable information about the dose equivalent rate.

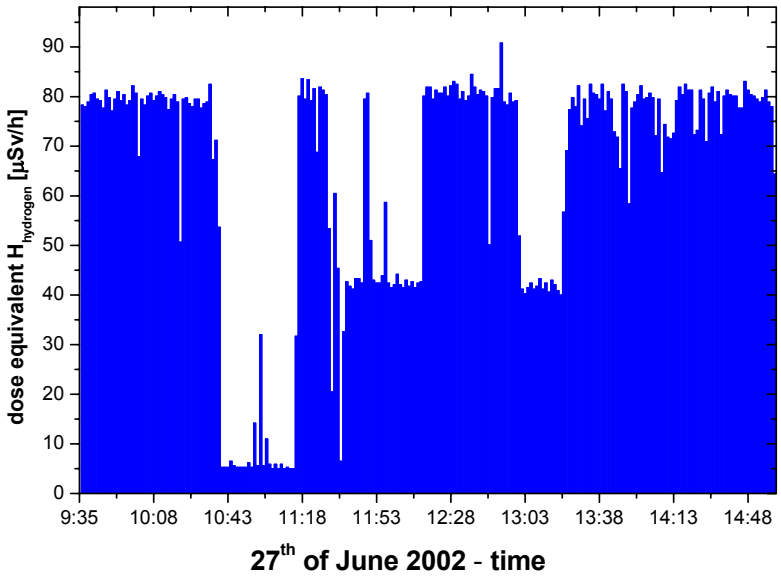

Fig. 8-5 Record of the hydrogen-filled chamber PAXS43 on the 27th of June 2002. Data was recorded every 84 s.

8.2.2 Argon-filled chamber and RIC chamber

In addition to the observations with the permanently installed PAXS43 chamber we used a high-pressure argon-filled chamber (serial no. 2619), IG5A20, and a rem ionisation chamber (serial no. 3046), RIC, which are routinely used at CERN to characterise an unknown radiation field. The chambers were calibrated in terms of ambient dose equivalent *H*(10)* in the calibration laboratory. The IG5A20 chamber has a calibration factor of K_A = 1.01±0.05 nSv/count determined in a ^{137}Cs field on the 23rd of May 2002. The calibration factor K_R =106.41±8.31 nSv/count for the RIC chamber was evaluated in a ^{238}Pu-Be field on the 14th of March 2002. The readings of the instruments are shown in Fig. 8-6 in comparison to the hydrogen-filled chamber versus time on the 27th of June 2002. The argon-filled chamber measures a dose equivalent of 13.1±0.9 µSv/h and the RIC chamber a dose equivalent of 56.6±4.3 µSv/h in the period when the monitor chamber PAXS43 indicates a dose equivalent of 78.2±5.1 µSv/h. The background was measured in the time period from 10:40 to 11:15 on the 27th of June. The summary of the results is presented in Table 8-2. The results are given only with one standard deviation.

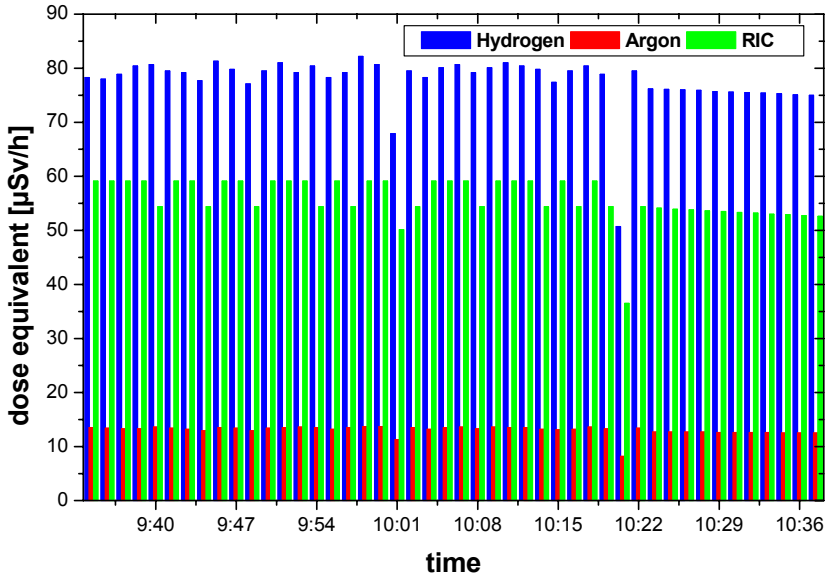

Fig. 8-6 Dose equivalent rates recorded by the hydrogen-filled chamber PAXS43, the argon filled chamber IG5A20 and the rem ionisation chamber RIC. The figure displays a section from the measurement record of the 27th of June 2002. Data is plotted every 84 s for each instrument.

Table 8-2 Dose equivalent rates measured on the 27th of June 2002 on the PS-bridge.

27th of June	Dose equivalent rates [µSv/h]		
Chambers:	PAXS43	IG5A20	RIC
9:35 to 10:30	78.2±5.1	13.1±0.9	56.6±4.3
Backround: 10:40 to 11:15	7.1±5.6	1.2±0.7	4.5±3.7

8.2.3 Sievert Instrument

The measurements have been performed with the two detectors of the Sievert Instrument, (detector **A** closer than **B** to the permanently installed PAXS43 chamber) to determine the dose equivalent applying the variance-covariance method. The exposures were done with an operating voltage of 900 V on the detector wall. For evaluations a (*W/e*)-value of 28 J/C recommended by Kyllönen *et al*. [Kyl01b] for a mixed radiation field was chosen.

The radiation field is pulsed with a very complex pulse structure, shown in Fig. 8-7. The instrument measures the voltage over a capacitor every 0.1 s and the variance-covariance analysis is performed over the data set consisting of the voltage differences between successive voltages of 0.3 s. The interval containing the discharging of the capacitor is not included.

In Table 8-3 the radiation quality factors are evaluated with three $\overline{Q}_D$ - relations [Kyl01b] assuming different dominance of neutron energies in a mixed radiation field. These results show, that applying the variance-covariance analysis leads to inconsistent results in a series of measurements at the PS-bridge. Here the intensity fluctuations between the short SFTPRO pulses are large and rapid. As it can be seen from the figure, the SFTPRO pulses are more than four times higher then the other pulses.

However, to get more consistent information about the radiation quality factor, we set a data filter between the intense SFTPRO pulses and the rest of the pulse spectrum (see Fig. 8-7). In Fig. 8-8 the data is plotted after setting the data filter. Now the variance-covariance analysis is applied to the data within the filter and beneath the filter. The radiation quality factor is determined assuming radiation fields with neutrons (1) below a few MeV, (2) of all energies and (3) above a few MeV, using the appropriate $\overline{Q}_D(\bar{y}_D)$ - relation. A time interval of 0.3 s for analysis was set. Uncertainties are given with one

standard deviation multiplied with an overall covering factor of 2 [ISO95]. The results after setting the data filter is presented in Table 8-4. The results of the quality factor determined for the reading of the instrument beneath the filter are shown in Table 8-5. Comparing the three evaluations, of the raw data, the data after setting the filter and the data beneath the filter, shows that the evaluations with filter give nearly constant values for the radiation quality factor between the different measurements. However, the choice of the $\overline{Q}_D(\bar{y}_D)$-relation has important influence on the results. The results for the quality factor beneath the filter are still varying between different measurements, but the variations are smaller compared to the analysis with no filter.

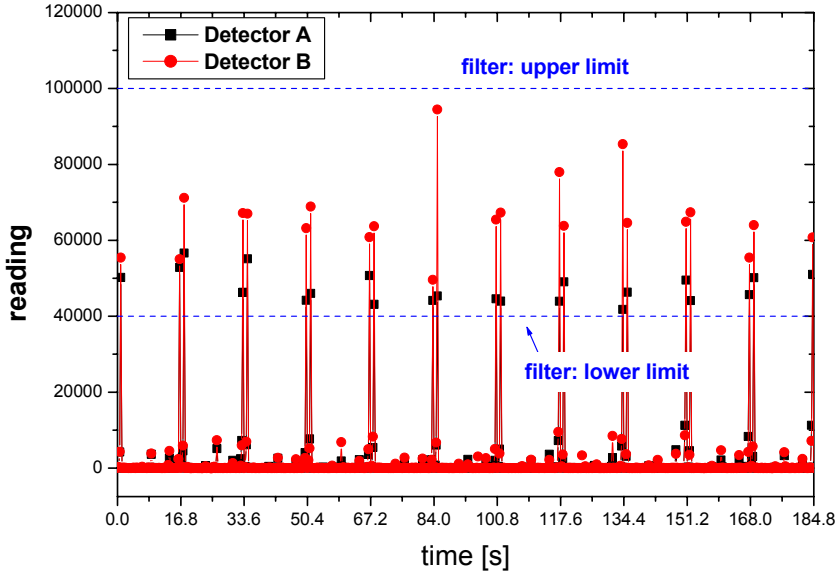

Fig. 8-7 Radiation field at the PS-bridge recorded by the Sievert Instrument. For evaluations of the quality factor a data filter was set, so that the mean lineal energy of the SFTPRO beam losses could be determined.

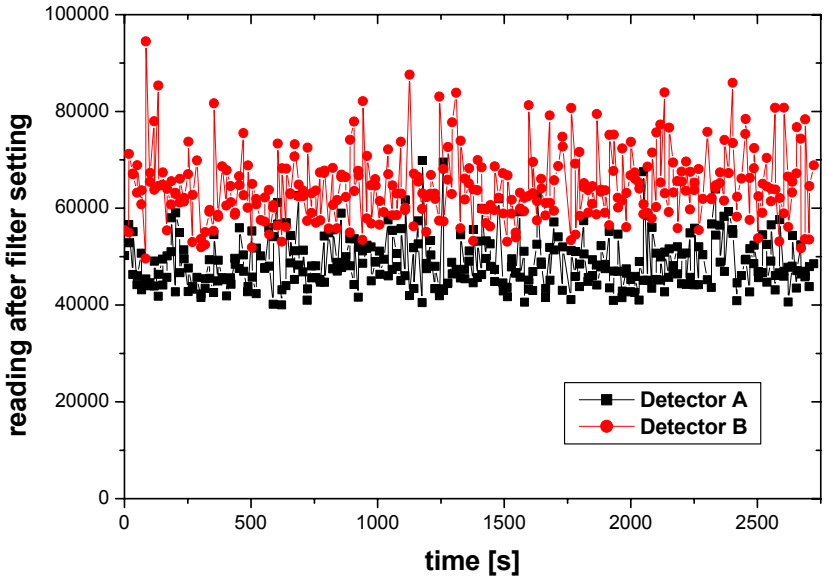

Fig. 8-8 Reading of the Sievert Instrument after setting a data filter. Now the variance-covariance method is applied for evaluating the radiation quality factor.

Table 8-3 Radiation quality factors evaluated with three $\overline{Q}_D$ - relations [Kyl01b] assuming different dominance of neutron energies. Uncertainties of the quality factor are given with one standard deviation multiplied by a covering factor of 2.

Neutrons		(1) below a few MeV $\overline{Q}_D = 0.52 + 0.28\overline{y}_D$		(2) of all energies $\overline{Q}_D = 0.73 + 0.17\overline{y}_D$		(3) above a few MeV $\overline{Q}_D = 0.88 + 0.09\overline{y}_D$	
Date	Time	A	B	A	B	A	B
27th of June	11:26 to 11:44	26.8	-1.1	16.7	-0.3	9.3	0.3
1st of July	11:36 to 12:17	14.5	13.1	9.2	8.3	5.4	4.9
1st of July	12:24 to 14:12	18.7	15.0	11.8	9.5	6.7	5.5
1st of July	15:04 to 15:50	13.3	14.4	8.5	9.1	5.0	5.3
3rd of July	23:57 to 4:57	8.9	17.6	5.8	11.1	3.6	6.4
	Average	15.5±12.1	14.1±13.3	9.8±7.4	9.0±8.0	5.7±3.9	5.3±4.3
Background: 27th June	10:53 to 11:15	2.8	-	2.1	-	1.6	-

Table 8-4 Radiation quality factors evaluated with three $\overline{Q}_D$- relations [Kyl01b] assuming different dominance of neutron energies. Uncertainties of the quality factor are given with one standard deviation multiplied by a covering factor of 2. Data filter is set according to Fig.8-7.

Neutrons		(1) below a few MeV $\overline{Q}_D = 0.52 + 0.28\overline{y}_D$		(2) of all energies $\overline{Q}_D = 0.73 + 0.17\overline{y}_D$		(3) above a few MeV $\overline{Q}_D = 0.88 + 0.09\overline{y}_D$	
Date	Time	A	B	A	B	A	B
27th of June	11:26 to 11:44	11.4	12.6	7.3	8.1	4.4	4.8
1st of July	11:36 to 12:17	10.7	14.3	6.9	9.1	4.1	5.3
1st of July	12:24 to 14:12	13.2	12.9	8.4	8.2	5.0	4.9
1st of July	15:04 to 15:50	11.9	12.3	7.7	7.9	4.6	4.7
3rd of July	23:57 to 4:57	11.1	13.3	7.2	8.5	4.3	5.0
	Average	11.7±2.0	13.1±1.6	7.5±1.2	8.4±0.9	4.5±0.6	4.9±0.5

Table 8-5 Radiation quality factors evaluated with three $\overline{Q}_D$- relations [Kyl01b] assuming different dominance of neutron energies. Uncertainties of the quality factor are given with one standard deviation multiplied by a covering factor of 2. Data filter is evaluated beneath data filter (i.e. reading: -10^6 to 40000).

Neutrons		(1) below a few MeV $\overline{Q}_D = 0.52 + 0.28\overline{y}_D$		(2) of all energies $\overline{Q}_D = 0.73 + 0.17\overline{y}_D$		(3) above a few MeV $\overline{Q}_D = 0.88 + 0.09\overline{y}_D$	
Date	Time	A	B	A	B	A	B
27th of June	11:26 to 11:44	13.1	15.6	8.3	9.9	4.9	5.7
1st of July	11:36 to 12:17	14.0	15.7	8.9	9.9	5.2	5.8
1st of July	12:24 to 14:12	10.1	14.3	6.5	9.1	3.9	5.3
1st of July	15:04 to 15:50	11.6	27.0	7.4	16.8	4.4	9.4
3rd of July	23:57 to 4:57	10.5	13.3	6.8	8.5	4.1	5.0
	Average	12.3±3.0	17.9±9.9	7.9±1.8	11.3±6.0	4.7±1.0	6.5±3.2

In Table 8-6 we present the results for the absorbed dose rate without data filter and beneath the data filter. The latter results are for estimating the part of absorbed dose measured without the SFTPRO pulses. As it can be seen from the table, the values of absorbed dose evaluated beneath the data filter are similar to the values evaluated during the background study. Therefore, for determining the dose equivalent we take the absorbed dose measured without filter and multiply with the quality factor determined after setting the data filter. Here, the choice of the appropriate $\overline{Q}_D(\overline{y}_D)$-relation is a crucial factor for the results of dose equivalent.

We assume that the relation (1) for neutrons below a few MeV is not applicable in stray radiation fields around accelerators. Based on the assumptions that the radiation field is dominated by neutrons of all energies, the average quality factor becomes 7.5±1.2 measured with detector **A** and 8.4±0.9 measured with detector **B**. On the other hand, based on the relation for neutrons above a few MeV, the quality factor becomes 4.5±0.6 for detector **A** and 4.9±0.5 for detector **B**. Thus the dose equivalent is evaluated according to $H^* = N \cdot D \cdot \overline{Q}_D$, where N is the *H*(10)*-calibration factor for the detectors determined in a ^{137}Cs field.

In Table 8-7 the dose equivalents for different days and $\overline{Q}_D(\overline{y}_D)$-relation are summarised. Note that all measurements were performed during approximately stable conditions, where the monitor chamber PAXS43 indicated a dose equivalent of about 80 µSv/h.

Although at CERF the relation for neutrons above a few MeV gives the best agreement with the reference values, we assume that here the choice of the $\overline{Q}_D = 0.73 + 0.17\overline{y}_D$ relation (for neutrons of all energies) is more appropriate, because we assume that the beam losses occurred 50 m upwards the beam line. That means, we measure the stray radiation in backward direction, where the neutron component is produced mainly by evaporation neutrons (i.e. low energy neutrons). At CERF the stray radiation field is measured in forward direction.

Table 8-6 Dose and dose equivalent rates for measurements between the 27th of June and 3rd of July 2002. The measurement times are indicated in column 2. Absorbed dose rates are presented for detector **A** and **B** without setting a data filter in column 3 and 4. In column 5 and 6, the absorbed dose beneath the data filter (i.e. reading: -10^6 to 40000) is determined.

		Absorbed dose rate (without filter) $\dot{D}$ [µGy/h]		Absorbed dose rate (beneath filter) $\dot{D}$ [µGy/h]	
Date	Time	A	B	A	B
27th June	11:26 to 11:44	17.4	16.5	2.2	2.3
1st July	11:36 to 12:17	17.3	16.8	3.6	3.5
1st July	12:24 to 14:12	17.2	16.7	3.1	2.9
1st July	15:04 to 15:50	17.7	17.4	2.9	2.8
3rd July	23:57 to 4:57	16.1	15.7	1.0	0.9
	Average	17.1±0.8	16.6±0.9	2.4±1.8	2.4±1.8
Background: 27th of June	10:53 to 11:15	2.2	2.1		

Table 8-7 Dose equivalent rates for measurements between the 27th of June and 3rd of July 2002. The measurement times are indicated in column 2. Dose equivalent rates assuming the $\overline{Q}_D(\overline{y}_D)$-relation for neutrons of all energies are presented for detector **A** and **B** in column 3 and 4. The dose equivalent rates for the $\overline{Q}_D(\overline{y}_D)$-relation assuming neutrons above a few MeV are given in column 5 and 6.

		Dose equivalent rate (2) neutrons of all energies $\overline{Q}_D = 0.73 + 0.17\overline{y}_D$ H [µSv/h]		Dose equivalent rate (3) neutrons above a few MeV $\overline{Q}_D = 0.88 + 0.09\overline{y}_D$ H [µSv/h]	
Date	Time	A	B	A	B
27th June	11:26 to 11:44	128.0	132.8	72.7	78.4
1st July	11:36 to 12:17	119.1	152.8	69.5	89.2
1st July	12:24 to 14:12	144.8	137.3	82.7	80.9
1st July	15:04 to 15:50	135.9	137.0	79.2	81.1
3rd July	23:57 to 4:57	115.2	133.0	67.1	78.1
	Average	128.6±15	138.6±10	74.1±7.8	81.8±5.5
Background: 27th of June	10:53 to 11:15	4.7	-	4.7	-

During the background studies (condition: no beam) detector **B** had some technical problems. Therefore, the estimated dose equivalent of 4.7 µSv/h of the background was evaluated with the detector **A** (Table 8-7).

In Fig. 8-9 the two SFTPRO pulses are displayed with a sampling frequency of 0.1 s. Although the pulse duration of the SFTPRO pulse is 10 µs, the recorded pulse does not show its peak within 0.1 s. Additionally one can also see a data point on the trailing edge. Two interpretations are possible: First this could be some detector problem due to the pulsed field itself. Second, if the accelerator frequency is not an exact multiple of the instrument sampling frequency of 0.1 s, a phase shift effect would occur.

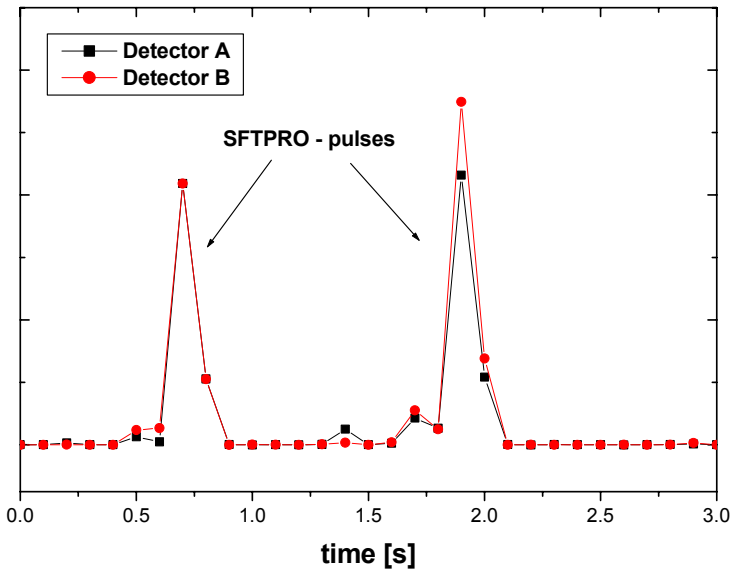

Fig. 8-9 SFTPRO pulses displayed with a sampling frequency of 0.1 s. Although the pulse duration of the SFTPRO pulse is 10 µs, the recorded pulse does not show its peak within 0.1 s. Additionally one can see also a data point on the trailing edge.

8.2.4 HANDI-TEPC

Although tissue equivalent proportional counters (TEPCs) are generally considered to be ideal for the determination of dose equivalent in mixed radiation fields, they suffer from pile-up effects (the random overlapping of pulses) in strongly pulsed fields.

At the PS-bridge, the microdosimetric spectra measured with the HANDI-TEPC are presented in Fig. 8-10. The pile-up effects lead to a distortion of the spectrum. In comparison to the spectra at the PS-bridge we present typical spectra from the CERF-field in Fig. 8-11, where the HANDI-TEPC is used as reference device for mixed radiation. At the PS-bridge similar spectra are expected, because the stray radiation is also shielded by concrete.

In Fig. 8-12, we plot the absorbed dose spectrum measured on the PS-bridge together with the spectrum measured at CERF. This shall illustrate the difference between the absorbed dose spectra, when the same ordinate scaling is used. The large peak above 100 keV/µm for the PS-bridge spectrum is a clear evidence for the pile-up effect.

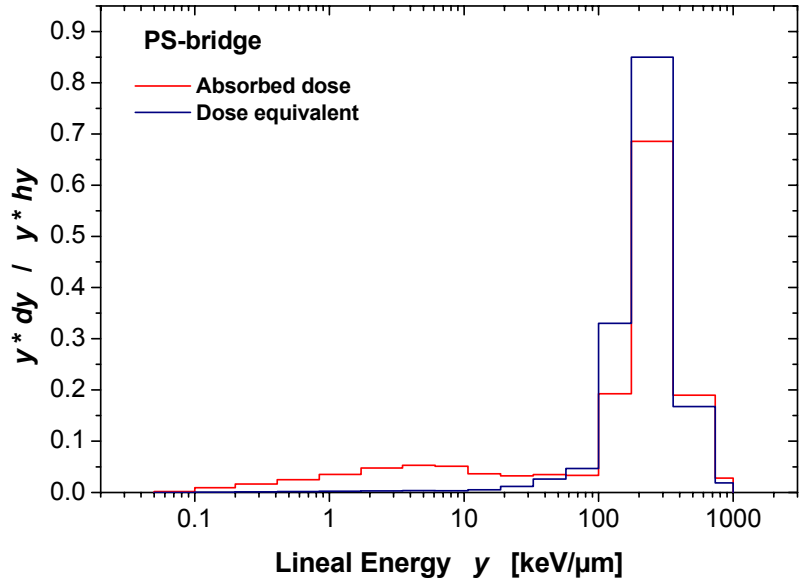

Fig. 8-10 Microdosimetric spectra measured with the HANDI-TEPC on the PS-bridge, where the shielding is of 260 cm concrete. The radiation field is strongly pulsed, so that the instrument records data only in the high *y*-channels. The detector can't separate all radiation events. This effect is known as "pile up".

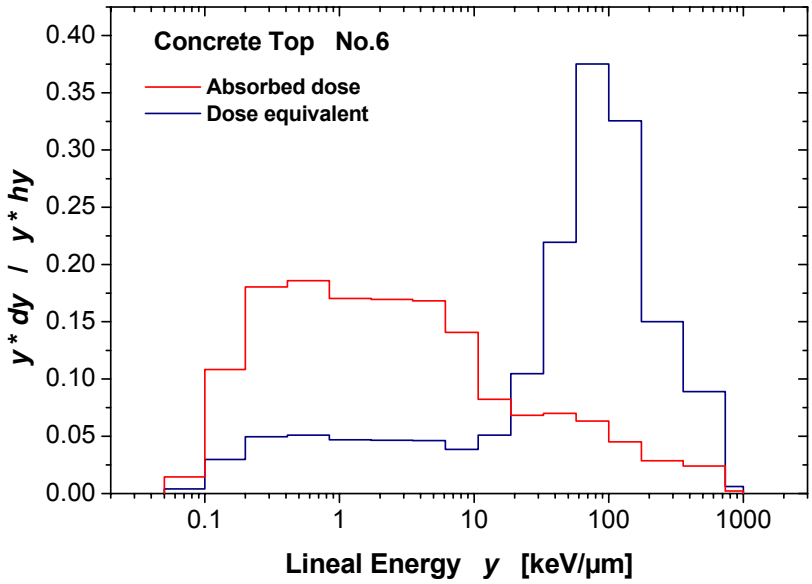

Fig. 8-11 Microdosimetric spectra measured at CT6 on the concrete roof shielding (thickness: 80 cm) with the HANDI-TEPC. Here, the pulse length was 4.8 s. The spectra are shown for comparison to the PS-bridge, where similar spectra have been expected.

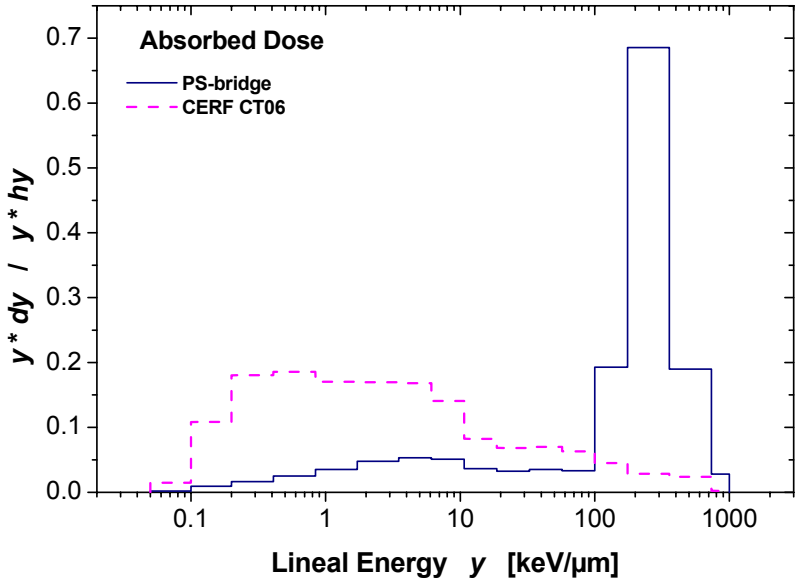

Fig. 8-12 Comparison of absorbed dose microdosimetric spectra on the PS-bridge and at CERF. On the PS-bridge one can see clearly a pile-up effect in the spectrum.

8.2.5 Recombination chamber

The measurements were performed with two recombination chambers: one (serial no.027) was used for the determination of saturation curves and the other one (serial no.004) served as monitor chamber. For this experiment a monitor chamber is especially important in order to correct for little intensity variations in the pulsed field. Both chambers were connected via electrometric cables to PTW-UNIDOS electrometers, where the charge was collected over a time interval of 84 s. The monitor chamber was supplied all the time with a voltage of 1200 V. After each time interval the data was written to a file. The start of ion collection was synchronised each time between the monitor chamber and the other chamber, where a sequence of voltages in the range of 8 V to 1200 V was applied. The charge was collected three times per applied voltage of negative and positive

polarisation. The values of ion collection efficiency obtained at the same voltage were averaged according to

$$f(|U|) = \frac{f(U) + f(-U)}{2} \tag{8.1}$$

In Fig. 8-13, the saturation curves obtained at the PS-bridge and in the calibration field of a ^{137}Cs source are shown together with the saturation curve determined in the field of a ^{238}Pu-Be source. The latter is presented here only to get a qualitative comparison, whether the quality factor is higher or lower in unknown field. From the plot we obtain an upper limit of 8.62 for the quality factor, which was determined in the field of ^{238}Pu-Be.

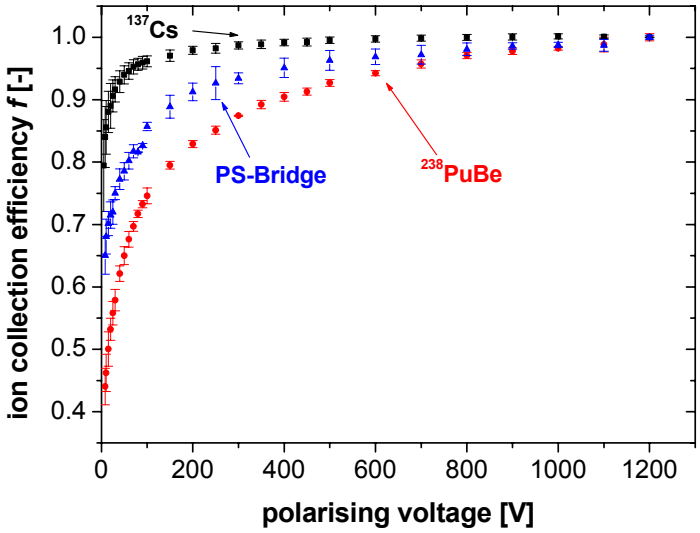

Fig. 8-13 Saturation curves measured with the REM-2 chamber in the field of ^{137}Cs, at the PS-bridge and in the field of ^{238}Pu-Be. The latter is presented to get a qualitative comparison and it sets an upper limit of 8.62 for the unknown quality factor.

Recombination chambers are generally operated under conditions of initial recombination, when general recombination is negligible. However, in the case of repetitive pulsed radiation the amount of general recombination may be considerable or slight. Initial recombination is independent of dose rate whereas general recombination increases with dose rate and sets an upper limit to the dose rate that can be measured accurately by a particular ionisation chamber.

Two methods can be applied to determine the corrections for the collection efficiency:

A plot of the reciprocal measured charge against the reciprocal applied voltage should become a straight line as saturation is approached, thus allowing the initial charge density to be estimated from the value at which the straight line cuts the 1/charge axis. Fig. 8-14 demonstrates this method and it shows in addition, that in fact a straight line approximates better the plot over 1/voltage than a plot over 1/(voltage)^2. Using this method we obtain an initial value for the charge of q_{sat} = 195.3 pC for the measurement interval of 84 s.

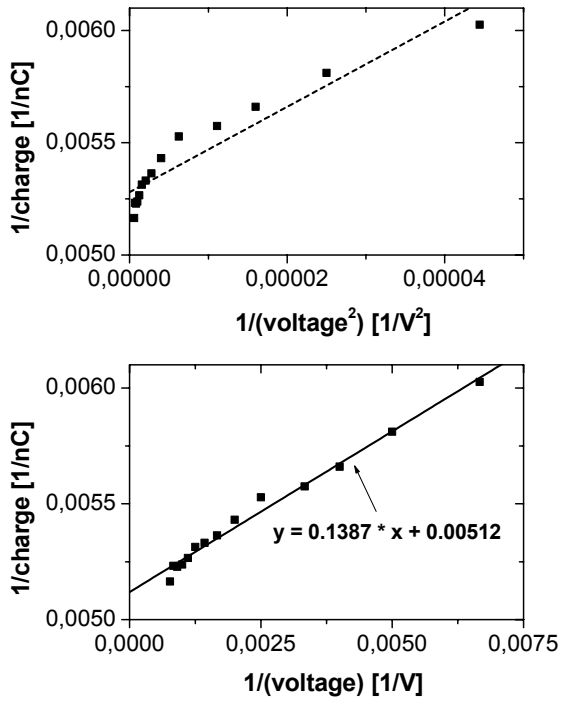

Fig. 8-14 Determination of the charge collected at saturation. A straight line approximates better the plot over 1/voltage than a plot over 1/(voltage)^2. The initial charge density is estimated from the reciprocal value at which the straight line cuts the 1/charge axis.

However, it is known that this graphical method is liable to yield sometimes too low estimate of q_{sat} and that paradoxically the way that has been found to be most reliable is the two-voltage method. The condition for this second method described by Boag [Boa87] is that the total ionisation per pulse occurs instantaneously and that the ions produced by each pulse are collected before the next pulse occurs. This is a valid assumption whenever the pulse is very short (a few microseconds or less) and the interval between the pulses is long compared to the transit time of ions between the chamber electrodes (for the REM-2 chamber the collection time is of the order of hundreds milliseconds at low voltages).

Here a second measurement at considerably lower applied voltage V_2 is done with all other conditions unchanged. These two measurements are used to extrapolate to the asymptotic value. The chart in Fig. 8-15 provides solutions for several discrete values of V_1/V_2. The recombination correction factors F obtained by the two voltage method are shown in Table 8-8. The initial charge q_{sat} is then given by F times q_1 (charge collected at V_1).

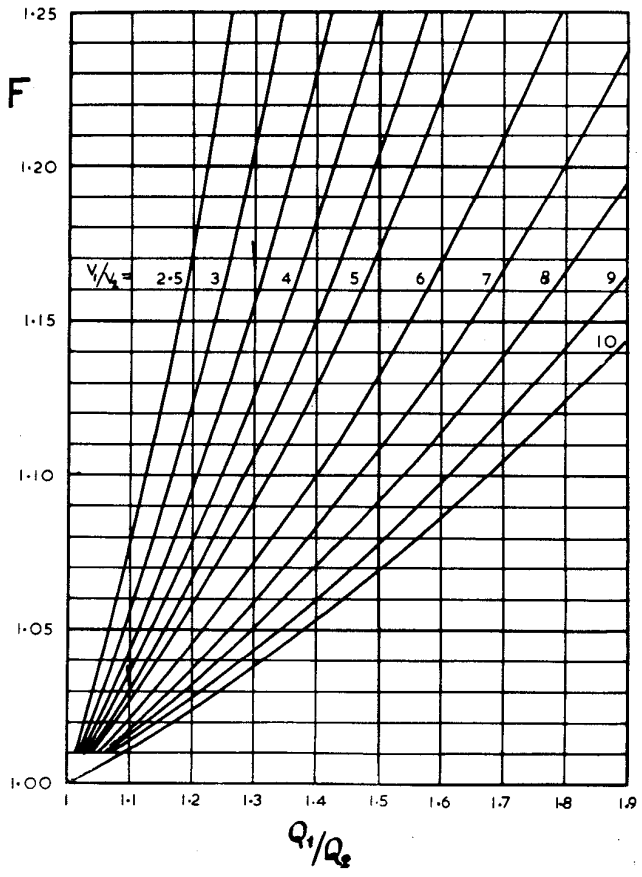

Fig. 8-15 Recombination correction factors F for several discrete values of V_1/V_2.

Table 8-8 Recombination correction factors *F* read from Fig. 8-15 after applying the two voltage method.

V_1 = 1200 V V_2	V_1/V_2	Q_1/Q_2	F	q_1 = 191.12 pC $q_{sat}=F.q_1$
400 V	3	1.0564	1.028	196.47 pC
300 V	4	1.0654	1.021	195.13 pC
200 V	6	1.1106	1.021	195.13 pC
150 V	8	1.1516	1.025	195.71 pC

Comparisons between the two reported methods deliver very good agreement for the initial charge in a time interval of 84 s measured at the PS-bridge. It seems that the lack of saturation at the highest voltage is only about 3%. In most of the practical cases the plot of the reciprocal measured charge per pulse against the reciprocal applied voltage, does not work for neutron radiation because of its broad LET spectrum [Gol03]. This time however, both the plot and the value of q_{sat} seem to be reasonable. An explanation for this could be the large fraction of low-LET radiation at the PS-bridge, which we evaluated by using the fitting procedure developed by Golnik [Gol96a], where f_{mix} is plotted against f_γ (Fig.8-16) and equation (8.2) is fitted to the graph.

$$f_{mix}(U) = \mathcal{D}_{low} \cdot f_\gamma(U) + \sum_{j=2}^{6} \mathcal{D}_j(L) \cdot s_j \qquad (8.2)$$

Here, $f_{mix}(U)$ and $f_\gamma(U)$ are ion collection efficiencies determined at voltage U in mixed and gamma radiation field, respectively; $\mathcal{D}_j$ are the absorbed dose contributions associated with a considered LET numbered by index j and s_j are analytical functions of the ion collection efficiency, averaged over the interval j; the parameter $\mathcal{D}_{low}$ is the low-LET contribution to the absorbed dose. The fitting parameters and the results are presented in Table 8-9.

Table 8-9 Dosimetric parameters evaluated after analysing the complete saturation curve with the fitting method by Golnik[Gol96a].

$\mathcal{D}_{low}$ [%]	65.1±2.4
$\dot{D}^*_{total}$ [μGy/h]	19.6±1.0
Q_{ICRP60}	7.5±1.0
$\dot{H}^*_{total}$ [μSv/h]	148.0± 29

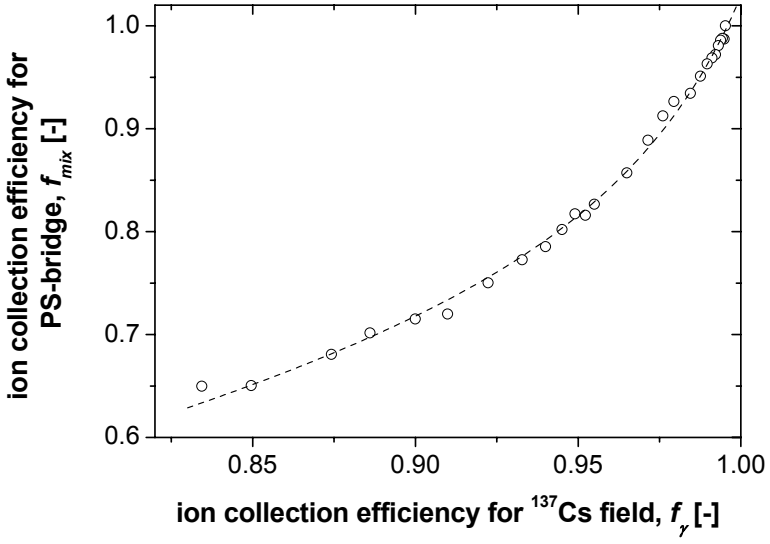

Fig. 8-16 Ion collection efficiency for PS-bridge, f_{mix} , is plotted against ion collection efficiency of the reference field ^{137}Cs, f_γ. The dashed line presents the fit according to equation (8.2) developed by Golnik [Gol96a].

The fitting method delivers a low-LET component of $\mathcal{D}_{low}$ = 65.1±2.4 % to the absorbed dose. From this we can estimate the quality factor for neutrons to be about Q_{high} = 19 according to:

$$\begin{aligned} Q_{ICRP60} &= \mathcal{D}_{low} \cdot Q_{low} + (1 - \mathcal{D}_{low}) \cdot Q_{high} \\ &= 0.651 \cdot 1 + (1 - 0.651) \cdot Q_{high} = 7.5 \end{aligned} \tag{8.3}$$

The REM-2 chamber overestimates neutron ambient dose equivalent for 0.5-0.9 MeV neutrons by a factor of about 1.5, compared to measurements in a ^{238}Pu-Be field [Gol03, Gol96a]. Due to the large value of Q_{high}, we can expect a considerable contribution from neutrons of this energy region. For this reason we use the corrected calibration factor of K_{corr} = 417.3 µC/Gy (corrected for the response of a ^{238}Pu-Be field) as in chapter 6 to take into account the slightly higher sensitivity to neutrons up to 5 MeV. Thus the dose equivalent rate is $\dot{H}^*_{total}$ =148.0±29 µSv/h.

8.3 Summary of measurements at the PS-bridge

In Table 8-10 the dosimetric results determined with the different instrument are summarised for the PS-bridge. The photon component of the mixed field was measured with an argon-filled chamber. This result agrees very well with the estimation of the REM-2 chamber for the low-LET component $\mathcal{D}_{low}$ = 65.1±2.4 % of the absorbed dose, which equals 12.8±0.8 µGy/h. The quality factors determined by the recombination chamber and the Sievert Instrument show very good agreement, under the condition that the relation $\overline{Q}_D = 0.73 + 0.17\bar{y}_D$, which assumes a radiation field with neutrons of all energies, is taken for evaluations with the Sievert Instrument. Consequently also the dose equivalent rate obtained with the recombination chamber and the Sievert Instrument agree very well within measurement uncertainties.

If the relation $\overline{Q}_D = 0.88 + 0.09\bar{y}_D$ is taken for evaluations with the Sievert Instrument, in which case a radiation field with neutrons above a few MeV is considered, the dose equivalent rate is a factor 0.6 lower and would agree very well with the dose equivalent rate determined by the hydrogen-filled chamber. However, this lower value of dose equivalent has to be doubted. In case of the hydrogen-filled chamber volume recombination in the detector gas cannot be excluded and the dependence of the chamber response in this field is not known. In case of the Sievert Instrument, we assume that the $\overline{Q}_D(\bar{y}_D)$-relation for neutrons of all energies is justified, because on the PS-bridge we deal with stray radiation produced in backward direction. Probably, the main beam losses occur about 50 m upstream the beam line. Thus, we measure mainly the neutron radiation produced by evaporation processes, which are emitted isotropically (i.e. also in backward direction). Therefore the energy range of neutrons is shifted to lower energies. At CERF, the relation for neutrons above a few MeV was the appropriate one, but there we measured a stray radiation field in forward direction. Therefore at CERF, the neutron spectrum is dominated by neutrons above a few MeV.

Unfortunately the HANDI-TEPC available at CERN is not able to provide reasonable microdosimetric spectra of absorbed dose and equivalent dose at the PS-bridge. Pile-up effects (a random overlapping of pulses due to multiple events within a spill) are identified in the spectra. The results for the HANDI-TEPC measurements in Table 8-10 are included for completeness. The consequence of the pile-up effect can be mainly seen in the high value of the quality factor. The measured total absorbed dose, which results from the integral over the microdosimetric spectrum for absorbed dose, should be equal or less the absorbed dose measured by the recombination chamber or the Sievert Instrument,

because the pile-up is not an exact adding of pulses. The value of 8.7±0.5 µSv/h measured of absorbed dose by the HANDI-TEPC is in conformity with our considerations.

The dose equivalent component for neutrons measured by the RIC chamber seems to be underestimated by a factor 1.5 to 2. The reason for this is that the RIC chamber is restricted to neutrons with energy less than 15 MeV, because its moderator cannot moderate neutrons of higher energy sufficiently to be detected by the BF_3 detector.

The recombination chamber and the Sievert Instrument seem to be capable of assessing the total dose equivalent correctly provided that the response is interpreted carefully by using appropriate calibration factors.

Table 8-10 Summary of results obtained by the different instrument used at the PS-bridge. For the Sievert Instrument two different $\overline{Q}_D(\overline{y}_D)$ -relations are possible, which result in different dose equivalent rates.

Instrument	Absorbed dose rate [µGy/h]	Quality factor [-]	Dose equivalent rate [µSv/h]	comments
Hydrogen-filled chamber PAXS43	13.1±0.9	1.0	78.2±5.1	
Argon-filled chamber			13.1±0.9	
RIC chamber			56.6±4.3	
HANDI-TEPC	8.7±0.5	15.4±1.4	134±8	
Sievert Instrument (Detector A/B)	17.1±0.8 / 16.6±0.9	7.5±1.2 / 8.4±0.9	128.6±15 / 138.6±10	$\overline{Q}_D = 0.73 + 0.17\overline{y}_D$
	17.1±0.8 / 16.6±0.9	4.5±0.6 / 4.9±0.5	74.1±7.8 / 81.8±5.5	$\overline{Q}_D = 0.88 + 0.09\overline{y}_D$
REM-2 chamber	19.6±1.0	7.5±1.0	148.0±29	

Chapter 9

Summary and outlook

The objective of the work described in the thesis was to investigate if the recombination chamber and the Sievert Instrument are capable of assessing the ambient dose equivalent correctly in mixed stray radiation fields behind the shielding of high-energy accelerators even when they are pulsed. Since the mixed stray radiation fields differ strongly from those applied in standard calibration, the instrument response to all particles in the field is usually not well known. For this reason the investigation of the instrument under reference condition is the basis for improving the reliability and accuracy of measurements in mixed fields. The instruments were therefore tested under reference conditions in the fields of calibration sources and in the mixed reference field at CERF. After showing that the recombination chamber and the Sievert Instrument agree very well with the HANDI-TEPC, which is the reference instrument for total dose equivalent at CERF, the instruments were tested in an unknown mixed radiation field with short pulses (i.e. the PS-bridge). The results were compared with those obtained by the instruments currently used at CERN (i.e. an argon-filled chamber, a hydrogen-filled chamber and a rem ionisation chamber).

The work is grouped in following topics:

The recombination chamber:

The recombination method enables the determination of radiation protection quantities, in particular ambient dose equivalent, in stray radiation fields whose composition is unknown. Both the absorbed dose and the quality factor are determined simultaneously by means of the same ionisation chamber operated under conditions of initial recombination. In addition to the determination of the average quality factor of the field, it appears possible to make an estimate of the dose fraction contributed to the ionisation by low-LET radiation. The recombination chambers were calibrated and characterised in the field of ^{137}Cs, so they could be used for measuring the dose equivalent in mixed radiation fields.

The Sievert Instrument

The Sievert Instrument was developed for radiation protection applications and cosmic ray measurements based on two tissue-equivalent proportional counters (TEPC) applying the variance-covariance method. In order to measure in mixed radiation fields the instrument was calibrated and parameters necessary for further evaluations were determined.

Detectors for radiation monitoring

The chambers used for comparison with the recombination chamber and the Sievert Instrument are described. The HANDI-TEPC is introduced, which is used as a reference instrument at CERF for assessing the total dose equivalent. Moreover high-pressure ionisations chambers and the rem counter are briefly presented.

Measurements in the fields of reference sources

In particular the field of a ^{238}Pu-Be source in the calibration laboratory is characterised with two neutron insensitive chambers i.e. a CO_2-filled chamber of type G5 and an argon-filled chamber of type IG5 in order to determine the photon contribution to ambient dose equivalent in the given geometry. The results were evaluated and compared applying the distance law. Scattered neutrons and neutrons from (n,γ)-reactions were accounted for by an extrapolation method. These straightforward measurements were confronted with the more complex method using the recombination chamber REM-2, which in addition allows the determination of the low-LET component of a mixed radiation field. In comparison measurements with the Sievert Instrument in the field of ^{238}Pu-Be were carried out.

In order to obtain a sufficiently accurate estimate of the dose equivalent $H_{n,cal}$ coming from neutrons of a small ^{241}Am-Be source, measurements were carried out with the Sievert Instrument in the field of ^{241}Am and ^{241}Am-Be in the same geometry. The measurements in the field of ^{241}Am allow estimating the dose component coming from 60 keV photons for the ^{241}Am-Be source. After appropriate correction, the results for the neutron dose equivalent were compared to results obtained by the rem counter.

The CERF field:

The CERF field provides a controlled environment in which detector systems for measuring radiation hazards in high-energy radiation environments can be intercompared. Here, the recombination chamber and the Sievert Instrument were investigated at different

beam intensities. This allowed estimating the "concurrent" (background) radiation encountered at CERF. The already established HANDI-TEPC was taken as reference device. The agreement of the results obtained with the recombination chamber, the Sievert Instrument and the HANDI-TEPC is very good at CERF. This can be taken as sufficient evidence that the investigated methods are all very suitable to measure dose equivalent in unknown mixed fields.

In addition measurements with an argon-filled and a hydrogen-filled chamber were carried out. The objective of these measurements was to determine the dose equivalent obtained by photons, muons and charged particles by means of the argon-filled chamber and to evaluate the results of the hydrogen-filled chamber at different beam intensities. The hydrogen-filled chamber, however, overestimated the dose equivalent by a factor of two on the top locations.

Measurements at the PS-bridge

While at CERF the stray radiation field is caused by an intended target interaction with controlled beam intensity and therefore well known, the stray radiation field at the PS-bridge is produced by varying beam losses in form of short pulses and less well known. Measurements were carried out with a set of detectors to obtain as much information as possible about the unknown field. A permanently installed hydrogen-filled chamber, which is connected to the radiation protection survey net of CERN, was used as a monitor chamber for recording the beam stability (stray radiation of the beam) during the experiment. An argon-filled chamber was used to determine the photon component of the mixed field. A rem ionisation chamber (RIC) was applied to estimate the field component by neutrons up to 20 MeV. Measurements with the HANDI-TEPC, which is usually the preferred reference instrument in mixed radiation fields of unknown composition, showed expected problems. Due to the measurement principle it is not to resolve the single events of detected radiation. Thus pile-up effects in the microdosimetric spectra were observed.

The Sievert Instrument was capable to illustrate the complicate pulse structure versus time. With this information it was possible to identify beam losses occurred at the ejection of the beam to certain experiments. Applying the variance-covariance method gave in a straightforward way inconsistent results, but the setting of appropriate data filters to the dominating radiation pulses allowed the calculation of the radiation quality factor. These pulses were assumed to represent the radiation hazard and their radiation quality factor was taken for evaluations of the dose equivalent. However, it is shown that the appropriate selection of the $\overline{Q}(\bar{y}_D)$-relation is an important factor for assessing the dose equivalent.

Although the recombination chamber was not able to resolve the time structure of the pulsed field one could measure saturation curves, which provided information about the average quality factor of the field. Thus combining the measured absorbed dose and the quality factor one got the dose equivalent of the field. In addition the analysis of the saturation curve delivered an estimation of the low-LET component to absorbed dose of the field. With special care the possible general recombination in the REM-2 chamber was considered and necessary corrections were introduced.

Outlook

The HANDI-TEPC, the recombination chamber and the Sievert Instrument allow to determine the absorbed dose, the quality factor and hence the dose equivalent in complex radiation fields. The HANDI-TEPC has the advantage that it provides in addition information about the microdosimetric spectrum of the radiation field.

At CERF it was shown that the results for the main dosimetric parameters obtained with the recombination chamber and the Sievert Instrument agreed very well with the HANDI-TEPC, which has itself established as reference instrument at CERF. This can be taken as sufficient evidence that the investigated methods are all very suitable to measure dose equivalent in unknown mixed fields.

At the PS-bridge, where a mixed strongly pulsed field encounters, the recombination chamber showed reasonable results in a straightforward way, whereas the data recorded by the Sievert Instrument had to be interpreted specially for applying the variance-covariance method. Then these two instruments appeared to agree within measurement uncertainties. The HANDI-TEPC failed at the PS-bridge because of the pronounced pile-up effect in the microdosimetric spectra.

The reasonable agreement of the results of dose equivalent measurements between the recombination chamber and the Sievert Instrument in strongly pulsed fields must be treated with some caution since a better understanding of the field encountered at the PS-bridge is needed for final conclusions. One way to enlarge the knowledge about the relevant composition of this field would be the measurements with a passive Bonner sphere spectrometer to obtain information about the neutron spectrum. Another way would be to perform radiation transport calculations by Monte Carlo simulations.

Appendix A

A.1 Calibration results of the Sievert Instrument

Table A-1 Calibration parameters and multiplication factors for detector **A**

Laboratory	Sweden	CERN (source 3609)				Sweden	Average
Date	2002-06-03	2002-07-25	2002-07-25	2002-07-25	2002-07-27	2002-08-06	
r [m]	2.5±0.01	2.5±0.01	2±0.01	1.5±0.01	1.1±0.01	2.5±0.01	
H*(10) [μSv/h]	10728±322	9221±277	7618±229	4092±128	2298±69		
I_{sat} [pA]	3.458±0.069	0.465±0.010	0.737±0.016	1.301±0.029	2.455±0.055	3.402±0.076	
$p_{working}$ [kPa]	1.45±0.03	1.45±0.03	1.44±0.03	1.43±0.03	1.45±0.03	1.43±0.03	1.445 ± 0.3
$m_{working}$ [kg]	(3.14±0.63) E-05	(3.08±0.62) E-05	(3.12±0.62) E-05	(3.10±0.62) E-05	(3.14±0.63) E-05		(3.14 ± 0.62) E-05
M (200V)				2±0.1			2±0.1
M (300V)				3±0.1			3±0.1
M (400V)				7±0.2			7±0.2
M (500V)				17±0.5			17±0.5
M (600V)	42± 1	42± 1	41± 1	42±1	42± 1		41 ± 1
M (700V)	106±3	106±3	105±3	106±3	106±3		106 ± 3
M (800V)	274±8	276±8	273±8	275±8	274±8		274 ± 8
M (900V)	746±22	759±21	748±21	754±21	752±21		752 ± 21

Table A- 2 Calibration parameters and multiplication factors for detector **B**

Laboratory	Sweden	CERN (source 3609)			Sweden	Average
Date	2002-06-03	2002-07-25	2002-07-25	2002-07-25	2002-08-06	
r [m]	2.5±0.01	2.5±0.01	2±0.01	1.5±0.01	2.5±0.01	
H*(10) [µSv/h]	10728±322	1468±44	2298±69	4092±123		
I_{sat} [pA]	3.324±0.074	0.449±0.10	0.700±0.16	1.241±0.28	3.218±0.072	
$p_{working}$ [kPa]	1.40±0.03	1.38±0.03	1.37±0.03	1.37±0.03	1.37±0.03	1.378 ± 0.03
$m_{working}$ [kg]	(3.02±0.6) E-05	(2.98±0.6) E-05	(2.97±0.59) E-05	(2.96±0.59) E-05		(2.98 ± 0.59) E-05
M (200V)				2±0.1		2±0.1
M (300V)				4±0.1		4±0.1
M (400V)				9±0.3		9±0.3
M (500V)				22±0.6		22±0.6
M (600V)	56±2	56±2	56±2	56±2		56 ± 2
M (700V)	149±4	148±4	148±4	149±4		149 ± 4
M (800V)	396±11	397±11	396±11	399±11		397 ± 11
M (900V)	1075±30	1075±30	1088±31	1084±31		1080 ± 31

Table A-3 Measured mean lineal energy ($\bar{y}_D$) in ^{137}Cs fields with different equivalent dose rates for detector **A**. The results are presented with statistical uncertainties.

Source	Cs(3609)					Cs(3740)	Cs(3739)
H(10)* [µSv/h]	1018±31	1468±44	2298±69	4092±128	7618±229	517±16	58.8±1.8
Distance [m]	3±0.01	2.5±0.01	2±0.01	1.5±0.01	1.1±0.01	1.5±0.01	1.5±0.01
$\bar{y}_D$ (600V)		1.720±0.025					
$\bar{y}_D$ (700V)	1.670±0.025	1.628±0.024	1.651±0.024	1.57±0.023	1.682±0.025	1.634±0.024	1.815±0.027
$\bar{y}_D$ (800V)		1.621±0.024					
$\bar{y}_D$ (900V)	1.634±0.024	1.673±0.025	1.615±0.024	1.659±0.024	1.644±0.024	1.613±0.024	1.627±0.024
average - $\bar{y}_D$	1.647±0.024						

Table A- 4 Measured mean lineal energy ($\bar{y}_D$) in ^{137}Cs fields with different equivalent dose rates for detector **B**. The results are presented with statistical uncertainties.

Source	Cs(3609)			Cs(3740)	Cs(3739)
H(10)* [µSv/h]	1468±44	2298±69	4092±128	517±16	58.8±1.8
Distance [m]	2.5±0.01	2±0.01	1.5±0.01	1.5±0.01	1.5±0.01
$\bar{y}_D$ (700V)	1.686±0.025	1.672±0.025	1.779±0.026	1.742±0.026	1.649±0.024
$\bar{y}_D$ (900V)	1.708±0.025	1.681±0.025	1.689±0.025	1.683±0.025	1.695±0.025
average - $\bar{y}_D$	1.703 ± 0.025				

Table A-5 Detector A: Measurements of H^* for different applied voltages and different calibration factors, *N,* in the field of three ^{137}Cs sources at different dose equivalent rates. *Diff* denotes $\frac{H^* - H^*(10)}{H^*(10)}$.

N	Source	Cs(3739)			Cs(3740)			Cs(3609)		
	H(10)* [µSv/h]	58.8±1.8			517±16			7618±229		
	Distance [m]	1.5±0.01			1.5±0.01			1.1±0.01		
	Voltage [V]	*H** [µSv/h]	$R_{H^*(10)}$	*Diff* [%]	*H** [µSv/h]	$R_{H^*(10)}$	*Diff* [%]	*H** [µSv/h]	$R_{H^*(10)}$	*Diff* [%]
0.9842	700	59.9±3.1	1.02	1.9	510±27	0.99	-1.4	7634±397	1.02	0.2
	900	58.8±3.0	1.00	0.0	512±27	0.99	-0.9	7629±396	1.00	0.2
1.0001	700	59.6±3.1	1.01	1.4	500±26	0.97	-3.3	7523±391	1.01	-1.2
	900	57.7±3.0	0.98	-1.9	502.26	0.98	-2.9	7495±389	0.98	-1.6

Table A-5 Continued

N	Source	Cs(3609)			Cs(3609)		
	H(10)*[µSv/h]	4092±128			2298±69		
	Distance [m]	1.5±0.01			2.0±0.01		
	Voltage [V]	*H** [µSv/h]	$R_{H^*(10)}$	*Diff* [%]	*H** [µSv/h]	$R_{H^*(10)}$	*Diff* [%]
0.9842	700	4041±210	0.99	-1.2	2273±118	0.99	-1.1
	900	4094±213	1.00	0.0	2279±119	0.99	-0.8
1.0001	700	3946±205	0.96	-3.6	2233±116	0.97	-2.8
	900	4027±209	0.98	-1.6	2234±116	0.97	-2.8

Table A-5 Continued

N	Source	Cs(3609)			Cs(3609)		
	H(10)*[µSv/h]	1468±44			1018±31		
	Distance [m]	2.5±0.01			3.0±0.01		
	Voltage [V]	*H** [µSv/h]	$R_{H^*(10)}$	*Diff* [%]	*H** [µSv/h]	$R_{H^*(10)}$	*Diff* [%]
0.9842	600	1469±76	1.00	0.1			
	700	1445±75	0.98	-1.6	1001±52	0.98	-1.7
	800	1448±75	0.99	-1.4			
	900	1459±76	0.99	-0.7	1006±52	0.99	-1.2
1.0001	600	1452±75	0.99	-1.1			
	700	1417±74	0.97	-3.5	985±51	0.97	-3.2
	800	1420±74	0.97	-3.3			
	900	1436±75	0.98	-2.2	987±51	0.97	-3.0

Table A- 6 Detector B: Measurements of H^* for different applied voltages and different calibration factors, *N,* in the field of three ^{137}Cs sources at different dose equivalent rates. *Diff* denotes $\frac{H^* - H^*(10)}{H^*(10)}$.

N	Source	Cs(3739)			Cs(3740)			Cs(3609)		
	H(10)* [µSv/h]	58.8±1.8			517±16			4092±128		
	Distance [m]	1.5±0.01			1.5±0.01			1.5±0.01		
	Voltage [V]	H^* [µSv/h]	$R_{H^*(10)}$	*Diff* [%]	H^* [µSv/h]	$R_{H^*(10)}$	*Diff* [%]	H^* [µSv/h]	$R_{H^*(10)}$	*Diff* [%]
0.978	700	58.8±3.1	1.00	0.0	511±26	0.99	-1.2	4049±210	0.99	-1.0
	900	59.3±3.1	1.01	0.9	518±27	1.00	0.2	4075±212	1.00	-0.4
0.991	700	58.8±3.1	1.00	0.3	511±26	0.98	-1.7	4073±212	1.00	-0.5
	900	59.3±3.1	1.01	0.7	518±27	1.00	0.1	4076±212	1.00	-0.4

Table A-6 Continued

N	Source	Cs(3609)			Cs(3609)		
	H(10)* [µSv/h]	2298±692			1468±44		
	Distance [m]	2.0±0.01			2.5±0.01		
	Voltage [V]	H^* [µSv/h]	$R_{H^*(10)}$	*Diff* [%]	H^* [µSv/h]	$R_{H^*(10)}$	*Diff* [%]
0.978	700	2259±117	098	-1.7	1445±75	0.98	-1.6
	900	2283±119	0.99	0.7	1462±76	1.00	-0.4
0.991	700	2253±117	098	-2.0	1443±75	0.98	-1.7
	900	2279±118	0.99	-0.9	1460±76	0.99	-0.6

A.2 Uncertainty considerations for the Sievert Instrument

All uncertainties discussed in this work refer to standard uncertainties evaluated as type A or type B according to the ISO-guide [ISO95]. The results in all tables of chapter 3 are only presented with an estimated statistical uncertainty with the exception of the presentation of the dose equivalent, which is given with a standard uncertainty of the combination of type A and B.

The uncertainty due to combined detector and electronic noises in $\bar{y}_D$ is estimated to less than 2% in a low LET field and even less in a high LET field for signals above 1 pA [Kyl01b]. The contribution of this uncertainty in the quality factor is less than 1%. The statistical uncertainty in $\bar{y}_D$ is estimated to be less than 5% in a static calibration field. The statistical uncertainty of the dose is assumed to be less than 2%.

Contributions of type B are coming from the calibration 5% (1σ), temperature dependence 1% (1σ), (W/e)-value 5% (1σ) and approximations of the method to ICRP 60 *Q(L)* values of 10%[Kyl01c]. Type A and B sum up together to 13.5% to the measured dose equivalent.

Table A- 7 Standard uncertainties of 1h measurements

Type	A(%)	B(%)
Dose	2	
Quality factor	5	1
Calibration (source, distance, etc.)		5
Temperature		1
W/e –factor		5
Approximations in method		10
A & B (%)	**13.5**	

Appendix B

Uncertainty calculations for the graphite chamber type G5

The uncertainties are calculated according to the "Guide to the Expression of Uncertainty in Measurement" [ISO95] and the EA recommendations [EA99].

B.1 Uncertainty considerations at the calibration

1. The calibration of a pen-like chamber type G5 (serial number 8) was carried out with a ^{137}Cs source (No.3609) in CERN calibration laboratory. The detector was irradiated in different distances to obtain certain dose equivalents. The charge was collected by a PTW-UNIDOS electrometer (CERN-No.07077). The chamber was supplied via electrometric cables with a power supply (ORTEC MODEL 456, 0-3kV). The working voltage of –20V was monitored with a KEITHLEY 197 AUTORANGING MICROVOLT DMM. Before every measurement a zero-adjustment was done.

2. We assume that the calibration factor K can be expressed as:

$$K = \frac{M + \delta m + \delta d + \delta k_{el} + \delta k_{p,T,h}}{H^{*}(10)} + \delta H^{*}$$

where the variables signify:

- M - reading of the electrometer
- δm - observed difference for readings
- δd - displacement correction
- δk_{el} - correction for electrometer
- $\delta k_{p,T,h}$ - correction for pressure, temperature and humidity to the chamber
- δH^* - uncertainty of ambient dose equivalent of source

All corrections are supposed to be distributions with mean zero and a certain standard deviation which expresses the uncertainty to which this correction is known.

Calibration factor (K): The calibration factor is the ratio of the charge measured and the source strength including all uncertainties.

Statistical uncertainty for readings (δm): The observed differences of the charge readings of the chamber at certain $H^*(10)$ gives a standard uncertainty for the readings, which is of statistical nature.

Displacement (δd): The standard uncertainty according to positioning of the chamber is estimated to be within ±0.005m. ($\delta d = 2r^{-1}dr$)

PTW-electrometer(δk_{el}): Following uncertainties are given by the manufacturer's literature [PTW98]:

Resolution: ±0.2 %
Zero Drift: <±0.2 %
Long-term stability: <±0.5 % per year
Stabilization Time: <±0.5 %
Temperature: <±0.5 %
Humidity: <±0.5 %
Stray radiation effect: <±0.5 %
Battery condition: <±0.5 %
Mains voltage and frequency: <±0.5 %

This results in an overall uncertainty for the electrometer of $(1.35/\sqrt{3}) = 0.8$ %.

Source: The standard uncertainty for sources in the CERN calibration laboratory are estimated to be <= 3%[2,3].

Temperature, pressure, humidity ($\delta k_{p,T,h}$): No corrections are made for temperature and humidity changes effecting the chamber due to the controlled climate of the laboratory.

Correlation: None of the input quantities are considered to be correlated to any significant extent.

3. Five measurements are made to record the charge q. Before every measurement a zero-adjustment was done. The standard deviation of these five measurements yields δm:

arithmetic mean:	-3.646 pC
standard deviation:	0.28 pC
standard uncertainty:	0.13 pC
standard uncertainty in percent:	3.4 %

4. Uncertainty budget:

Quantity X_i	Estimate X_i	Standard uncertainty $u(x_i)$	Probability Distribution	Sensitivity Coefficient c_i	Uncertainty Contribution $u_i(y)$	Uncertainty Contribution $u_i(y)$ [%]
$M, \delta m$	-3.646 pC	0.13 pC	normal	1	0.13 pC	3.4
δd	1.784 m	0.005 m	normal	4.084 pC/m	0.020 pC	0.56
δk_{el}	-	0.028 pC	rectangular	1	0.028pC	0.78
δH^*	50µSv	2 µSv	normal	0.055 pC/µSv	0.109 pC	3
$\delta k_{p,T,h}$	-	-	normal	1	-	-
K	-1.31 pC/µSv				0.070 pC/µSv	4.66

5. Reported result:

The determined uncertainty of the calibration factor K for the G5 chamber is $u_{cal} = 4.66\%$.

B.2 Uncertainty considerations for the evaluation of the photon-contribution of the ^{238}Pu-Be source

For the measurements with the G5 chamber the same set up as during the calibration was used. The unknown photon-contribution and its uncertainty is obtained from the following procedure:

(1) The charge was collected five times after zeroing of the chamber at certain distances *d*, respectively. This delivered for the measurements a statistical uncertainty per percent u_{stat}.

(2) For each measurement point was considered an uncertainty due to the electrometer and the distance of u_1=*1%***.**

(3) The uncertainty for each measurement point u_m then was given by

$$u_m = \sqrt{u_{stat}^2 + u_1^2}$$

(4) Each measurement point together with its uncertainty was then plotted and a trend line was added using the program Origin 6.0. As a result of the trend line we got the value for the intercept and its uncertainty u_{int}.

(5) The value obtained for the intercept divided by the calibration factor of the chamber delivered the photon-contribution of the ^{238}Pu-Be source. The standard uncertainty u_{tot} was calculated by:

$$u_{tot} = \sqrt{u_{int}^2 + u_{cal}^2}$$

Appendix C

Results obtained in the CERF-field

C.1 HANDI-TEPC

Table C-1 Main dosimetric parameters per PIC count for the HANDI-TEPC in several positions. *Q* denotes the radiation quality factor according to ICRP 60. The presented results are from the CERF runs of the year 2002.

Position	Average Intensity PIC counts per spill	*Q*	*D* per PIC count [pGy/PIC]	*H** per PIC count [pSv/PIC]
CT02	6308±149	4.0±0.4	74±7	292±30
CT03	4096±96	4.2±0.5	71±7	300±33
CT04	4046±157	4.3±0.5	58±6	250±28
CT06	8420±259	4.2±0.4	84±8	354±36
	6213±228	3.9±0.4	97±10	376±39
	4098±140	3.7±0.4	109±11	398±42
	2074±112	2.9±0.3	141±14	415±45
	959±78	2.2±0.2	211±21	469±52
CT07	7956±163	4.2±0.4	79±8	336±35
CT08	8206±226	4.2±0.4	68±7	286±30
	5963±179	3.9±0.4	79±8	304±32
	4059±44	3.7±0.4	87±9	326±36
	2102±76	2.7±0.3	122±12	334±37
	1029±47	2.2±0.2	192±19	416±46
CT10	8344±224	4.3±0.4	83±8	355±36

Table C–1 Continued

Position	Average Intensity PIC counts per spill	*Q*	*D* per PIC count [pGy/PIC]	*H** per PIC count [pSv/PIC]
CS01	6162±88	4.3±0.4	49±5	212±22
CS02	6270±107	4.7±0.5	109±11	510±52
	3829±98	4.3±0.5	107±11	464±49
	1854±66	4.6±0.5	111±11	513±56
	689±87	4.2±0.5	114±12	482±59
	403±45	4.5±0.6	112±11	505±62
CS03	6225±198	4.9±0.5	98±10	479±49
	3723±125	4.9±0.5	99±10	482±51
	1046±68	4.6±0.5	98±10	453±53
	184±22	5.0±0.6	104±10	522±57
CS04	6147±156	4.9±0.5	77±8	377±39
	4153±176	5.0±0.5	76±8	378±40
CS06	6684±201	4.6±0.5	79±8	365±38
CS07	6698±136	5.0±0.5	71±7	357±36
CS08	6666±172	5.1±0.5	58±6	297±31
	5378±159	5.3±0.6	59±6	313±36
IT02	266±18	3.0±0.3	504±51	1497±167
IT05	1410±161	6.3±0.7	210±21	1327±137
	1183±179	6.1±0.6	225±23	1363±142
	646±45	4.3±0.5	365±37	1569±167
	247±28	2.3±0.2	924±93	2068±223
IT06	1466±98	6.9±0.7	220±22	1523±157
	1198±168	6.2±0.7	238±24	1482±155
	662±76	4.5±0.5	383±38	1726±184
	235±31	2.8±0.3	729±73	2047±231
IT07	265±35	2.6±0.3	1044±105	2721±285
IT09	1456±43	6.8±0.7	179±18	1212±126
	1242±9	5.3±0.6	269±27	1420±148
	670±51	4.9±0.5	277±28	1365±142
	263±4	2.3±0.2	853±85	1929±203
IT10	235±37	2.9±0.3	759±76	2187±240
IT13	265±29	1.8±0.2	1129±113	1979±207

C.2 Recombination chamber

Table C-2 Main dosimetric parameters per PIC count for the recombination chamber in several positions. Q_4 denotes the radiation quality factor according to ICRP 21. In order to approximate the Q-LET-relationship from ICRP 60, Golnik introduced Q_{4new}, however its results are identical to the ICRP21-procedure of Q_4<5, which is here the case. The presented results are from the CERF runs of the year 2002.

Position	Average Intensity PIC counts per spill	Q_4	D per PIC count [pGy/PIC]	H^* per PIC count [pSv/PIC]
CT02	5984±34	3.6±0.5	90±1.1	327±45
	3987±17	3.7±0.7	99±2.4	363±67
	2044±210	3.5±0.7	120±2.5	422±82
	951±104	3.3±0.7	176±2.1	577±125
CT02 – no target	2048±210	2.3±1.3	42±2.3	97±53
	5686±652	2.3±1.3	15±0.5	34±19
CT05	6389±265	3.3±0.5	138±1.7	455±62
CT06	8551±147	3.7±0.5	115±1.4	427±57
CS03	6340±105	3.8±0.5	131±1.6	502±68
CS04	6409±125	3.9±0.5	110±1.3	433±60
	6191±126	4.5±0.6	110±1.7	497±71
	3826±97	4.0±0.6	107±1.6	424±61
	1927±48	4.2±0.6	109±1.3	457±65
	1043±32	3.6±0.7	109±1.6	391±73
IT02	1579±289	8.0±1.1	201±3	1612±226
	677±116	5.2±0.7	337±4	1757±238
	233±6	3.3±0.5	605±11	1987±331
IT02 – no target	229±5	2.6±0.9	414±10	1068±371
IT05	272±4	2.8±0.4	915±11	2544±396
IT05 – no target	271±6	1.4±0.4	621±9	892±256
IT06	264±8	2.2±0.4	1321±24	2902±589
	268±6	2.8±0.4	950±12	2693±378
	1236±27	5.4±0.7	405±5	2166±299
IT09	1411±57	5.7±0.8	267±3	1530±209
IT10	268±4	3.1±0.4	819±10	2505±341
	269±8	2.8±0.4	1072±13	3008±433
	1238±27	5.6±0.8	371±4	2086±281

C.3 Sievert Instrument

Table C-3 Main dosimetric parameters per PIC count for the Sievert Instrument in several positions. The quality factor, $\overline{Q}_D$, was evaluated according to $\overline{Q}_D = 0.88 + 0.09\overline{y}_D$. The presented results are from the CERF runs of the year 2002.

Position	Average Intensity PIC counts per spill	$\overline{Q}_D$	*D* per PIC count [pGy/PIC]	*H** per PIC count [pSv/PIC]
CT04	6342±183	3.5±0.8	70±1	242±28
	4238±30	3.5±0.8	73±1	255±30
CT05	4156±18	3.3±0.7	117±2	379±43
CT06	8134±58	3.3±0.8	121±2	404±46
	5963±90	3.3±0.7	130±3	430±49
	4097±95	2.8±0.6	137±3	387±42
	2102±72	2.3±0.4	185±4	428±41
	1029±55	2.1±0.4	274±5	583±54
CT08	8237±95	3.5±0.8	93±2	321±35
	6388±168	3.3±0.7	100±2	328±37
	4137±175	3.1±0.7	108±2	332±37
	2074±150	2.3±0.4	161±3	363±35
	959±66	2.1±0.4	250±5	512±46
CT09	4134±123	2.9±0.6	135±3	389±42
CT10	8111±128	3.8±0.9	122±2	469±56
	5948±21	3.8±0.9	132±3	497±59
	3983±65	3.6±0.8	147±3	521±61
	2102±78	3.3±0.7	190±4	619±71
	994±49	2.3±0.4	275±6	633±62

Table C-3 Continued

Position	Average Intensity PIC counts per spill	*Q*	*D* per PIC count [pGy/PIC]	*H** per PIC count [pSv/PIC]
CS01	6460±14	3.7±0.9	123±2	456±54
CS02	6329±217	4.0±0.9	130±3	514±62
	3920±192	4.1±1.0	129±3	530±65
	1949±60	4.0±0.9	132±3	523±63
	1056±6	3.9±0.9	129±3	502±60
CS03	6758±124	4.0±1.0	117±2	472±57
	6203±216	3.9±0.9	117±2	461±56
	3926±248	3.9±0.9	120±2	468±56
	2038±187	3.8±0.9	119±2	451±54
	1038±20	3.9±0.9	116±2	455±55
CS04	6046±226	4.1±1.0	94±2	383±46
	3926±198	4.0±1.0	88±2	353±43
CS06	6470±145	3.9±0.6	93±2	366±44
CS07	6391±117	4.1±1.0	85±2	345±42
	3870±134	4.3±1.0	85±2	364±45
	1914±50	4.0±1.0	86±2	348±42
	1061±37	3.7±0.9	86±2	322±38
CS08	6460±14	4.1±1.0	67±1	276±34
IT02	1254±36	4.7±0.6	218±4	1031±70
	266±24	2.1±0.2	789±16	1674±90
IT05	1478±68	5.1±0.7	249±5	1280±88
	1209±45	4.3±0.6	274±5	1178±79
	667±89	3.3±0.4	436±9	1457±92
	208±13	2.1±0.2	1232±25	2550±136
IT06	1422±27	5.0±0.7	274±5	1365±93
	1190±33	4.8±0.6	291±6	1398±95
	649±62	3.4±0.4	470±9	1618±102
	229±28	1.8±0.2	1022±20	1810±87
IT07	270±9	1.8±0.2	1177±24	2071±99
IT09	268±16	1.8±0.2	1029±21	1849±90
IT10	1450±40	6.9±1.0	255±5	1751±127
	1222±45	5.8±0.8	304±6	1741±123
	658±13	5.0±0.7	397±8	2002±139
	233±6	3.4±0.4	768±15	2626±168
IT11	270±11	2.3±0.2	1027±21	2327±129

C.4 Argon-filled chamber

Table C-4 Main dosimetric parameters per PIC count for the argon-filled chamber in several measurement positions. The presented results are from the CERF runs of the year 2002.

Position	Average Intensity PIC counts per spill	H^* per PIC count [pSv/PIC]
CT06	1045±6	217±11
CT07	8096±43	78±4
	3986±14	108±5
	2087±3	145±7
	944±9	229±11
CT07-no target	5878±18	26±1
	2089±5	73±4
CT08	2940±75	118±6
	2013±10	132±7
CT11	5984±20	101±5
	3989±11	115±6
	2085±4	156±8
	1034±4	240±12
CT11-no target	5939±64	27±1
	2081±8	76±4
CS01	6495±58	95±5
CS02	6400±79	96±5
CS03	6405±91	91±5
	3996±57	91±5
	2064±26	92±5
	1059±10	94±5
	391±5	98±5
CS04	6400±38	73±4
CS06	6499±90	76±4
CS07	6399±67	68±3
CS08	6458±53	51±3

Table C-4 Continued

Position	Average Intensity PIC counts per spill	H^* per PIC count [pSv/PIC]
IT01	1476±8	112±6
IT02	272±2	512±26
IT02-no target	270±4	394±20
IT05	266±3	751±38
IT06	1045±6	217±11
	270±3	764±38
IT06-no target	272±3	564±28
IT07	1428±4	160±11
	1204±2	177±9
	660±9	333±17
	231±3	816±41
IT08	1764±45	118±6
	1208±6	132±7
IT09	270±3	611±31
IT10	265±2	627±31

C.5 Hydrogen-filled chamber

Table C-5 Dose equivalent per PIC count measured with a hydrogen-filled chamber in several positions. The presented results are from the CERF runs of the year 2002.

Position	Average Intensity PIC counts per spill	H^* per PIC count [pSv/PIC]
CT06	6196±71	506±25
	3831±94	556±28
	1971±32	598±30
	1015±22	926±47
CS01	6767±67	528±26
CS02	6427±77	528±26
CS03	6511±150	501±25
	6453±93	492±25
	3971±206	512±38
	2056±34	502±25
	1053±32	503±26
	394±8	525±29
CS04	6499±86	418±26
CS06	6423±81	384±19
CS07	6114±49	338±17
CS08	6170±99	322±16
IT02	266±5	3133±158
IT05	264±6	4165±212
IT06	1250±35	2028±102
	269±4	4365±221
IT07	1241±21	2034±102
IT09	266±3	3775±189
	102±2	8786±456
IT10	258±9	3963±199

Bibliography

[Alb95] Alberts, W.G., Ambrosi, P., Böhm J., Dietze G., Hohlfeld, K., Will, W., *New Dose Quantities in Radiation Protection*, Physikalisch-Technische Bundesanstalt, PTB-Bericht Dos-23e, 1995.

[Alb99] Alberts, W.G., Alevra, A.V., Ferrari, A., Otto, T., Schrewe, U.J., Silari M., *Calibration Problems, Calibration Procedures and Reference Fields for Dosimetry in Flight Altitudes*. Radiat. Prot. Dosim. 86, p. 289-295, 1999.

[Aro93a] Aroua, A., *Some Spectrometric and Microdosimetric Results of the CERN-CEC May and July 1993 Experiments (H6M93 and H6J93),* Technical Memorandum, CERN/TIS-RP/TM/93-39, 1993.

[Aro93b] Aroua, A., Höfert, M., Sannikov, A.V., *HANDI-TEPC Results of the CERN-CEC July and September 1993 Experiments (H6J93, H6S93*), Internal Report, CERN/TIS-RP/IR/93-45, 1993.

[Aro95] Aroua, A., Höfert, M., Sannikov, A.V., *Effects of High Intensity and Pulsed Radiation on the Response of the HANDI-TEPC*, Radiat. Prot. Dosim. 61, No.1-3, p. 227-232, 1995.

[Ben03] Benedikt, M., *private communication*, CERN, 2003.

[Bir97] Birattari C., Ferrari A., Höfert M., Otto T., Rancati, T., Silari M., *Recent Results at the CERN-EC High Energy Reference Field Facility*, Proc: Satif-3 Shielding Aspects of Accelerators, Targets and Irradiation Facilities, Sendai, Japan 1997. NEA/OECD, p. 219-234, Report CERN/TIS/RP/97-12/CF, 1997.

[Boa87] Boag, J. W., *Ionization Chambers*, *The dosimetry of ionizing radiation*, vol. II, p.169ff, Academic Press, 1987.

[Cos84] Cossairt J.D., Grobe D.W., Geradi M.A., *Measurements of radiation quality factors using a recombination chamber*, Fermilab, Technical Memorandum, TM-1248 1103.00, 1984.

[Dis66] Distenfeld C.H. and Markoe A.M., *Determination of the quality factor through the utilization of a balanced, tissue equivalent, ionization chamber*, Nucl. Instr. and Meth. 45, p. 181-189, 1966.

[EA99] EA, European co-operation for Accreditation, *Expression of the Uncertainty of Measurement in Calibration*, EA-4/02, December 1999.

[Fas93] Fassò, A., Ferrari, A., Ranft, J., Sala, P.R., *FLUKA: Present Status and Future Developments*, Proc. IV Int. Conf. on Calorimetry in High-Energy Physics, La Biodola, Italy, 21-26 Sept. 1993, Ed. A. Menzione and A. Scribano, World Scientific, p. 493, 1993.

[Fas97a] Fassò, A., Ferrari, A., Ranft, J., Sala, P.R., *An Update about FLUKA*, Proc. 2nd Workshop on Simulating Accelerator Radiation Environments, CERN, Geneva, Switzerland, 9-11 Oct 1995, Ed G. R. Stevenson, CERN Report TIS-RP/97-05, p. 158-170, 1997.

[Fas97b] Fassò, A., Ferrari, A., Ranft, J., Sala, P.R., *New Developments in FLUKA Modelling Hadronic and EM Interactions*, Proc. 3rd Workshop on Simulating Accelerator Radiation Environments, KEK, Tsukuba, Japan 7-9 May 1997, Ed. H. Hirayama, KEK Proceedings 97-5, p. 32-43, 1997.

[Fer97] Ferrari, A., Rancati, T., Sala, P.R., *FLUKA Application in High-energy Problems: from LHC to ICARUS and Atmospheric showers*. Proc. 3rd Workshop on Simulating Accelerator Radiation Environments, KEK, Tsukuba, Japan 7-9 May 1997, Ed. H. Hirayama, KEK Proceedings 97-5, p.165-176, 1997.

[Gol85] Golnik, N., Pliszczynski, T., Wysocka, A., Zielczynski, M., *Determination of Dose Components in Mixed Radiation Fields by means of Recombination Chambers*, 5th Symp. Neutr. Dosim., Neuherberg (Ed. H. Schraube, G. Burger and J. Booz, Luxembourg, ISBN 92-835-5618-2, EUR 9762), p. 717-725, 1985.

[Gol88] Golnik, N., Wilczynska-Kitowska, T., Zielczynski, M., *Determination of the Recombination Index of Quality for Neutrons and Charged Particles Emloying High Pressure Ionisation Chambers*, Radiat. Prot. Dosim. 44, p. 57-60, 1988.

[Gol92] Golnik, N., Zielczynski, M., *Determination of Quality Factor in Mixed Radiation Fields using Recombination Chamber*, Kernenergie 34, p. 311-313, 1992.

[Gol93] Golnik N., *Application of recombination chamber during the September 1993 CERN-CEC experiment*, Technical Memorandum, CERN/TIS-RP/TM/93-50, 1993.

[Gol94] Golnik N., Zielczynski, M.*, Determination of Resticted LET Distribution for Mixed (n, γ) Radiation Fields by High Pressure Ionization Chambers*, Radiat. Prot. Dosim. 52(1/4), p. 35-38, 1994.

[Gol96a] Golnik N., *Recombination Methods in the Dosimetry of Mixed Radiation*, Raport IAE – 20/A, Institute of Atomic Energy, Otwock-Swierk, 1996.

[Gol96b] Golnik N., Zielczynski M., *The concept of RIQ and its adaptation to recent recommendations of ICRP for external neutron fields*, Nukleonika 41(2), p. 119-126, 1996.

[Gol98] Golnik N., *Characterization of CERN-EU High Energy Reference Radiation fields with Recombination Chamber*, Raport IAE-34/A, Institute of Atomic Energy, Otwock-Swierk, 1998.

[Gol99] Golnik N., Silari, M., Otto, T., *On the Use of a Recombination Chamber for Radiation Measurements in CERN-EU High Energy Reference Radiation Fields*, Radiat. Prot. Dosim. 86, p. 175-179, 1999.

[Gol02b] Golnik, N., *private communication*, 2002

[Gol03] Golnik, N., *private communication*, 2003

[Höf94] Höfert, M., Stevenson, G.R., The CERN-CEC High-energy Reference field facility, Proc: 8th International Conference on Radiat. on Shielding, Arlington, Texas, April 1994. American Nuclear Society, Inc., p. 635-642, 1994.

[ICR73] ICRP, International Commission on Radiological Protection*, Recommendations of the ICRP*, Publication 21, Supplement to ICRP 15, Pergamon Press, 1973.

[ICR77] ICRP, International Commission on Radiological Protection*, Recommendations of the ICRP*, Publication 26, Annals of the ICRP 1, No.3, Pergamon Press, 1977.

[ICR83] ICRU, International Commission on Radiation Units and Measurements, *Microdosimetry*, ICRU Report 36, Bethesda, Maryland, 1983.

[ICR90] ICRP, International Commission on Radiological Protection, *Recommendations of the ICRP*, Publication 60, Annals of the ICRP 21, No.1-3, Pergamon Press, 1990.

[ICR93] ICRU, International Commission on Radiation Units and Measurements, *Quantities and Units in Radiation Protection Dosimetry*, ICRU Report 51, Bethesda, Maryland, 1993.

[ICR95] ICRP, International Commission on Radiological Protection, *Recommendations of the ICRP*, Publication 74, Pergamon Press, 1995.

[IAE88] IEAE, International Atomic Energy Agency, *Radiological Safety Aspects of the Operation of Proton Accelerators*, Technical reports series No. 283, Vienna, 1988.

[IAE00] IEAE, International Atomic Energy Agency, *Absorbed Dose Determination in External Beam Radiotherapy*, *An International Code of Practice for Dosimetry Based on Standards of Absorbed Dose to Water*, Technical reports series No. 398, Vienna, 2000.

[ISO95] ISO, International Standards Organisation, *Guide to the Expression of Uncertainty in Measurement*, Switzerland, 1995.

[ISO01] ISO, International Standards Organisation, *Reference neutron radiations: calibration of area and personal dosimeters and the determination of their response as a function of photon energy and angle of incidence*, ISO Report 8529 1-1. 1999-2001.

[Lim97] Lim T., Bottollier-Depois, J.F., Festag, J.G., Golnik, N., Grillmaier, R.E., Höfert, M., Lindborg, L., *Tissue-equivalent proportional counters in a high-energy neutron field at CERN*, SPIE Vol.2867, p. 300-305, 1997.

[Kel84] Kellerer, A.M., Rossi, H. H., *On the determination of Microdosimetric Parameters in Time-Varying Radiation Fields: the Variance-Covariance Method.* Radiat. Res. 97, p.237-245, 1984.

[Kel85] A. M. Kellerer, *Fundamentals of Microdosimetry in The Dosimetry of Ionising Radiation*, Ed. K. R. Kase, B. E. Bjärngard and F. H. Attix, Academic Press, Vol. 1, Chapter 2, p. 77, 1985.

[Kun92] Kunz, A., Arend, E., Dietz, E., Gerdung, S., Grillmaier, R.E., Lim, T., Pihet, P., *The Homburg Area Neutron Dosemeter HANDI: Characteristics and Optimisation of the Operational Instrument*, Radiat. Prot. Dosim. 44 , No.1/4, p. 213-218, 1992.

[Kyl97] Kyllönen, J.-E., Lindborg, L., Samuelson, G., *Paired TEPC for Variance Measurements. In: Microdosimetry: An Interdisciplinary Approach,* Eds D. Goodhead, P. O'Neil, and H.G. Menzel (The Royal Society of Chemistry, Cambridge) Special Publication No 204, 1997.

[Kyl01a] Kyllönen, J.-E., Lindborg, L., Samuelson, *Cosmic Radiation Measurements Onboard Aircraft with the Variance Method*, Radiat. Prot. Dosim. 93(3), p. 197-205, 2001.

[Kyl01b] Kyllönen, J.-E., Lindborg, L., Samuelson, *The Response of the Sievert Instrument in Neutron Beams up to 180 MeV*, Radiat. Prot. Dosim. 94(3), p. 227-232, 2001.

[Kyl01c] Kyllönen, J.-E., Grindborg, J.-E., Lindborg, L., *Response Investigations of TEPC in High Energy Proton and Neutron Beams Using the Variance Method*, Presented at 13th Symposium on Microdosimetry in Stresa, Italy, May 2001.

[Kyl02a] Kyllönen, J.-E., Mayer, S., Response Investigations of the Sievert Instrument in Neutron Beams between 0.5 and 19 MeV at PTB, Internal Report, CERN-TIS-2002-037-RP-IR, 2002.

[Kyl02b] Kyllönen, J.E., *private communication*, 2002.

[May02a] Mayer, S., Zielczynski, M., M^{c}Lay, F., Dimovasili, E., Otto, T., *Measurements with a Recombination Chamber made at the CERN-EC High Energy Reference Field, CERF, in August 2001,* Technical Note, CERN/TIS-RP/TN/2002-03

[May02b] Mayer, S., Dimovasili, E., Otto, T., *Further Investigations of the Recombination Chamber REM-2 as a Mixed Field Dosimeter at CERF in October 2001*, Technical Note, CERN/TIS-RP/TN/2002-06

[May02c] Mayer, S., Otto, T., *Investigations of a Recombination Chamber as a Mixed Field Dosimeter in Comparison with a Tissue-Equivalent Proportional Counter at CERF*, in Proc: RMA, 10th Symp. On Radiation Measurements and Applications, Ann Arbor, Michigan, USA, 21-23 May 2002. Divisional Report CERN-TIS-2002-015-RP-CF, (Nucl. Instr. and Meth. A (in press)

[May02e] Mayer, S., Otto, T., Golnik, N., *Determination of the Photon-Contribution of a ^{238}Pu-Be Source*, in Proc: IRRMA-V, 5th Internat. Topical Meeting on Industrial Radiat. And Radioisotope Measurement Applications, Bologna, Italy, 9-14 June 2002. Divisional Report CERN-TIS-2002-014-RP-CF, Nucl. Instr. and Meth. B (in press)

[May02f] Mayer, S., Golnik, N., Otto, T., Carbonez, P., *The Photon-Contribution of the ^{238}Pu-Be Source in the TIS-RP Calibration Laboratory,* Internal Report, CERN-TIS-2002-036-RP-IR, 2002.

[Men89] Menzel, H.G., Lindborg, L., Schmitz, Th., Schuhmacher, H., Waker, A.J., *Intercomparison of Dose Equivalent Meters based on Microdosimetric Techniques: Detailed Analysis and Conclusions*, Radiat. Prot. Dosim., 29 No.1/2, p. 55-68, 1989.

[Mit02] Mitaroff, A. and Silari, M. *The CERN-EU High-Energy Reference Field (CERF) Facility for Dosimetry at Commercial Flight Altitudes and in Space*. CERN-TIS-2001-006-RP-PP, 2001, Radiat. Prot. Dosim., 102 No.1, p. 7-22, 2002.

[McL01] M^{c}Lay, F., Mayer, S., Otto, T., *Characterisation of the CERN REM-2 recombination chambers,* Technical Memorandum, CERN/TIS-RP/TM/2001-038, 2001.

[McC81] McCaslin, J.B., Thomas, R.H., *Practical neutron dosimetry at high energies, Radiation Protection quantities for External Exposure* (Burger, G., Harder, D., Kramer, R., Wagner, S., Eds), Rep. EUR-71-1-EN, p.137, Harwood Academic Publishers, Chur, Switzerland, 1981.

[Mul02] Muller, A., Pangallo, M., Perrin, D., Otto, T., Rettig, M., *Preliminary assessment of radiation measuring equipment in framework of the RAMSES project*, Technical Note, CERN-TIS-2002-032-RP-TN, 2002.

[Nac72] Nachtigall, D., Burger, G., *Dose Equivalent Determination in Neutron fields*, in Topics in Radiation Dosimetry, Attix, F., Ed. (Academic Press, New York), pages 385-459, 1972.

[Nav97] Nava, E., Otto, T., Silari, M. *Reference Dose Equivalent Values for the 1997 CERN-EC Runs*. Technical Memorandum, CERN TIS-RP/TM/97-22, 1997.

[NCR91] NCRP, National Council on Radiation Protection and Measurements, *Calibration of Survey Instruments used in Radiation Protection for the Assessment of Ionizing Radiation Fields and Radioactive Surface Contamination*, NCRP report, no.112, 1991.

[Ott98] Otto T., *Application of International Standard ISO10647 to CERN's Neutron Calibration Filed*, CERN/TIS-RP/TM/98-19, 1998.

[Ott99a] Otto T., *Traceability to International Standards of CERN's Calibration Sources*, Internal Report, CERN/TIS/IR/99-05, 1999.

[Ott99b] Otto, T., *private communication*: Modified version of the evaluation program of the HANDI-TEPC, 1999.

[Ott02] Otto T., *Preliminary Simulation Results for the Sensitivity of Centronic High-pressure Ionisation Chambers*, Technical Note, CERN/TIS/TN/2002-011, 2002.

[Ott03] Otto T., *private communication*, 2003.

[Pol73] Polon, *Recombination Chamber Type REM-2*, Technical manual, Metronex-Warsaw, Poland, 1973.

[PTW98] PTW-UNIDOS, *Instruction Manuel-Universal Dosemeter*, Firmware No. 2.20, PTW-Freiburg, 1998.

[Roe93] Roesler S., Stevenson G.R., *July 1993 CERN-CEC Experiments: Calculation of Hadron Energy Spectra from Track-Length Distribution using FLUKA*. CERN/TIS-RP/IR/93-47, 1993.

[Rus98] Rusinowski Z., Golnik N., *Performance tests of the IAE dose equivalent meter in radiation field of high energy calibration facility at SPS-CERN*, Nucl. Instr. and Meth. A, 408, 600-602, 1998.

[San94] Sannikov, A.V., *HAN93 Program for Evaluation of Dosimetric Values and Microdosimetric Distributions from HANDI-TEPC Measurement Data*, Internal Report, CERN/TIS-RP/IR/94-03, 1994.

[Sul63] Sullivan, A.H., Baarli, J., *An Ionization Chamber for the Estimation of the Biological Effectiveness of Radiation*. CERN-Report-63-17, 1963.

[Sul69] Sullivan A.H., *The estimation of the distribution of energy loss of ionizing radiation from observations of the initial recombination of the ions in a gas*, CERN 69-1, 1969.

[Wah01] Wahl W., *αβγ-Table – Radionuclide-Handbook – for Laboratory Workers in Spectrometry, Radiation Protection and Medicine*, Institute for Spectrometry and Radiation Protection, p. 105, 2001.

[Wak85] Waker, A. J., *Principles of Experimental Microdosimetry*, Radiat. Prot. Dosim. 61(4), p. 297-308, 1995.

[www02] Website of the AB Divisions (PS Divisions) Operation Group (internal) http://srv1ps.cern.ch/psop/ComplexPS/beamref.html, 2002.

[Zie62] Zielczynski, M., *Use of Columnar Recombination for Determination of Relative Biological Efficiency of Radiation*, Nukleonika 7, 175-182, 1962.

[Zie80] Zielczynski, M., Golnik, N., Makarewicz, M., Sullivan, A.H., *Definition of Radiation Quality by Initial Recombination of Ions*, in: 7th Symp. on Microdosimetry, EUR 7147, Eds J. Booz, H. G. Ebert and H.D. Hartfield (Luxembourg: CEC), 853-862,1980.

[Zie92] Zielczynski M., Golnik N., *Investigation of REM-2 Recombination Chambers at CERN Calibration Laboratory, CERN Report*, TIS-RP/TM/92-32, 1992.

[Zie94] Zielczynski M., Golnik N., *Recombination Index of Quality – Measuring and Applications,* Radiat. Prot. Dosim., 52, 419-422, 1994.

[Ziel96] Zielczynski M., Golnik N., Rrusinowski, Z., *A Computer Controlled Ambient Dose Equivalent Meter Based on a Recombination Chamber*, Nucl. Instr. and Meth. A, 370, p. 563-567, 1996.

[Zie99] Zielczynski M., Golnik N., *Dosimetry of TRIGA Reactor Fields using High Pressure Ionization Chambers,* Raport IAE-61/A, ISSN 1232-5317, Institute of Atomic Energy, Otwock-Swierk, 1999.

[Zie00] Zielczynski M., Golnik N., *Microdosimetry for Neutron Capture Therapy Using Recombination Chamber,* Proc. Ninth Int. Symp. On Neutron Capture Therapy for Cancer, October 2-6, Osaka, Japan, p. 81-82, 2000.

[Zie01] Zielczynski, M., *private communication*, 2001.

Acknowledgements

First of all I want to thank Prof. Hannes Aiginger, my supervisor at the Vienna University of Technology, for his support during my doctoral studies. I would not have been able to finish this thesis without his constant encouragement. Furthermore, I wish to express my gratitude for giving me the possibility to write my thesis in the stimulating environment of CERN.

I would like to thank Thomas Otto, my supervisor at CERN, who taught me a lot in many fruitful discussions about radiation physics. He always encouraged me in my scientific work and was a constant source of inspiration.

I am very grateful to Hans Menzel, who showed a lot of interest in my work. I learnt a lot by his helpful criticism and valuable suggestions. Many thanks to him for a very careful reading of the manuscript.

Furthermore, I would like to express my sincere thanks to Natalia Golnik and Mietek Zielczynski, who I really admire for their competence and dedication. Even during their holidays they were ready to deal with my questions and to give helpful advice.

I am also indebted to Jan Erik Kyllönen and Lennart Lindborg, who made it possible for me to use the Sievert Instrument for my work. Especially, I want to thank Jan Erik for many valuable discussions and the excellent collaboration.

I also do not want to miss many fruitful discussions with my friends and colleagues at the AI in Vienna, Thomas Berger and Michael Hajek.

Further thanks are addressed to the whole staff of the Radiation Protection Group at CERN. I am especially thankful to Doris Forkel-Wirth for her selfless support. Many thanks to the "girls" on my corridor, Luisa Ulrici, Joanne Madden and Antonella Vignes, who always provided a good atmosphere. Thanks also go to Isabel Brunner, Pierre Carbonez, Evangelia Dimovasili, Hubert Müller, Daniel Perrin and Markus Rettig for their support and help.

ACKNOWLEDGEMENTS

There are a lot of people who are responsible for so many unforgettable moments at CERN. Most importantly I would like to mention Claudia and Andi ("The Big B"), who were always there to rely on. A lot of fun was provided by the Austrian gang with German support: Axl, Christian, Christoph, Daniel, Edda, Harald I., Karsten, Manfred, Martin, Stefan, Werner. Thanks to Katharina and Martin for showing me how much fun running can be and to Ingrid for countless hours we spent together swimming and chatting. Last but not least I am very grateful to Angela and Hannes for their friendship and for explaining to me "savoir vivre" in Geneva.

I would like to address many thanks to Julia, Nina, Michael, Tante Christa and Onkel Karli for the short but intense moments we spent together during my stays back in Vienna. I missed them a lot in Geneva.

I am grateful to the Austrian Ministry of Science for the financial support, which made my stay at CERN possible.

Most importantly I want to thank my parents. I am very grateful to my mother for the good times we had together. I will always carry her memory in my heart. Special thanks to my father for arousing my interest in technology. Without his never ending support and confidence I would not have got this far.

I am of course most grateful to Harald for his patience and support. He adds the meaning to my life far beyond what physics could do.

CURRICULUM VITAE

Sabine Mayer

Date of Birth: 25.01.1975
Nationality: Austrian

EDUCATION:

Oct. 2000 – March 2003	Doctoral student in the Radiation Protection Group at CERN. Thesis topic: *Dose equivalent* m*easurements in mixed and time varying radiation fields around high-energy accelerators*
19 Jan. 2000	Dipl.-Ing. (M.S.) in Technical Physics with distinction
1994 – 2000	Studies of Physics at the Vienna University of Technology Diploma thesis at the Atomic Institute of Vienna ("Atominstitut der Österreichischen Universitäten") and at the department of Radiotherapy and Radiobiology of the General Hospital Vienna, topic*: "Messung und klinische Auswirkung der Anisotropie von ^{192}Ir-Quellen in der Brachytherapie"* (Measurement and clinical effects of the anisotropy of ^{192}Ir sources in brachytherapy)
1989 – 1994	TGM – Institute of technology, Vienna (Vocational School) Branch of study: communication engineering - medical technology "Maturaproject" (School leaving examination project): "Bau und Ansteuerung eines Blutdruckmessgeräts" (Design and construction of a blood pressure meter) Graduation with distinction
1985 – 1989	BG XI, Vienna (Grammar School)

CURRICULUM VITAE

PUBLICATIONS:

[1] **Mayer, S.**, *Messung und klinische Auswirkung der Anisotropie von ^{192}Ir-Quellen in der Brachytherapie,* Diploma Thesis at the Vienna University of Technology, Austria, 2000.

[2] Mitaroff, A., Dimovasili, E., **Mayer, S.**, Birattari, C., Wiegel, B., Silari, M., Aiginger, H., *Kalibrierung und Experiment eines Bonnerkugel-Spektrometers mit erweitertem Meßbereich. Proc. of Conf. Strahlenschutz für Mensch und Gesellschaft im Europa von morgen,* 17-21 Sep. 2001, Eds. K. Mück, Hefner, A., Vana, N., p 21-25, 2001.

[3] M^{c}Lay, F., **Mayer, S**., Otto, T., *Characterisation of the CERN REM-2 recombination chambers,* Technical Memorandum, CERN/TIS-RP/TM/2001-038, 2001.

[4] **Mayer, S.**, Zielczynski, M., M^{c}Lay, F., Dimovasili, E., Otto, T., *Measurements with a Recombination Chamber made at the CERN-EC High Energy Reference Field, CERF, in August 2001,* Technical Note, CERN/TIS-RP/TN/2002-03, 2002.

[5] **Mayer, S.**, Dimovasili, E., Otto, T., *Further Investigations of the Recombination Chamber REM-2 as a Mixed Field Dosimeter at CERF in October 2001*, Technical Note, CERN/TIS-RP/TN/2002-06, 2002.

[6] **Mayer, S.,** Mitaroff, A., Golnik, N., *Measurements of Dose Equivalent with a Recombination Chamber in a Complex High Energy Radiation Field*, in Proc: IRRMA-V, 5th Internat. Topical Meeting on Industrial Radiat. and Radioisotope Measurement Applications, Bologna, Italy, 9-14 June 2002. Divisional Report CERN-TIS-2002-016-RP-CF (EDMS # 359068), Nucl. Instr. And Meth. B (in press), 2002.

[7] **Mayer, S.**, Otto, T., *Investigations of a Recombination Chamber as a Mixed Field Dosimeter in Comparison with a Tissue-Equivalent Proportional Counter at CERF*, in Proc: RMA, 10th Symp. On Radiation Measurements and Applications, Ann Arbor, Michigan, USA, 21-23 May 2002. Divisional Report CERN-TIS-2002-015-RP-CF (EDMS # 355538). Nucl. Instr. And Meth. A (in press), 2002.

[8] Dimovasili, E., **Mayer, S.**, Mitaroff, A., Silari, M., *HANDI TEPC measurements during the 1999, 2000 and 2001 CERF runs*, Technical Note, CERN/TIS-RP/TN/2002-020, 2002.

[9] Golnik, N., **Mayer, S.**, Zielczynski, M., *Recombination Index of Radiation Quality of Low-LET Radiation*, in Proc: IRRMA-V, 5th Internat. Topical Meeting on Industrial Radiat. and Radioisotope Measurement Applications, Bologna, Italy, 9-14 June 2002, Nucl. Instr. and Meth. B (in press), 2002.

[10] **Mayer, S.**, Otto, T., Golnik, N., *Determination of the Photon-Contribution of a ^{238}Pu-Be Source***,** in Proc: IRRMA-V, 5th Internat. Topical Meeting on Industrial Radiat. and Radioisotope Measurement Applications, Bologna, Italy, 9-14 June 2002. Divisional Report CERN-TIS-2002-014-RP-CF (EDMS # 355488), Nucl. Instr. and Meth. B (in press), 2002.

[11] **Mayer, S.**, Golnik, N., Otto, T., Carbonez, P., *The Photon-Contribution of the ^{238}Pu-Be Source in the TIS-RP calibration laboratory,* Internal Report*,* CERN-TIS-2002-036-RP-IR, 2002.

[12] Kyllönen, J.-E., **Mayer, S.**, *Response Investigations of the Sievert Instrument in Neutron Beams between 0.5 and 19 MeV at PTB*, Internal Report*,* CERN-TIS-2002-037-RP-IR, 2002.

PRESENTATIONS AT CONFERENCES WITH BOOK OF ABSTRACTS ONLY

[1] **Mayer, S**., Fellner, C., Aiginger, H., Pötter, R., *Messung der Anisotropie von ^{192}Ir-Quellen in der Brachytherapi,* ÖPG (Österreichische Physikalische Gesellschaft) – Tagung, Universität Innsbruck, Austria, 1999.

[2] Loew, H.G., **Mayer, S**., Fellner, C., Aiginger, H., Pötter, R., *Digitale Gradienten-Filmdosimetrie zur Auflösung steiler Dosisverläufe in der Brachytherapie und Teletherapie*. *Physikalische Charakterisierung eines neuen UMAX-Filmscanners zur dosimetrischen Analyse von GAF-Chromic Filmen*, 50. ÖPG-Jahrestagung "Physik-Event 2000", 25-29 September 2000, Graz, Austria, Book of Abstracts: p. 207, 2000.